THICKNESS EVALUATION OF ASPHALT AND BASE LAYERS OF SOME MAJOR AND MINOR ARTERIAL ROADS IN KUMASI USING GROUND PENETRATING RADAR

By

Mohammed Hadi, BSc Physics (Hons)

A Thesis Submitted to the Department of Physics,
Kwame Nkrumah University of Science and Technology, Kumasi
in partial fulfillment of the requirements for the degree

of

MASTER OF SCIENCE (GEOPHYSICS)

College of Science

Supervisor (Dr. Kwasi Preko)

June, 2012

Declaration

I hereby declare that this submission is my own work towards the award of MSc Geophysics degree and that, to the best of my knowledge, it contains no material previously published by another person nor material which has been accepted for the award of any other degree of the University, except where due acknowledgement has been made in the text.

MOHAMMED HADI		15-03-13
Student	Signature	Date

Certified by: Dr. I.K. Preko		15/03/13
Supervisor	Signature	Date

Prof. S.K. Danuor		15/03/13
Head of Dept.	Signature	Date

Abstract

The asphalt and base layer thicknesses of major and minor arterial roads in Kumasi were investigated to determine possible structural defects. The evaluated roads included both newly constructed flexible pavements and older ones. The MALA GPR unit was used with the 800 MHz ground-coupled shielded antenna in the common offset mode and the equipment was calibrated to probe up to a depth of 1 m. A longitudinal profile of average length 1.5 km each was taken on ten different flexible pavements, at approximately 1.5 m from the outer edge of the respective pavements. In addition, transverse profiles were taken across the pavements at 100 m intervals. The estimated average asphalt layer thickness range of the major arterial pavements was 110 - 141 mm as compared to the designed thickness range of 102 - 200 mm, implying a RMSD of ±13.6 mm. The average base layer thicknesses estimated was 155 - 171 mm as against the designed range of 150 - 200 mm, with a RMSD of ±21 mm. Although the estimated layer thicknesses were within the acceptable range, it was found that the layer thicknesses measured were just about the minimum values (per the Equivalent Single Axis Loads of the roads studied). The minor arterial roads had an average asphalt layer thickness range of 96 - 110 mm, showing a RMSD of ±22 mm against the designed thickness of 50 - 150 mm. A few structural defects were found especially along the Lake road and the Kaase Ind. road. Even though no cores were picked from the studied pavements to calibrate the results from the GPR, the fast and non-destructive survey possible with the equipment has proven useful as an alternative to the destructive pavement condition evaluation techniques used in Ghana.

Acknowledgments

My deepest appreciation goes to the Almighty God for His unending mercy and grace towards me throughout the duration of this work. I wish to express my sincerest gratitude to my supervisor Dr. Kwasi Preko for his motivation, encouragement and the invaluable suggestions that helped me to improve this work. I am really indebted to him for all the opportunities he gave me and it is my fervent prayer that God grants him his wishes and protects him. I also wish to thank Prof. S K Danuor for his encouragement and motivation. I sincerely thank Mr. Vandycke Asare for the advice and training that he gave me on the GPR equipment as well as all the lecturers in the Physics department including; Mr. A. A. Aning, Mr. D. D. Wemegah, Mr R. M. Noye for the knowledge they imparted to me. I would not forget the brotherly assistance of the engineers at the Department of Urban Roads in Kumasi, especially, Mr. Botway and Mr. Smith. Further, I wish to extend my profound gratitude to my fellow MSc. students; Nana Andrew Davidson, Mr. Benjamin Boadi and Mr. Evans Manu, for the brotherly support they offered me during the field work as well as their assistance with regards to the use of some software. I just could not have done the field work without them. Finally, I acknowledge the friendly working atmosphere created by the entire staff of the Physics Department of KNUST.

Contents

List of Tables

List of Figures

Appendix A

Appendix B

List of Symbols and Acronyms

α	Attenuation constant
B	Magnetic flux density
c	Electromagnetic wave velocity
D	Electric flux density
E	Electric field strength
f	Frequency
G_{mm}	Maximum specific gravity
G_{mb}	Bulk specific gravity
h	Pavement layer thickness
H	Magnetic field strength
i	$\sqrt{-1}$
j	Free current density
k^*	Complex dielectric constant

k'	Real part of dielectric constant
k''	Imaginary part of dielectric constant
n	Refractive index
v	Velocity
V_a	Percentage air voids
V_{air}	Fractional volume of air
V_{agg}	Fractional volume of aggregate
V_w	Fractional volume of water
ω	Angular velocity ($2\pi f$)
$\emptyset$	Void ratio of asphalt
ρ_f	Fractional density of asphalt
ρ_{emp}	Emplaced density of asphalt
ε	Dielectric constant
ε_0	Dielectric constant of free space
ε_r	Relative dielectric constant
ε_{eff}	Effective dielectric constant
ε_{HMA}	Dielectric constant of Hot Mix Asphalt
r	Reflection coefficient
τ	Transmission coefficient
t	Time
μ	Magnetic permeability
μ_0	Magnetic permeability of free space
μ_r	Relative magnetic permeability
∇	Nabla operator $(\frac{\partial}{\partial x}, \frac{\partial}{\partial y}, \frac{\partial}{\partial z})$
χ	Electric polarization
χ_m	Magnetic polarization

AASHTO	American Association of State Highway and Transportation Officials
AC	Asphalt Concrete
ACP	Asphalt Concrete Pavement
CRCP	Continuous Reinforced Concrete Pavement
CMP	Common Midpoint
CSAH 61	County State-Aid Highway 61
DFR	Department of Feeder Roads
DUR	Department of Urban Roads
DVLA	Driver and Vehicle Licensing Authority
ESAL	Equivalent Single Axle Loads
FHWA	Federal Highway Administration
GDP	Gross Domestic Product
GHA	Ghana Highway Authority
GTTC	Government Technical Training Centre

HMA	Hot Mixed Asphalt
JPCP	Joint Plain Concrete Pavements
JRCP	Joint Reinforced Concrete Pavements
NDT	Non-Destructive Testing
NMO	Normal Moveout
NRSC	National Road Safety Commission
PCC	Portland Cement Concrete
PCP	Prestressed Concrete Pavements
PMS	Pavement Management System
RMSD	Root Mean Square Deviation
SPA	Seismic Pavement Analyzer

CHAPTER 1

INTRODUCTION

1.1 Traffic Infrastructure in Ghana

Road development is of high priority on the development agenda of the government of Ghana and considers good roads as one of the main catalysts for accelerating Ghana's economic growth. However, the existing urban road system in Ghana is greatly short of its functional and structural capacity to sustain high magnitude of stress imposed by heavy axle loads and ultimately a premature failure of road pavements results. Heavy investments are needed for the restoration of the road network of urban areas in Ghana to a desired serviceability level. In fact, Ghana was one of the first countries in the world to establish a road fund in 1985. However, road maintenance continued to face difficulties such as irregular and insufficient releases, inadequate financial management system and in 1997 a "second generation" Road Fund came into place through a Road Fund Act. This established a Board with private and public sector participation (Andreski, 2005). The rising cost of constructing road infrastructure worldwide and the subsequent premature degradation of the roads have necessitated the establishment of comprehensive scientific tools for evaluating finished contractor jobs as well as assessing the conditions of existing roads to plan rehabilitation strategies. In terms of road pavement facilities, an annual estimate of 34.72 % of the 2007-2008 national budget was dedicated to improving traffic infrastructure (Ministry of Transport, 2007-2008). Such budget allocations are spent on new construction, maintenance, and rehabilitation efforts in Ghana. When a pavement deteriorates to a point where it no longer satisfies the criteria under which it was designed, whether it is in terms of reduced structural capacity, increased roughness, reduced surface friction, or other circumstances, premature failure may occur. The existence of the Road Fund in Ghana suggests the premium the nation

attaches to its road infrastructure and more importantly, their maintenance. Pavement designers expect certain treatments to last a minimum amount of time. For example, a new continuously reinforced concrete pavement (CRCP) should last about 25 years or more before needing its first overlay; an asphalt concrete pavement (ACP) overlay should last 10 to 12 years; and a seal coat should last 5 to 8 years (Victorine et al., 1997). However, most roads in Ghana experience pavement failures shortly after their construction as manifested in road surface defects such as rutting, stripping, cracks etc thereby necessitating prompt maintenance interventions. Atto-Okine (1992) carried out a study to determine the cause of pavement failure of a major two-lane, low-volume road in Accra only 2 years after it had been constructed. The failure included excessive pavement distress in the form of settlement, cracking, differential subsidence, and outer-wheel path ruts. It was revealed that this failure was caused partly by a lack of specialized geotechnical tests to determine reliable input parameters, and partly by poor construction practices for placing geosynthetics used on the project. Structural degradation of asphalt road pavements has a considerable impact on traffic safety. Roadway surface defects or discontinuities make driving uncomfortable and increase the possibility of accidents. If damages to road pavements are not objectively and efficiently monitored and prevented with adequate maintenance, they may significantly increase the possibility of accidents and the severity of the damages.

Ghana has about 64,000 km of roads made up of 11,000 km paved and 53,000 km unpaved (gravel and earth surfaces). However, one of the key challenges is the lack of effective road maintenance leading to hazardous surface conditions, with its attendant effect on road safety. Detailed and accurate information about the road network is the foundation for comprehensive management and planning of transportation infrastructure and assets. Quality standards for the required data have evolved considerably over the last decades as traffic and

applications have become more demanding, and include a wide range of variables such as road centerline and geometry, pavement type, and road surface conditions. Table 1.1 below shows the details of road network in Ghana and their condition as at 2005:

Table 1.1: Ghana's Road Network, Length and Condition, (2002)

	Paved [km]	%Good	Unpaved [km]	%Good	Total [km]	%Good
Trunk	6992	52	6659	3	13151	26
Feeder	1097	55	31497	31	32594	32
Urban	1935	39	2128	13	4063	25
Total	9524	50	40284	26	49808	30

Source: Department of Urban Roads, 2002

1.2 Urban Roads in Ghana

An urban road, just like most other roads is a multi-layered flexible or rigid structure overlaying a subgrade. Most often, water pipes, electricity and telephone cables are buried under these road structures at various depths and orientations. This accordingly necessitates the use of non-destructive methods to evaluate urban roads. In many developed countries urban transport involves an integrated network of transportation modes, and urban roads are essential for the efficient movement of goods and people in towns and cities.

Road transport in Ghana accounts for approximately 97 % of passenger miles. Road transport in Ghana may be categorized into four main segments, namely; urban, express services, rural-urban and rural. All these road infrastructure require regular assessment and maintenance.

However, only one-fifth of the total road network is paved (see table 1.1). Most of the roads have been subject to periodic overlaying or reconstruction as traffic demand and loading has increased over the course of many years, developing from a track into a primitive road, into a paved road and finally into a major or minor arterial road structure. Such roads may have variable and non standard construction materials particularly in the sub-base, where new road materials have been laid over the top of the existing structure as the road has evolved. In such situations, the ability to undertake efficient site investigation of the road structure and underlying ground to determine the thickness and nature of the materials is particularly important. The urban transport in Ghana is characterized by congested central districts of the cities, poor quality of service from public transport operators, high exposure to road accidents and poor environmental standards. The Kumasi metropolis has a circulatory road network pattern comprising five major arterials primary roads linking the city to other parts of the country and beyond, all radiating from the center of the city. There are also four other primary roads that link the city to other districts. The total length of the road network in Kumasi is 430 km. Of this, the asphaltic cement standards. The Kumasi metropolis has a circulatory road network pattern comprising five major arterials primary roads linking the city to other parts of the country and beyond, all radiating concrete is about 26 % and that of surface dressing is 53 %, while gravel and earth roads account for 21 %. The record on road network quality is quite reasonable, with 75 % of the paved network in good or fair condition and, more impressive, 74 % of the unpaved network in good or fair condition (Kwakye et al., 1998).

1.3 Management of Urban Roads in Ghana

In Ghana, the Ministry of Transport has oversight responsibility for the management of the road transport sector and its subsidiary departments and agencies are broadly divided into

two: the road infrastructure sub-sector which is responsible for road construction and maintenance and they include the Ghana Highway Authority, Department of Feeder Roads and the Department of Urban Roads. The other is the transport services sub-sector, including; Driver and Vehicle Licensing Authority, National Road Safety Commission, Metro Mass Transit, Government Technical Training Centre, and the Ghana Road Fund Secretariat. The Department of Urban Roads is responsible for the maintenance and rehabilitation of urban roads infrastructure. Routine inspection of urban road conditions in Ghanaian cities is usually done through visual surveys. In most cases the investigations are ad-hoc and subjective and also the results from studies taken at certain discrete points (such as coring) which are used to draw conclusions about the conditions of several kilometers of roads should be supported with continuous survey results. Areas which require maintenance can be caused by problems in the pavement, sub-base and/or subgrade, and often the first indication that maintenance may be required is noted by the appearance of features such as cracks or rutting of the road surface. The Ghana Highway Authority pavement design manual AASHTO (1993) sets forth the policy and the nation's approved standards to be adopted for the design and assessment of conditions of roads in Ghana. Until recently, the structural design of new bitumen surfaced roads in Ghana was based on a combination of Road Notes 29 and 31, published by the British Transport and Road Research Laboratory, 1966. These notes were not specifically designed to cater for the current needs of the country. Thus, the method selected is the AASHTO Guide for Design of pavement structures. This method was selected because it represents the state of the art in asphalt road pavement design and has been extensively adopted for local conditions. The various techniques described in the AASHTO Guide are also used for the investigation of urban roads. Once areas of a road have been identified as requiring detailed investigation, there are several methods which can be used to determine the properties of the pavement, sub-base and supporting underlying ground, both intrusively and

non-intrusively. It is these subsequent detailed investigations that are used to plan maintenance treatments.

1.4 Problem Statement

Engineers at the Ghana Highway Authority, Urban Roads Department and Local Government Ministries routinely assess the conditions of road infrastructure in the country. The key information needed from these surveys is the remaining life of existing roads and thus their rehabilitation strategy. Such information enables the engineers identify, prioritize and schedule roads that require rehabilitation either immediately or in the nearest future, and estimate the cost as well. Unfortunately, the mode of evaluation of finished contractor jobs by these engineers is usually visual and destructive. Usually, since several kilometers of roads are often evaluated, the techniques used should be fast, economical, repeatable and cause little delay to motorists. Most importantly, the technique must be objective enough to generate results that can be processed with computer algorithms.

1.5 Objectives of this Research

Results from studies taken at certain discrete points are used to draw conclusions about the conditions of several kilometers of roads. This requires an alternative method that is continues, fast and non-invasive. Accordingly, to attempt demonstrate the use of such alternative methods for evaluating the conditions of urban road infrastructure in both finished contractor job inspection and assessment of the deterioration levels of the existing road pavements in general, this research was conducted with the following objectives in mind;

- To evaluate the thicknesses of surface asphalt layers and base layers of some major and minor arterial roads in Kumasi with the GPR method.

- Determine the uniformity in the thicknesses of asphalt and base layers in newly constructed roads in the Asokwa Sub-Metropolis of Kumasi.
- To map out general subsurface anomalies underneath the road pavements.
- Demonstrate the capabilities and limitations of ground penetrating radar (GPR) for use in local road condition evaluations.

1.6 Expected Contribution from the Study

As outlined in the study objectives, results from this study is expected to provide an insight into a fast, objective and scientific approach to the evaluation of traffic infrastructure in the country. Accurate layer thickness estimation is an important issue for pavement engineers, for both newly constructed and old pavements. For new pavements, layer thickness measurement is essential to ensure that the placed layers meet the design specifications, as part of quality control and quality assurance. For old pavements, layer thickness measurement and subsurface defect localization are important to make appropriate economical rehabilitation decisions. It is also expected to provide a better alternative to engineers at the various local government departments tasked with the management and maintenance of pavement facilities in the country.

1.7 Types of Road Pavements in Ghana.

Pavements are planar-layered media with different materials composing each layer. Figure 1.1 shows a typical cross-section of a road pavement structure. There are two main categories of road pavements in Ghana: flexible (hot-mix asphalt) pavements and rigid (concrete) pavements.

1.7.1 Flexible Pavements

Flexible pavements are layered systems composed of different layers that are placed in such a way that layer strength is greater at the top, where the stresses caused by traffic loading are high. In conventional flexible pavements (figure 1.2(a)), the top layer is called the wearing surface, which is usually made of a dense graded hot-mixed-asphalt (HMA) to resist distortion under traffic and to provide a smooth and skid-resisting riding surface. Under this layer, an HMA base course exists which is made of a lower quality HMA. The base course may be composed of crushed stone, crushed slag, or other untreated or stabilized materials. The sub-base course is an optional layer used primarily for economical purposes since it is made of cheaper material than that used for the base. The flexible pavement may consist of all or part of the above layers. In addition, other modified materials of the above layers and/or geosynthetics may be used. The aforementioned layers are supported by the existing or stabilized soil, which is called subgrade. In full-depth flexible pavement, one or more layers of HMA are placed directly on the subgrade. The asphalt base course thickness usually varies between 50 mm and 250 mm (2 - 10 in). The base courrse is usually between 100 mm and 300 mm (4 - 12 in) thick. Subgrade is the bottom layer supporting all the aforementioned layers. It can be either the original in-situ soil or a placed layer of selected material. In both cases, the subgrade should have a high density attained by good compaction.

It should be noted that a typical pavement is composed of any combination of two or more layers in the order specified above (top to bottom). A flexible pavement should have, at least, an HMA layer and an aggregate (base course) layer. The layer thicknesses used in the design depend primarily on the importance of the road, the volume of traffic it is expected to carry, the properties of the construction materials used, and the local environmental conditions.

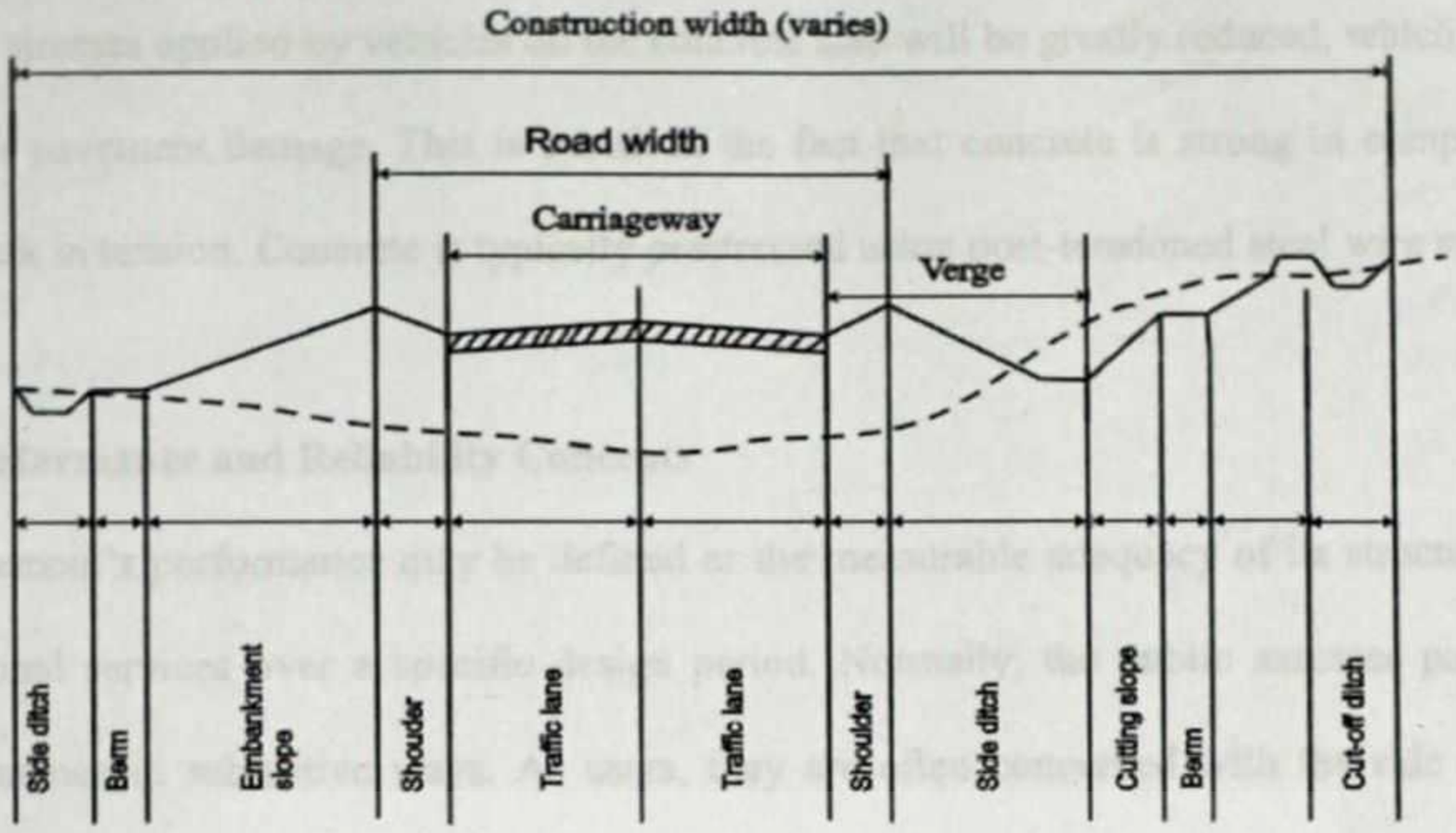

Figure 1.1: Cross-section of a typical road pavement (AASHTO,1993).

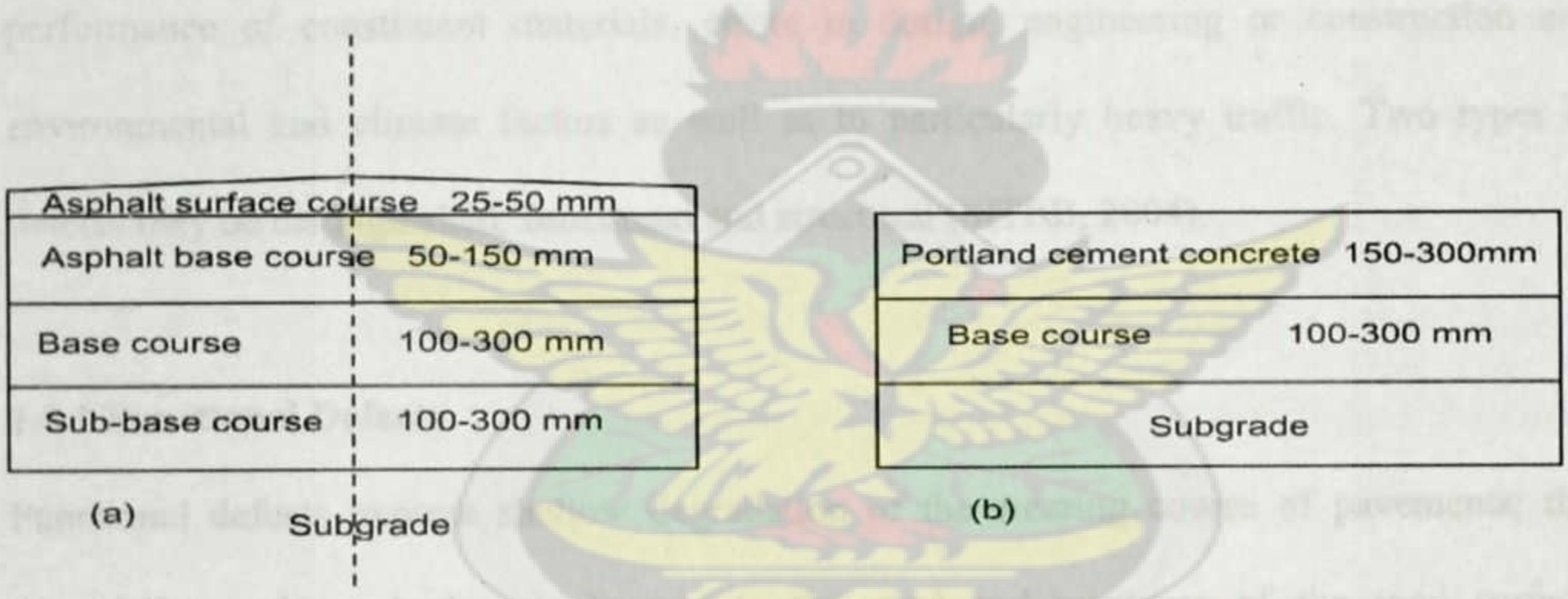

Figure 1.2: Typical Sections of (a) Flexible Pavement and (b) Rigid Pavement.

1.7.2 Rigid Pavements

In rigid pavements, a concrete slab is placed over the existing soil. A base and sub-base, which are typically used, are optional layers. Rigid pavements are constructed with 150 mm to 300 mm thick (6 - 12 in) Portland cement concrete (PCC) slabs as illustrated in figure 1.2(b). Prestressed Concrete Pavements (PCP) are built in such a way that a compressive stress is naturally imposed on the slabs in the absence of any traffic load. Consequently,

tensile stresses applied by vehicles on the concrete slab will be greatly reduced, which in turn reduces pavement damage. This is based on the fact that concrete is strong in compression but weak in tension. Concrete is typically prestressed using post-tensioned steel wire strands.

1.8 Performance and Reliability Concepts

A pavement's performance may be defined as the measurable adequacy of its structural and functional services over a specific design period. Normally, the public assesses pavement performance in subjective ways. As users, they are often concerned with the ride quality, safety, appearance, and convenience. As taxpayers, they expect pavements to last long enough to justify the cost of their construction (AASHTO, 1993). Defects in flexible pavements are indicative of road distress and impaired efficiency. They may be due to poor performance of constituent materials, errors in design, engineering or construction and environmental and climate factors as well as to particularly heavy traffic. Two types of defects may be distinguished: functional and structural (SITEB, 2004).

1.8.1 Functional Defects

Functional defects express shallow degradation of the wearing course of pavements; this degradation reduces both vehicle grip to the road and evenness of the road surface, jeopardizing traffic safety. Factors responsible for this type of degradation and giving rise to skid resistance problems include leveling (or polishing) of aggregates; surface exposure of bitumen (known as bitumen blooming); desegregation and detachment of aggregates. Smoothness problems comprise longitudinal undulations, transverse undulations (more commonly called ruts); hollows or bulges; dips on extensive surfaces; edge cracking. A pavement provides functional service by giving users a safe and comfortable ride for a

specific range of speeds. Functional services is comprised of several factors including the following:

- Acceptable ride quality (smoothness)
- Adequate surface friction for safety
- Appropriate geometry for safety
- Appearance (aesthetics)

1.8.2 Structural Defects

Conversely, structural defects arise in the supporting courses of the superstructure. They are due to deterioration of its load-bearing capacity and have major repercussions on pavement durability, if they are not timely cured. Defects of this type encompass surface cracks and breaks and, more recurrently, longitudinal, and transverse cracks, longitudinal cracks only, transverse cracks only, ramified cracks (spider or alligator cracks), and failures (CNR, 1988). Now, it is worth reviewing the potential factors which trigger structural degradation of flexible road pavements. These factors may be related both to problems occurring upon construction and to effects supervening during road use. In particular, permanent deformation of the subgrade and of the loose and bound granular materials making up the pavement (taking place during construction) may result from a combination of different (and usually concurrent) factors; unevenness of the subgrade-supporting course; poor workmanship in the placing of layers; poor or uneven compaction; incorrect finishing (water puddles); nonhomogeneous thickness. Deformations due to repeated traffic stresses during road use chiefly originate in the loose granular layers and subgrade of the pavement. They are caused by the use of unsuitable materials, such as granular mixes with crushable aggregates; granular mixes with excess of fines; granular mixes with plastic fines; aggregates of inappropriate grain size; plastic or compressible subgrades. During road use, bituminous-concrete layers

may also contribute to structural degradation of the road surface for the following reasons: presence of crushable aggregates; inappropriate grain size curve; bitumen unsuitable for local climate and traffic conditions; incorrect batching of bitumen; inadequate thickness (under sizing); bituminous concretes that are too stiff with respect to the unbound underlying layers. Structural service of a pavement is provided by supporting traffic loadings and withstanding environmental influences. The types and thicknesses of materials used in the various pavement layers often dictate how the pavement will perform structurally.

Structural and functional adequacy of the road pavement are closely related, but are not entirely interdependent. Structural deterioration of a pavement is manifested to some extent in diminished functional adequacy, in the form of increased roughness, noise and even posing a hazard to vehicles and their occupants. But some types of structural deterioration can occur and progress to a fairly advanced stage without being noticeable to users. A pavement's functional adequacy can also decrease without any significant change in structural adequacy (such as by the loss of skid resistance).

1.8.3 Asphalt Road Performance Indicators

Road users would ordinarily assess the performance of pavements subjectively, and such a method cannot be directly utilized in pavement design. Nonetheless, certain characteristics of road pavements can be quantitatively measured and therefore can be correlated to the road users' subjective assessment of the pavement's performance. The characteristics are known as performance indicators and they include:

1. Visible distress
2. Structural adequacy
3. Surface friction

4. Roughness/serviceability

1.8.3.1 Visible Distress

Distress occurs in pavements as a result of complex interactions of design, construction, materials, traffic, environmental and maintenance procedures. Visible distress are quantified with respect to the following three parameters; type, severity and quantity. The most common asphalt road distresses often observed in Ghana are described below. The probable causes of these types of distress that occur in AC pavements and AC overlays are also included.

- Alligator Cracking

Alligator or fatigue is a series of interconnecting cracks caused by fatigue failure of the AC surface and surface treated (ST) under repeated traffic loading, and is considered a major structural distress. The cracking generally initiates at the bottom of the AC surface, where tensile stresses and strains are highest under a wheel load. The cracks propagate to the surface, and connect other areas, forming many-sided and sharp-angled pieces in a pattern resembling the skin of an alligator. The pieces are usually less than 0.3 cm on the longest side. Alligator cracking occurs only in areas that are subjected to repeated traffic loadings. Accordingly, it does not often occur on the entire area of the road pavement, unless the road were entirely subjected to intense traffic loadings all over.

- Stripping

Stripping is simply the removal of asphalt binder from the aggregate and it's a moisture-related defect in the asphalt. It is one of the contributing factors to the deterioration mechanism of AC pavements. Stripping may also contribute to the development of alligator cracking and other forms of cracking in AC pavements (Stuart (1990), Hicks (1991)).

- Bleeding/Flushing

It is the development of a film of bituminous material on the pavement surface which creates a shiny, glass-like, reflective layer that is often sticky. Bleeding is caused by excessive amount of asphalt cement in the mix and/or low air void contents.

- Longitudinal cracking

It is a cracking that runs more or less parallel to the pavement's centerline or paving lay down direction within the lane width. It may be caused by poorly constructed paving longitudinal joints or the shrinkage of the AC surface due to the hardening of the asphalt.

- Transverse cracking

Transverse cracks run perpendicular to the pavement centerline or lay down direction and are caused by the shrinkage of the AC surface due to hardening of the asphalt.

- Rutting

A rut is a longitudinal surface depression in the wheel path. In some cases, pavement uplift (shoving) may occur along the sides of the rut. Low-severity rutting may only be noticeable after a rainfall, when the wheel paths are filled with water. Rutting usually stems from permanent deformation in one or all of the pavement layers or subgrade, often caused by consolidation or lateral movement of the materials due to traffic loads.

1.8.3.2 Structural Adequacy

Structural adequacy can be defined as the ability of a pavement to carry the expected loads over the specified time period. The structural design of a pavement begins with a forecast of the types and volumes of vehicle traffic expected to use the pavement over a specified future

period of time. Pavement layer materials are then selected, and thicknesses of these layers are determined which will provide a structure capable of supporting the forecasted traffic over the desired time period without failure.

1.8.3.3 Surface Friction

Pavement surface friction, sometimes referred to as skid resistance, is the force developed at the tyre-pavement interface that resists sliding when breaking forces are applied to the vehicle tyres. Three factors influence a pavement's surface friction; microstructure, macrostructure and transverse slopes. Microstructure refers to the roughness of the surfaces of the individual coarse aggregate particles and of the binder. Microstructure contributes to friction by adhesion with vehicle tyres. Macrostructure is the overall texture of the pavement, which is controlled by coarse aggregate type and size in flexible pavements and by surface finish in rigid pavements. A good macrostructure helps to improve surface friction by providing escape channels for the surface water at the pavement-tyre interface. Finally, transverse slope contributes to surface friction by removing water from the pavement surface. Inadequate surface friction of a newly constructed pavement may be attributed to poor construction techniques, poor materials selection (mix design), or poor transverse slope.

1.8.3.4 Roughness/Serviceability

While distress, structural conditions and skid resistance are important engineering indicators of a pavement's condition, users assess the condition of a pavement largely in terms of ride quality. Serviceability is thus defined as the ability of a pavement to provide a safe and comfortable ride to users. Roughness is also defined as irregularities in the pavement surface adversely affect ride quality, safety, and vehicle maintenance costs.

CHAPTER 2

LITERATURE REVIEW

2.1 The Various Methods used in Traffic Infrastructure surveys

The practice of forensic engineering within the field of traffic infrastructure management has grown in response to the increasing number of facilities needing repair or replacement. When a pavement deteriorates to a point where it no longer satisfies the criteria under which it was designed, whether it be in terms of reduced structural capacity, increased roughness, reduced surface friction, or other circumstances, premature failure may be involved. This is partly due to the non-adherence of some road contractors in African countries to design specifications spelt out in contracts, thus carrying out shoddy works. Quality assurance of finished contractor jobs in most developing countries is often based on visual inspections, which does not reveal important details of the road pavements such as asphalt layer thickness, density etc. Visual condition surveys may include both structural and functional pavement conditions, but often serve as qualitative indicator of the condition of the roads and are also subjective. Road evaluations are carried out to assess the functional and structural conditions of road pavement sections either for purposes of routine monitoring or planned corrective action. Functional condition is primarily concerned with the ride quality or surface texture of a highway section. Structural condition is concerned with the structural capacity of the pavement as measured by deflection, layer thickness, and material properties. Such evaluation methods include visual surveys, destructive and non destructive tests. In response to this growing concern for detailed assessment of conditions of both flexible and rigid pavements, researchers worldwide have over the years applied various methods to study internal properties of pavements such as layer thickness, density, void ratio, moisture content, steel reinforcements in bridges locations etc. The various methods include destructive methods (such as coring,

drilling and pit excavations), which are often used for calibration and verification purposes only. Destructive tests provide more detailed data about the pavements such as;

- laboratory mechanical, physical and chemical properties which are obtained through coring, Shelby tubes and trenching.
- visual inspection of pavement layers at points where cores are picked.

The other category of methods are collectively termed the Non-Destructive Testing (NDT) techniques which include; the Benkelman beam, Falling Weight Deflectometer (FWD) or dynaflect, Spectral or Seismic Pavement Analyzer (SPA), linear polarization techniques, half-cell potentiometer, ultrasonic, infrared thermography, video imaging, profilometers and Ground Penetrating Radar (GPR) (Loulizi, 2001). Non-Destructive Tests (NDT) are the pavement evaluation methods conducted on pavements to assess in situ properties using scientific equipment. Results from NDTs can be used to evaluate the need for further destructive tests. Unlike the destructive methods, these methods do not require subsequent maintenance work at the site and they minimize disruption to traffic. NDTs could also assess both structural and functional conditions of a pavement. The choice of appropriate geophysical NDT method is guided by the following criteria:

1. Effectiveness - general technology maturity and success in road applications (such as pavement layer thickness evaluation, void detection or subsurface anomaly mapping).
2. Feasibility - operational costs/constraints, transportability, and availability, environmental limitations etc.
3. Invasiveness - extent of damage to pavement/base and cost for damage repairs.

4. Overall efficiency - rate of coverage (speed of the method), spatial sampling resolution etc.

The Non-Destructive Testing (NDT) of pavements is increasingly being recognized as an effective way to obtain information about the structural behaviour of pavements. Although the intrusive methods can provide extremely useful data on the pavement properties and condition, it is time consuming to excavate material from a pavement, and also further time and costs are incurred to repair the pavement after testing. The use of non-intrusive methods therefore provides a better alternative which allow pavement properties to be assessed without damage to the structure and often take less time to finish a comprehensive survey. Some of these NDT methods such as the falling weight deflectometer (FWD) are used to obtain information on the pavement's structural condition under a simulated vehicle loading, and from which data can be used to determine the stiffness of the pavement layers. This technique has been widely used in Europe, North America and Japan (Irwin, 2002). In this technique, a number of geophones are used to determine the static deflection bowls resulting from a vertical impact. The measured deflection bowls, together with the information on layer thickness, are used for the estimation of "in situ" bearing capacity (Antunes, 1993). The FWD is one of the nondestructive devices that has recently gained widespread acceptance (since the introduction of the static Benkelman beam at the WASHO Road Test in the early 1950s) for the structural evaluation of pavement deflection response (Graves and Drnevich,1991).

Evaluation of pavement surface roughness, which is a measure of the riding comfort, is carried out with the Profilometer. In this technique, the International Roughness Index (IRI), developed at the International Road Roughness Experiment held in Brazil in 1982 is adopted as a common quantitative basis for measuring the roughness (Sayers et al., 1986). The IRI is

defined as the ratio of the accumulated suspension motion to the distance traveled obtained from a mathematical model of a standard quarter car over a measured profile. It is expressed in units of m/km (in/mile). The longitudinal profile is usually measured using lasers and accelerometers.

The Seismic Pavement Analyzer (SPA) (Nazarian et al 1993) or the Spectral Pavement Analyzer (Metro Testing Laboratories, 1994) uses a suite of wave propagation techniques to determine shear modulus, layer thickness, support conditions and to detect delamination. The acoustic contrast at layer interfaces is used to determine layer thickness. Shear modulus is calculated from wave propagation velocities. The ability of the SPA to simultaneously determine thickness and deformation modulus, without recourse to coring and drilling, makes it an attractive tool for evaluating urban roads. Linear polarization techniques have been used to measure corrosion current density and therefore predict the state of reinforcement corrosion in bridge decks. Measurements are taken in the linear region of the polarization curve where the applied current to the corroding metal, in an ionic solution, is linearly related to the metal potential. Two devices that are currently used for these measurements are three linear polarization (3LP) and "Gecor" (Loulizi, 2001). The Half-cell potentiometer is a method widely used to determine the probability of reinforcement corrosion in concrete bridge decks (ASTM C876-91). The principle of this technique involves measuring the voltage difference between the reinforcing steel and a reference electrode.

Impact-echo is based on the use of transient stress waves produced by elastic impact from tapping a small steel ball against the surface of the material under test. The low-frequency stress waves propagate into the material and reflect from flaws or other interfaces. A transducer placed approximately 150 mm from the impact records surface displacements

caused by these reflected waves. The resulting waveform is transformed into the frequency domain using a Fast Fourier Transform. From the frequency spectrum, transient resonance frequencies, obtained from the multiple reflections of the waves, are identified. These frequency peaks are used to determine the integrity of the structure and to determine the location of flaws using the equation below;

$$d = \frac{c_p}{2f} \tag{2.1}$$

where d is the thickness at which the multiple reflections occur, c_p is the speed of the wave (typically 4000 m/s for normal concrete), and f is the frequency. Sansalone and Streett (1997) used the impact echo method for different applications including the determination of concrete slab thicknesses, detection of delaminations in bridge decks with and without HMA overlays, determining depth of surface opening cracks, locating unconsolidated concrete, and evaluation of bond quality at internal interfaces. Infrared thermography as applied to pavement condition assessment, is based upon the recognition that every material with a temperature above absolute zero (-273.15 °C) emits some form of radiant thermal energy that can be seen as a temperature pattern with a thermal camera. Therefore defects and inhomogeneities in the pavement would manifest themselves as local hot or cold regions in the isothermal mapping. That is, for an anomaly to be detected by thermography, it must create a temperature differential at the surface of the test object.

2.2 The Use of GPR in Traffic Infrastructure Studies

The recent development of the Ground Penetrating Radar (GPR) for use in pavement investigation has provided a new non-intrusive technique from which data can be used to both directly determine pavement properties, and to confirm the findings and enhance the

accuracy of other techniques. The use of GPR technique in traffic infrastructure surveys dates back to the early and mid 1970s when, according to Morey (1998), the Federal Highway Administration (FHWA) in the U.S.A. tested the feasibility of radar in tunnel applications and later on bridge decks. In the tests that followed Kovacs and Morey (1977) used it to detect moisture in construction materials, Cantor and Kneeter (1978) tested it for the inspection of bridge decks and More and Erhard (1978) employed it to detect voids under concrete highways. In the early 1980's, GPR surveys were also started in Canada (Manning and Holt (1983); Carter et al. (1992)).

The other active area in the late 1970's and early 1980's was Scandinavia, where the first GPR tests with ground coupled antennas were performed in Sweden (Ulriksen (1982); Johansson (1987); Carlsten (1988)) and in Denmark Berg (1984), and although the results were promising the method did not receive general acceptance at that time. However, after the first tests were conducted in Finland in 1986 Saarenketo (1992), the method rapidly became a routine survey tool in various road design and rehabilitation projects in Finland (Saarenketo and Scullion, 1994), and later as a pavement quality control tool (Saarenketo and Roimela, 1998).

With respect to pavement thickness evaluation, Maser and Scullion (1992) used the GPR method to determine the asphalt and base layer thicknesses of pavements in Texas in which the asphalt thickness was found to range from 2 - 10 inches whereas the base layer thickness varied from 5 - 12 inches. The accuracy of the radar predictions for asphalt thickness was within 0.32 inches (4%) using the radar data alone, and within 0.11 inches (1.4%) when one calibration core was used per site. The accuracy of the radar predictions for the base thickness was within 1 inch (17%). Moreover, fourteen asphalt test sections were evaluated in Kansas

by Roddis et al (1992) and the pavement thickness ranged from 3 - 22 inches. In this study, the GPR surveys were calibrated with 73 ground-truth measurements and the results indicated that blind estimates of asphalt thickness were found to be within 10% of actual thicknesses. Thus, when the core data were picked, the comparison improved to within 7%. When ground truth measurements were used, the accuracy improved to within 5%. Another project was carried out by Fernando and Maser (1992) in Florida to estimate asphalt pavement and aggregate base thicknesses at five test sites, again comparing the results to ground-truth measurements. The estimated asphalt thickness varied from 3 – 6 inches, and the aggregate base thickness varied from 8.5 to 12 inches. Blind estimates of asphalt thickness were within 0.5 inches of the actual thicknesses. Correspondingly, the blind estimates of base thickness were within 0.7 inches of core values taken at the test locations. When the results were calibrated with the ground-truth measurements the accuracy improved to 0.2 inches for asphalt thickness and 0.2 inches for the base thickness. The results from these studies demonstrated the ability of GPR as a non-destructive test technology for pavement and base layer thickness evaluation, with the accuracy of thickness calculations being 7.5% for asphalt and concrete pavements, and within 12% for unbound base layers. In recent years research on GPR has been focused on different types of applications on low traffic volume roads, both paved and gravel roads (Saarenketo and Vesa (2000); Roadex; Saarenketo and Aho, (2005)). Research has also begun on the transfer and utilization of GPR results by automated road construction machinery (Heikkilä et al., 2004). Amongst all the methods used in pavement surveys, the GPR appears to be the most appealing technique to assess bridge decks as well as pavements and becomes an important part of any pavement management system (PMS) or bridge management system (BMS). The advantages of using GPR include rapidity of measurements, non-invasive nature of the technique, and the ability to detect defects before they reach an advanced stage. The most important application of GPR in pavements is the

determination of different layer thicknesses. These data are useful for overlay design, predicting pavement life, and as input for other testing techniques such as FWD (Loulizi, 2001). In other recent studies, Yuejian et al. (2007) used the GPR to measure the asphalt and aggregate base layer thicknesses, road mix thickness and to detect areas of potential stripping in Pine County, Minnesota - USA. In their study, the GPR was successful at identifying the asphalt, road mix and aggregate base layer thicknesses along a ten mile stretch of CSAH 61, distinctly mapping the various layer interfaces, locating stripping in isolated zones. The Minnesota Department of Transportation has successfully used the GPR method for pavement layer thickness estimation and underground void detection and has been using the technology since 1998 and the method is known to work best for near-surface, dry soil conditions where the dielectric contrast is greatest, and conversely does not work well in wet, clayey soil conditions where the dielectric contrast is negligible. Most of the road pavement condition assessment methods described above have demonstrated high potential as tools for inspecting the roadway infrastructure, although each method has its own advantage as well as limitations. This research thesis investigates the use of GPR to estimate the layer thicknesses of asphalt concrete wearing course as well as base layer course in both newly constructed roads and already existing ones. No core samples were available for calibration, thus even though the GPR method used is expected to provide accurate asphalt and aggregate base layer thicknesses of the surveyed roads, some margin of error is anticipated. Nonetheless, one of the key objectives of the study is to demonstrate the use of the GPR technique for local urban roads condition assessment by estimating the longitudinal and transverse variation of the pavement thickness in both new and older roads. The results is expected to provide an alternative to the other destructive and more expensive methods used by local government engineers for quality assurance of pavements in Ghana among other things.

CHAPTER 3

THEORETICAL BACKGROUND

3.1 Mathematical Principles of the GPR

GPR technology involves the transmission of short pulses of electromagnetic energy into the ground, and the measurement of the time elapsed between the transmission and reception of the wave by a surface radar antenna, after reflection in an electrically inhomogeneous layer. The amplitudes and arrival times of the received pulses carry vital information about the electrical conductivities or the dielectric constants of the layer material. Depending on the dielectric constant of the layers penetrated, part of the transmitted energy is reflected whereas part is absorbed. Thus as shown in figure 3.1, the observed peaks in amplitudes represent the pavement surface reflection (A_1), the asphalt-base interface reflection (A_2), and the base-subgrade interface reflection (A_3) respectively. Further, the time interval (t_1) between the peaks A_1 and A_2 represents the two-way travel-time through the asphalt pavement layer, and the time interval (t_2) between peaks A_2 and A_3 represents the two-way travel-time through the base layer etc. The thicknesses of each layer (h_i) can be calculated by

$$h = \frac{v_i t_{WTT}}{2} \tag{3.1}$$

where v_i is the propagation velocity through each layer and t_{WWT} is the two-way travel time of the waves. The propagation velocity is again related to the electromagnetic property of the material by

$$v_i = \frac{c}{\sqrt{\varepsilon_i}} \tag{3.2}$$

where ε_i is the dielectric constant of each layer and c is the speed of light in air. c = 11.8 in/ns or 0.30 m/ns.

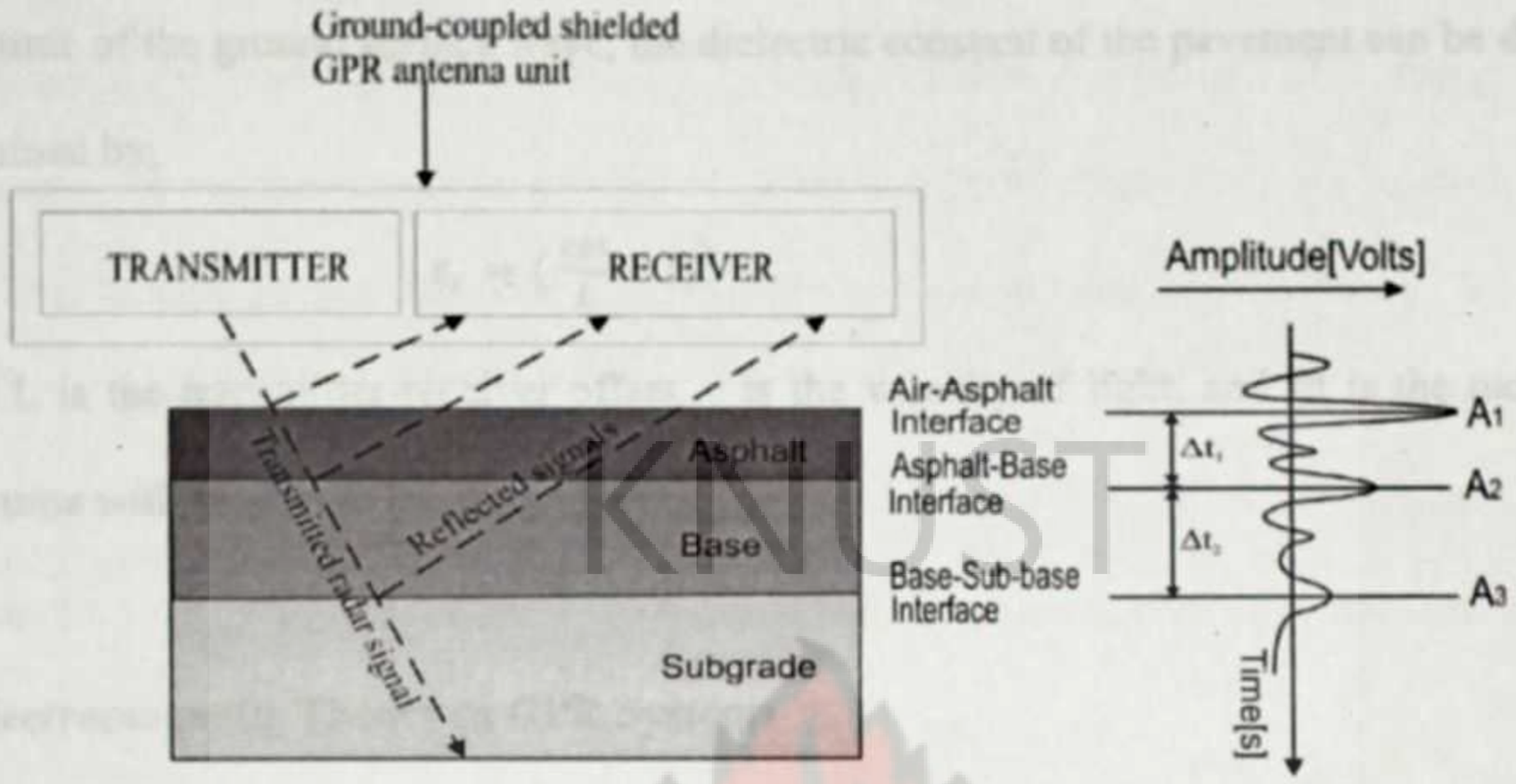

Figure 3.1: Typical GPR reflection in a road pavement and its waveform.

In air-coupled mode of GPR surveys, the dielectric constants of pavement materials are usually measured by the surface reflectivity method (equation 3.3). That is, the dielectric constant of the road pavement layer (ε_1) is found by:

$$\sqrt{\varepsilon_1} = (1+\rho_1)/(1-\rho_2) \tag{3.3}$$

where $\rho_1 = A_1/A_m$, A_1 is the amplitude of the GPR wave from the road pavement surface and A_m is the amplitude of the GPR wave from a metal plate. Similarly, the dielectric constant of the base layer (ε_2) is found by:

$$\sqrt{\varepsilon_2} = \sqrt{\varepsilon_1}\,(1-\rho_1^2+\rho_2)/(1-\rho_1^2\rho_2) \tag{3.4}$$

where $\rho_2 = A_2/A_m$, A_2 is the amplitude of the GPR wave from the base layer (Loken, 2007).

However, in a ground-coupled GPR survey the reflected wave and the direct wave arrive at the same time such that the amplitude of the surface reflection cannot be determined. Hence the surface reflectivity method of estimating the dielectric constants of the pavement layers does not apply to ground-coupled GPR studies (Liu et al., 2006). Thus by measuring the travel time of the ground surface wave, the dielectric constant of the pavement can be directly determined by;

$$\varepsilon_r = \left(\frac{c\Delta t}{L} + 1\right)^2 \tag{3.5}$$

where L is the transmitter-receiver offset, c is the velocity of light, and Δt is the measured travel time with respect to the direct wave.

3.2 Electromagnetic Theory in GPR Systems

The main mechanisms involved in the travel of EM waves between the transmitting and the receiving antennas are: the propagation of the waves through the homogeneous probed medium and the scattering of the EM waves from the inhomogeneous materials or layers encountered.

3.2.1 Electromagnetic Propagation

Electromagnetic wave propagation through a homogeneous medium is governed by Maxwell's equations and the constitutive relations. These equations relate the electric field and the magnetic field at every point to the sources that create them, and to the electrical properties of the medium. The Maxwell's equations describe all the classical electromagnetic wave phenomena. The first is Faraday's law of induction, the second is Ampere's law as amended by Maxwell to include the displacement current $\partial D/\partial t$, the third and fourth are Gauss' laws for the electric and magnetic fields.

$$\nabla \times \mathbf{E} = -\frac{\partial \mathbf{B}}{\partial t} \tag{3.6}$$

$$\nabla \mathrm{x}\, \mathbf{H} = \mathbf{J} + \frac{\partial \mathbf{D}}{\partial \mathrm{t}} \tag{3.7}$$

$$\nabla . \mathbf{D} = \boldsymbol{\rho} \tag{3.8}$$

$$\nabla . \boldsymbol{B} = \mathbf{0} \tag{3.9}$$

The displacement current term $\partial \mathrm{D}/\partial \mathrm{t}$ in Ampere's law is essential in predicting the existence of propagating electromagnetic waves. The quantities E and H are the electric and magnetic field intensities and are measured in units of [V/m] and [A/m], respectively. The quantities D and B are the electric and magnetic flux densities and are in units of [C/m^2] and [W/m^2], or [tesla]. D is also called the electric displacement, and B, the magnetic induction. The quantities ρ and J are the volume charge density and electric current density (charge flux) of any external charges (that is, not including any induced polarization charges and currents).

They are measured in units of [C/m^3] and [A/m^2]. The right-hand side of the fourth equation is zero because there are no magnetic monopole charges. The charge and current densities ρ and J may be thought of as the sources of the electromagnetic fields. For wave propagation problems, these densities are localized in space; for example, they are restricted to flow on an antenna. The generated electric and magnetic fields are radiated away from these sources and can propagate over large distances to the receiving antennas. Away from the sources, that is, in source-free regions of space, Maxwell's equations take the simpler form:

$$\nabla \mathrm{x}\, \mathbf{E} = -\frac{\partial \mathbf{B}}{\partial \mathrm{t}} \tag{3.10}$$

$$\nabla \mathrm{x}\, \mathbf{H} = \frac{\partial \mathbf{D}}{\partial \mathrm{t}} \tag{3.11}$$

$$\nabla . \mathbf{D} = 0 \tag{3.12}$$

$$\nabla . \mathbf{B} = 0 \tag{3.13}$$

The qualitative mechanism by which Maxwell's equations give rise to propagation of electromagnetic fields is shown in the figure below:

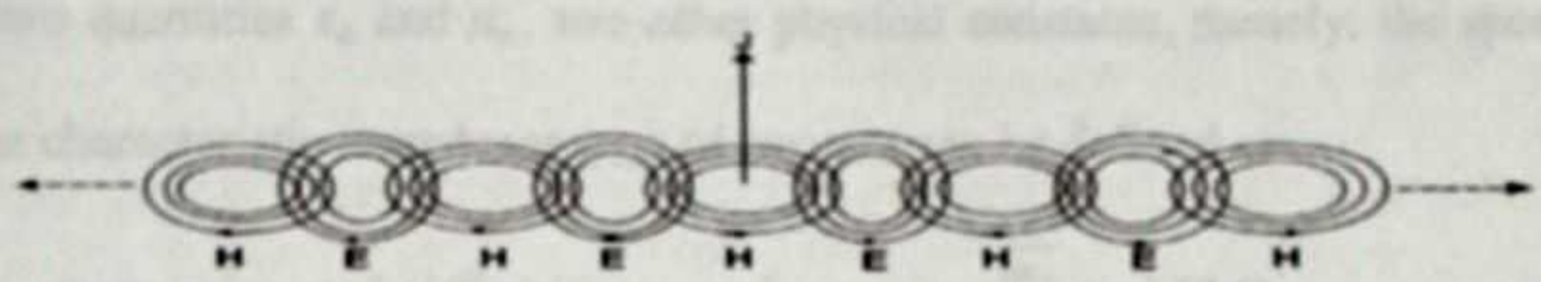

Figure 3.2: Propagation of electromagnetic fields.

For example, a time-varying current J on a linear antenna generates a circulating and time varying magnetic field H, which through Faraday's law generates a circulating electric field E, which through Ampere's law generates a magnetic field, and so on. The cross-linked electric and magnetic fields propagate away from the current source.

3.2.2 Constitutive Equations

The electric and magnetic flux densities D and B are related to the field intensities E and H via the so-called constitutive relations, whose precise form depend on the material in which the fields exist. In vacuum, they take their simplest form:

$$\mathbf{D} = \varepsilon_o \mathbf{E} \quad \text{and} \quad \mathbf{B} = \mu_o \mathbf{H} \tag{3.14}$$

where ε_0 and μ_0 are respectively the permittivity and permeability of free space, with numerical values;

$$\varepsilon_o = 8.854 \times 10^{-12}\,\mathrm{Fm}^{-1} \quad \text{and} \quad \mu_o = 4\pi \times 10^{-7} 10\,\mathrm{Hm}^{-1} \tag{3.15}$$

The units of ε_o and μ_o are the units of the ratios **D/E** and **B/H**, that is,

$$\frac{\text{coulumb/m}^2}{\text{volt/m}} = \frac{\text{coulumb}}{\text{volt . m}} = \frac{\text{farad}}{\text{m}} \tag{3.16}$$

$$\frac{\text{weber/m}^2}{\text{ampere/m}} = \frac{\text{weber}}{\text{ampere . m}} = \frac{\text{henry}}{\text{m}} \tag{3.17}$$

From the two quantities ε_o and μ_o, two other physical constants, namely, the speed of light (c_o) and the characteristic impedance (η_o) of vacuum can be defined as:

$$c_o = \frac{1}{\sqrt{\mu_o\, \varepsilon_o}} = 3\text{x}10^8 \text{ m/s} \quad \text{and} \quad \eta_o = \sqrt{\frac{\mu_o}{\varepsilon_o}} = 377\ \Omega \tag{3.18}$$

The next simplest form of the constitutive equations is for simple homogeneous isotropic dielectric and for magnetic materials:

$$\mathbf{D} = \varepsilon\mathbf{E} \quad \text{and } \mathbf{B} = \mu\mathbf{H} \tag{3.19}$$

These are typically valid at low frequencies. The permittivity ε and the permeability μ are related to the electric and magnetic susceptibilities of the material by:

$$\varepsilon = \varepsilon_o(1 + \chi) \text{ and } \mu = \mu_o(1 + \chi_m) \tag{3.20}$$

The susceptibilities χ and χ_m are measures of the electric and magnetic polarization properties of the material. More generally, constitutive relations may be inhomogeneous, anisotropic, nonlinear, frequency dependent (dispersive), or all of the above.

3.2.3 Signal Propagation

The movement of electromagnetic energy within the subsurface is governed by the propagation constant of the material through which it travels. The basic propagation constant of electromagnetic waves in free space (k_o) is defined as;

$$k_o = (\omega^2 \mu_o \varepsilon_o)^{0.5} \tag{3.21}$$

where ω is the frequency in radians, μ_o is the magnetic permeability of free space and ε_o is the electric permittivity of free space. In the ground, electromagnetic propagation is complicated by the electrical conductivity of the material it travels through. The calculation of the propagation constant becomes;

$$k = (\omega^2 \mu\varepsilon + \mathrm{i}\omega\sigma_{\mathrm{DC}}) \tag{3.22}$$

where μ, ε and σ_{DC} are the magnetic permeability, the electric permittivity and the DC electrical conductivity of the material, respectively, and i is $(-1)^{0.5}$. As the magnetic permeability of most sediments and water is of minor consequence in GPR applications (Telford et al, 1976), the value for free space, $\mu_o = 4\pi \times 10^{-7}\ \mathrm{Hm}^{-1}$ is usually used. The electric permittivity is of great importance in GPR applications and is usually expressed in the form of the relative permittivity or dielectric constant;

$$\varepsilon/\varepsilon_o = k^* = k'\varepsilon_o + \mathrm{i}k''\varepsilon_o \tag{3.23}$$

where k^* is the complex dielectric constant and k' and k'' are the real and imaginary components of k^*. Thus, the electromagnetic propagation factor in the subsurface can be expressed as;

$$k = [\omega\mu_o\varepsilon_o(\omega k' + \mathrm{i}\omega k'' + \mathrm{i}\,\sigma_{\mathrm{DC}})] \tag{3.24}$$

where $\omega k'$ is the dielectric constant factor, $\mathrm{i}\omega k''$ is the dielectric loss factor, and $\mathrm{i}\sigma_{\mathrm{DC}}$ is the DC conductivity loss factor. This equation demonstrates how the conductivity and the complex dielectric constant are both important in determining the amount of energy which will be dispersed in a given material. The rate at which electromagnetic energy is dissipated in the ground is measured by the attenuation coefficient, α which is defined as:

$$\alpha = \omega \mathrm{c}^{-1}\ \{[k'(1 + \tan^2\delta)^{0.5} + 1]\}^{0.5} \tag{3.25}$$

where $\tan^2\delta = \sigma_{DC}(\omega k'\varepsilon_o)^{-1}$ and c is the speed of light in free space, $3.0 \times 10^8\ \mathrm{ms}^{-1}$.

3.2.3.1 Wave Propagation in a conductive Media ($\neq 0$)

Within a conducting medium, the electric current density and the electric field are related by $\mathbf{J} = \sigma\mathbf{E}$, from which it follows that;

$$\nabla \cdot \mathbf{J} = \nabla\mathbf{E} = \frac{\sigma}{\varepsilon}\rho \tag{3.26}$$

Then by the continuity equation,

$$\frac{\partial \rho}{\partial t} + \frac{\sigma}{\varepsilon} = 0 \tag{3.27}$$

Which can be solved to yield

$$\rho_{(\vec{x},t)} = \rho_{(\vec{x},t)} \exp\text{-}(\frac{\sigma}{\varepsilon} t) \tag{3.28}$$

For good conductors, $\sigma/\varepsilon \approx 10^{14}\ s^{-1}$, thus, from eq. (3.25), it can be concluded that charges move almost instantly to the surface of the conductor. The ratio $\tau = \varepsilon/\rho$ is called the relaxation time of the conducting medium. For perfect conductors, $\sigma = \infty$, so that the relaxation time is vanishing. For times much larger than the relaxation time, there are practically no charges inside the conductor. That is, all of them will have moved to the surface of the conductor, where they form a charge density, $\sum$ .Within a conductor, the equation for the electric vector field **E** becomes;

$$[\nabla^2 - \mu\varepsilon \frac{\partial^2}{\partial t^2} - \mu\sigma\varepsilon \frac{\partial}{\partial t}]\mathbf{E} = 0 \tag{3.29}$$

For a monochromatic solution of the form $\mathbf{E} = \mathbf{E}_{(x)} \exp(-i\omega t)$, the above equation takes on the form;

$$[\nabla^2 + k^2]\mathbf{E}_{(x)} = 0 \tag{3.30}$$

where $k^2 = \mu\omega(\omega\varepsilon + i\sigma)$. This equation can be solved to yield for a plane wave solution traveling along an arbitrary direction $\vec{n}$,

$$\vec{\mathbf{E}} = \vec{\mathbf{E}}_0\, e^{i(\alpha\xi - \omega t)} e^{-\beta\xi} \tag{3.31}$$

where $\xi \approx \vec{n} \cdot \vec{x}$. The constants α, β have dimensions of l^{-1}, and are functions of σ.

For an insulator, $\sigma = 0$ and $\alpha = k$, $\beta = 0$. In this case, equation 3.28 reduces to an ordinary plane wave which is propagating with wave vector $\vec{k} = \vec{n}k$. For a very good conductor, the conductivity is large so that the range of frequencies with $\gg \varepsilon\omega$ is quite broad. In this case, the constants α, β are given by $\simeq \beta \simeq \delta^{-1}$, where δ is a constant called the *Skin Depth,* and it is given by the expression;

$$\delta = \sqrt{\frac{2}{\mu\sigma\omega}} \tag{3.32}$$

Accordingly, from equation 3.28, it can be noted that inside a good conductor; the field is attenuated in the direction of the propagation and its magnitude decreases exponentially ($\exp(-\xi/\delta)$) as it penetrates into the conductor. The depth of the penetration is set by δ and is smaller where there is higher conductivity, higher permeability and higher frequency.

3.2.4 Energy Loss and Penetration Depth

The electromagnetic wave travelling through the ground is attenuated by different processes on its way across the layers. Figure 3.3 gives an overview of the various processes that lead to the reduction of the signal strength.

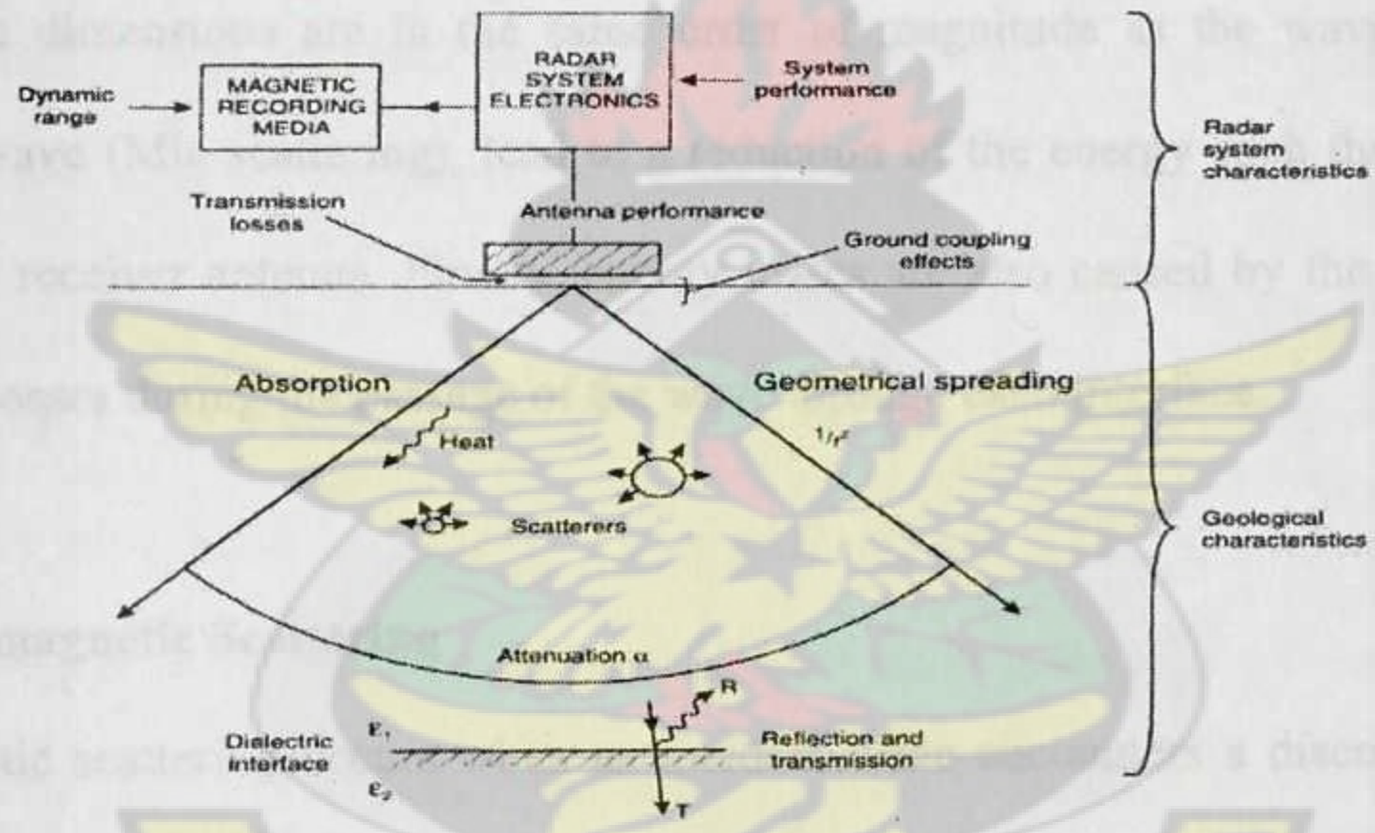

Figure 3.3: Processes that lead to the reduction of GPR signal strength (Reynolds, 1997)

The largest amount of energy loss results from damping of free charge carrier movement. The material dependent attenuation is induced by the direct current electric conductivity (σ_{DC}) of the medium. Depending on the distance (x) traversed, the amplitude, A of the electromagnetic wave decreases exponentially with respect to its starting value, A_0. Thus,

$$A_{(x)} = A_0 e^{\beta x} \tag{3.33}$$

For the loss constant,

$$\beta = \frac{\sigma_{DC}}{2c_0\varepsilon_0\sqrt{\varepsilon}} \tag{3.34}$$

The higher the σ_{DC} of the medium, the higher is the attenuation of the electromagnetic wave. Again in soils, electrical conductivity increases due to an increase in moisture content, clay, or dissolved solutes. The penetration depth of the electromagnetic wave;

$$\delta = \frac{1}{\beta} \tag{3.35}$$

β decreases with increasing electrical conductivity of the medium. Further, spherical losses caused by the field geometry of the measurement also contribute to the signal attenuation, that is, the energy density is reduced due to geometrical spreading with the inverse of the square of the traversed path. Scattering and diffraction of the electromagnetic energy at objects whose dimensions are in the same order of magnitude as the wavelength of the incident em wave (Mie scattering), lead to a reduction of the energy such that it cannot be picked by the receiver antenna. Finally, energy losses are also caused by the reflection and transmission losses during the passage of the wave through each interface.

3.2.5 Electromagnetic Scattering

Electromagnetic scattering occurs when an incident wave encounters a discontinuity in the electromagnetic properties of the traversed medium. Therefore, for road pavement evaluation with the GPR, where such discontinuities are either the interface between the pavement layers or the presence of an irregularly shaped objects embedded in a particular layer. This discontinuity causes the wave to be reflected, refracted, or diffracted depending on the geometry of the discontinuity, electrical properties of the materials, and the wavelength of the incident signal.

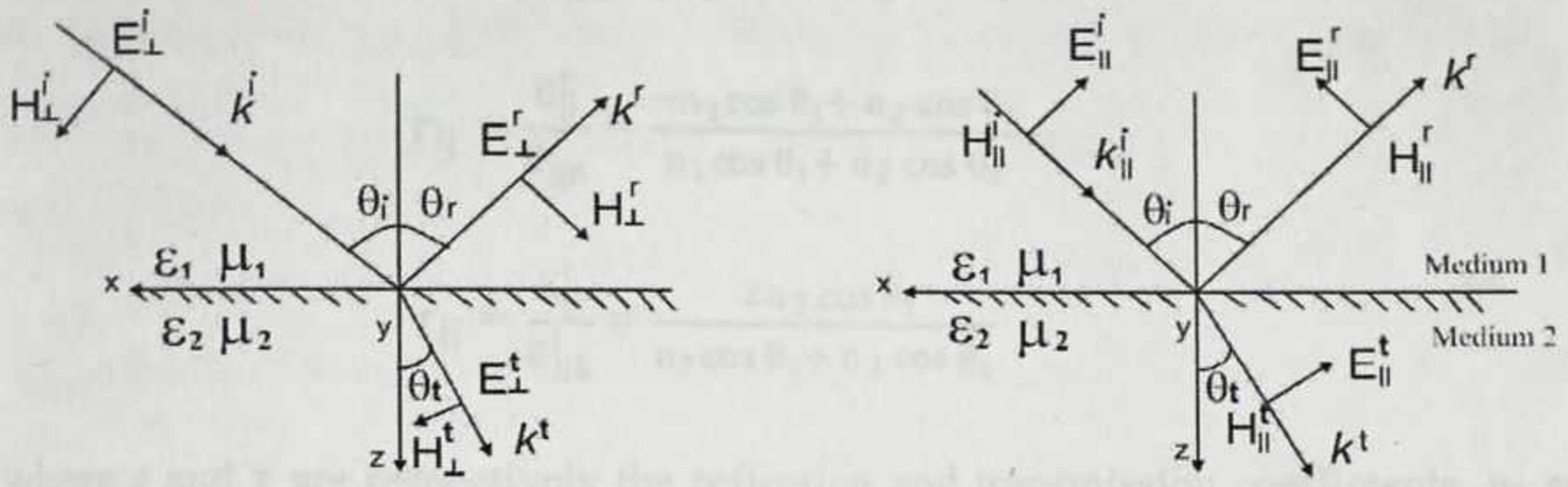

Figure 3.4: Oblique Reflection and Transmission from a flat interface (a) TE and (b) TM

As shown in figure 3.4, a planar interface such as a road pavement yields both reflected and transmitted signals. The reflection and transmission coefficients can be obtained using the boundary conditions at the interface (continuity of the tangential components of the electric and magnetic fields across the interface). For an oblique incident wave, two solutions can be found for the refection and transmission coefficients, depending on the polarization of the incident field. Polarization of the incident field is defined with respect to the plane of incidence, which is the plane formed by the normal to the interface and the direction of propagation of the incident wave. A transverse electric (TE or perpendicular) wave represents a wave with the electric field perpendicular to the plane of incidence. A transverse magnetic (TM or parallel) wave represents a wave with the electric field parallel to the plane of incidence (thus the magnetic field is perpendicular to this plane). By satisfying the boundary conditions at the interface between medium 1 with ε_1 and μ_1; and medium 2 with ε_2 and μ_2 , the reflection and transmission coefficients can be found as follows (Balanis, 1989):

For TE polarization,

$$r_\perp = \frac{E_\perp^r}{E_{\perp 0}^i} = \frac{-n_1 \cos\theta_t + n_2 \cos\theta_i}{n_1 \cos\theta_t + n_2 \cos\theta_i} \tag{3.36}$$

$$\tau_{\perp} = \frac{E_{\perp}^{r}}{E_{\perp 0}^{i}} = \frac{2n_1 \cos\theta_i}{n_1 \cos\theta_t + n_2 \cos\theta_i} \tag{3.37}$$

$$r_{||} = \frac{E_{||}^{r}}{E_{||0}^{i}} = \frac{-n_1 \cos\theta_i + n_2 \cos\theta_t}{n_1 \cos\theta_i + n_2 \cos\theta_t} \tag{3.38}$$

$$\tau_{||} = \frac{E_{||}^{r}}{E_{||0}^{i}} = \frac{2n_2 \cos\theta_i}{n_1 \cos\theta_i + n_2 \cos\theta_t} \tag{3.39}$$

where r and τ are respectively the reflection and transmission coefficients, n_1 and n_2 are the refractive indices of media 1 and 2 given by; $n_1 = \sqrt{\mu_1 \varepsilon_1}$, $n_2 = \sqrt{\mu_2 \varepsilon_2}$ or

$$n_{1,2} = \sqrt{\frac{\mu_{1,2}}{\varepsilon_{1,2}}} \tag{3.40}$$

and θ_i and θ_t are angles of incidence and transmission respectively and they are related by Snell's law of refraction via;

$$\frac{\sin\theta_t}{\sin\theta_i} = \frac{n_1}{n_2} \tag{3.41}$$

After the transmitter has emitted a signal, the first energy to arrive at the receiver is the direct air wave. This is the first because it travels directly from the transmitter to the receiver, through the air (at near the speed of light). As the travel time of the direct air wave is easily calculated and stays relatively constant, its arrival time is often used as a marker for static correction. The next to arrive is the direct ground wave. It travels directly into the subsurface only reflects when it encounters a media of different dielectric constant such as geological boundaries, buried objects or groundwater. When the electromagnetic wave velocity v is known, by measuring the travel time t of the wave, the depth of the reflecting object d can be found by:

$$d = \frac{v\Delta t}{2} \tag{3.42}$$

3.2.6 Signal Velocity and Depth Determination

The velocity at which the electromagnetic energy travels in the ground is important in determining the depth of reflectors. In free space electromagnetic energy travels at the speed

of light, 3.0×10^8 m/s . In the subsurface it travels at a fraction of the speed of light, usually in the range (0.01 – 0.16) m/ns . Both the dielectric constant and the DC conductivity strongly influence the propagation velocity v of a medium:

$$V = c\{(k'(1 + \tan^2\delta)^{0.5} + 1)/2\}^{-1} \quad (3.43)$$

An estimate of the propagation velocity [m/ns] was also determined by A-CUBED (1983) as follows

$$V = 0.3(k')^{0.5} \quad (3.44)$$

A more detailed analysis of the specific effects that the dielectric constant and the electrical conductivity have on the attenuation and velocity of electromagnetic energy at a given frequency is given by Olhoeft (1978). The depth to which GPR can image below the surface is dependent on three main factors:

- the number of interfaces that generate reflections and the dielectric contrast at each interface.
- the rate at which the signal is attenuated as it travels through the subsurface, and
- the centre frequency of the antennas. As the GPR pulse arrives at each interface, a portion of it is returned to the surface and the rest continues into the next layer.

As the number of interfaces increases, the proportion of energy that propagates to depth is reduced. In addition, the greater proportion of energy that is reflected back to the surface at each interface, the less energy that is available to propagate deeper into the ground. The conductivity of the material that a GPR signal is travelling through has a major influence on the depth to which the signal will penetrate. The conductive currents in a material are an energy dissipating mechanism for an EM field. In this case, energy is irreversibly extracted from the EM field and transferred to the medium it is in.

The frequency used is also of importance since the resolution of the system and the rate of signal attenuation is proportional to the frequency of the GPR system. At lower frequencies, the wavelength is longer and as a result there is less attenuation due to conductive losses and less scattering from the chaotic reflections from small clutter.

Table 3.1: Approximate depth ranges for different antenna frequencies.

Antenna Frequency [MHz]	**Approximate Radial Resolution [m]**	**Approximate Penetration Depth [m]**
25	100	50
50	50	40
100	25	25
250	10	8
500	5	6
800	3	2.5
1200	2.1	1
1600	1.6	0.5
2300	1.3	0.4

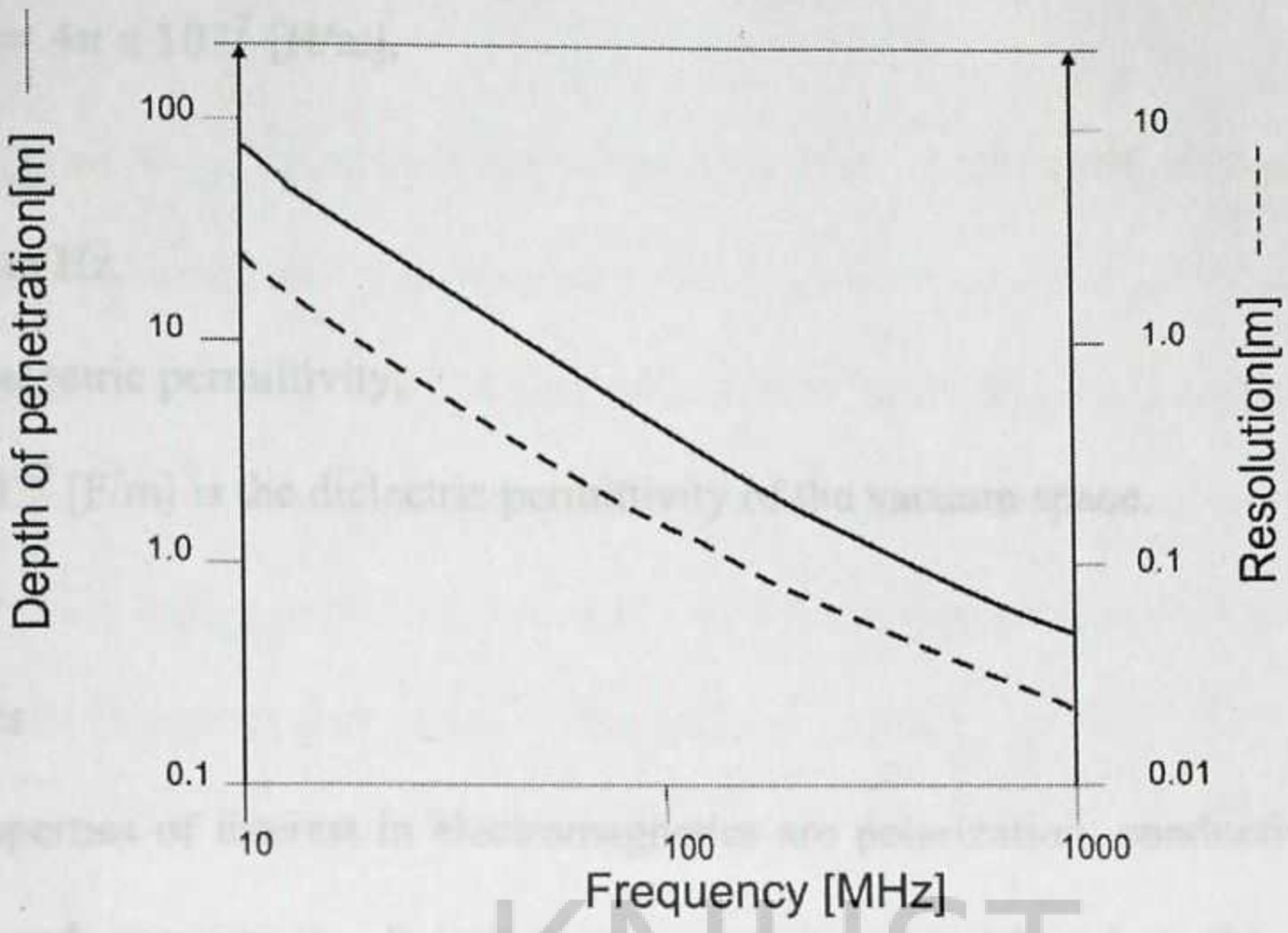

Figure 3.5: Antenna resolution and penetration depth as a function of frequency.

The main disadvantage of using very low frequencies is that the resolution decreases, such that the thickness of small layers can no longer be measured and small objects are not detected. A practical consideration is that, as the frequency decreases, the antennas increases in size and becomes more difficult to work with (Sellman et al. (1992); Moreman and Michel (1997)). EM wave propagation is governed by the Maxwell's equation, and most geological media are mainly influenced by the relative dielectric permittivity (ε) and electrical conductivity (σ), whereas the influence of the relative magnetic permeability is generally negligible. These parameters affect both wave propagation velocity (v) and radar energy attenuation (α). The parameters (v) and (α) are calculated from the theoretical formula (Franceschetti, 1983);

$$v = \frac{1}{\sqrt{(\mu \,.\, \varepsilon)}/2\left(\sqrt{\frac{1+\sigma^2}{(\omega^2 .\, \varepsilon^2)}}+1\right)} \tag{3.45}$$

$$\alpha = \omega\sqrt{\varepsilon\pi}\,\frac{1}{2}\left[\sqrt{1+\left(\frac{\sigma}{\omega\varepsilon}\right)^2}-\,1\right]^{1/2} \tag{3.46}$$

with $\mu = \mu_0 = 4\pi \times 10^{-7}$ [H/m],

$\omega = 2\pi f$,

f = frequency in Hz,

ε = relative dielectric permittivity,

$\varepsilon_0 = 8.85 \times 10^{-12}$ [F/m] is the dielectric permittivity of the vacuum space.

3.3 Dielectrics

The main properties of interest in electromagnetics are polarization, conductivity, magnetic permeability and permittivity. Polarization occurs in materials when the center of the negative charges in an atom or molecule does not coincide with that of the positive charges when an external electric field is applied. Conductivity is the inverse of the resistivity. It is denoted by the letter σ and has units of S/m. This means that conductivity is a measure of a material's ability to conduct electric current. Magnetic permeability is a measure of the susceptibility of materials to become magnetized. For free space, the magnetic permeability is denoted by μ_0 and is equal to $4\pi \times 10^{-7}$ [H/m]. The relative permeability of any material is the ratio of the permeability of the material to that of free space. It is, therefore, a dimensionless quantity and is denoted by μ_r.

Permittivity, on the other hand, is a property that shows a material's ability to be polarized and therefore its capability of storing a charge when an electric field is applied. The permittivity of free space, which is considered as a reference material, is equal to $\varepsilon_0 = 8{:}854 \times 10^{-9}$ [F/m]. Permittivity of different materials is expressed as a ratio to ε_0, called relative permittivity or *dielectric constant*. It is, therefore, a dimensionless quantity and is given by;

$$\varepsilon_r^* = \frac{\varepsilon^*}{\varepsilon_0^*} = \varepsilon_r' - i\varepsilon_r'' \qquad (3.47)$$

where $i = \sqrt{-1}$.

The dielectric constant is usually expressed as a complex number where the real part (ε_r') defines the property itself, and the imaginary part (ε_r'') represents the loss due to molecular friction (dielectric loss) and conduction (σ/ω, where ω is the angular frequency). The dissipation factor or loss tangent is a measure of the amount of power transformed into heat. Materials with very high loss factors are heated easily and rapidly. The loss factor is defined as the ratio of the imaginary part to that of the real part as shown in eq. (3.48) below;

$$\tan\delta = \frac{\varepsilon''}{\varepsilon'} \tag{3.48}$$

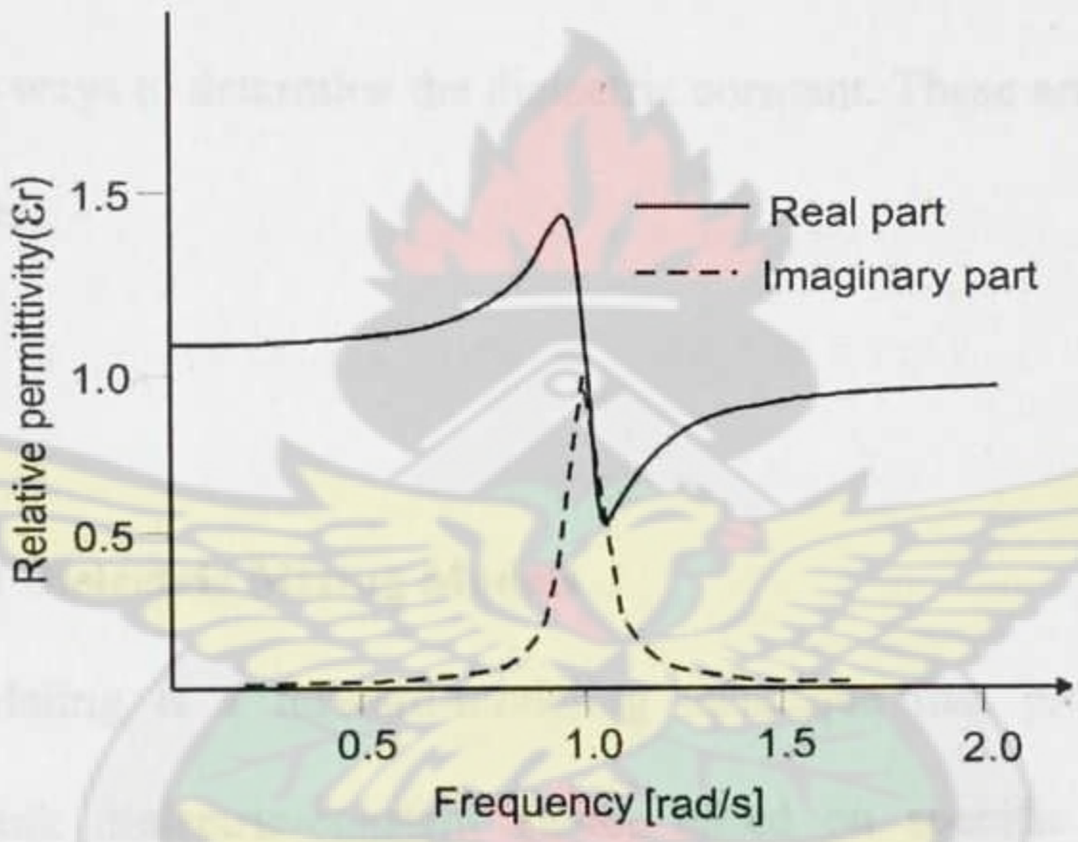

Figure 3.6: Real and imaginary parts of the effective dielectric.

3.3.1 Correlation of GPR with Dielectric Constant

Dielectric constant is a critical GPR parameter because it controls the propagation velocity of electromagnetic waves through a material and the reflection coefficients at interfaces, as well as affecting the vertical and horizontal imaging resolution. Therefore, knowing dielectric constant values of materials helps in planning GPR surveys and in better understanding and

interpreting GPR images. Measured dielectric-constant values for various rocks and minerals may be found in several publications (Davis and Annan (1989); Daniels (1996)).

The results of dielectric-constant modeling can be used in planning GPR data acquisition and in interpreting GPR data. For data acquisition, modeling results can be used to determine whether a feature or interface will result in measurable reflections, and if so, the expected two-way reflection travel-times (TWT) and antenna frequencies needed for imaging. For interpretation, dielectric modeling results can be used to better understand recorded travel-times and amplitude variations, the controlling factors on measured dielectric property values. A review of the equations governing GPR response illustrates the role of dielectric constant. There are two ways to determine the dielectric constant. These are the use of:

- measured values
- mixing models

3.3.2 Fundamentals of Dielectric Mixing Models

Dielectric mixing modeling is a forward-modeling technique that provides a basis for predicting expected bulk dielectric-constant values based on specific input parameters. Numerous dielectric-constant mixing models have been proposed, and all fall within four broad categories: effective medium, empirical and semi-empirical, phenomenological, and volumetric (Knoll, 1996). Mixing models can provide an estimate of the dielectric constant for a bulk material based

on specific parameters using;

- an empirical expression fulfilling the experimental data (Topp et al, 1980) or
- a semi-theoretical expression including volume fractions and dielectric constant of each constituent (Roth et al., 1990).

Topp et al. (1980) used a third order polynomial to describe the relation between effective dielectric constant and volumetric water content (VWC):

$$\varepsilon_{eff} = 3.03 + 9.3VWC + 146.0(VWC)^2 - 76.7(VWC)^3 \quad (3.49)$$

Conversely, the measurement of ε_{eff} can be used to determine VWC by a third order polynomial equation;

$$VWC = 5.3^{-2} + 2.29 \times 10^{-2}\varepsilon_{eff} - 5.5 \times 10^{-4}\varepsilon_{eff}^2 + 4.3 \times 10^{-6}\varepsilon_{eff}^3 \quad (3.50)$$

More generally, the polynomial model is written as;

$$VWC = A + B\varepsilon_{eff} + C\varepsilon_{eff}^2 + D\varepsilon_{eff}^3 \quad (3.51)$$

Another model suggested by Roth et al., (1990) uses the following equation;

$$\varepsilon_{eff} = [(1 - \eta)\varepsilon_s^n + (\eta - VWC)\varepsilon_a^n + VWC\varepsilon_w^n]^{1/n} \quad (3.52)$$

where η is the soil porosity, and the subscripts; *a, s, w* represent air, soil and water respectively, and n is a factor that accounts for the orientation of the electric field with respect to the geometry of the medium. Usually, the value of n used for isotropic medium is 0.5 (Birchak et al.,1974), hence simple physical interpretation of water content and ε was suggested by Herkelrath et al. (1991) as;

$$VWC = a\sqrt{\varepsilon_{eff}} + b \quad (3.53)$$

Similarly, Al-Qadi and Lahouar (2004) provided an expression to calculate the voids content in an asphalt sample by knowing parameters of dielectric constant and fractional volume of the aggregate and the binder;

$$\sqrt{\varepsilon_{HMA}} = V_{air}\sqrt{\varepsilon_{air}} + V_{agg}\sqrt{\varepsilon_{agg}} + V_b\sqrt{\varepsilon_b} + V_w\sqrt{\varepsilon_w} \quad (3.54)$$

where;

ε_{HMA} = dielectric constant of the hot mix asphalt layer

V_{air} = fractional volume of air

ε_{air} = dielectric constant of air, which is equal to 1

V_{agg} = fractional volume of the aggregates

ε_{agg} = dielectric constant of the aggrgates

V_b = fractional volume of the asphalt binder

ε_b= dielectric constant of the asphalt binder

V_w = fractional volume of water

ε_w = dielectric constant of water, which is equal to 81.

3.3.3 Dielectric Properties of Pavement Materials

Bitumen bound layers like asphalt are composed of aggregate, bitumen binders, air and in special structures, emulsion, water. Asphalt used in pavement structures can be divided into three groups;

1. asphalt cements
2. emulsified asphalts
3. cutback asphalts

Asphalt cement is obtained by distilling crude petroleum through different refining techniques. Emulsified asphalt, or emulsion, is a mixture of asphalt cement, water and an emulsifying agent. Cutback asphalts are like liquid asphalts in that they are manufactured by adding petroleum solvent to asphalt cements. Since the 1990's, mainly due to environmental reasons, emulsified asphalts have increasingly been substituted for cutback asphalts. Based on its composition, asphalt cement can be divided into asphaltens and maltens, which can be further divided into resins and oils (Roberts et al., 1991).

The most polar components in bitumen are asphaltens, ketons and karboxyl acids. Karboxyl acids have a greater ability to bond with a mineral surface, but they are easily replaced by water. The greatest resistance against water impact had ketons and fenols (Petersen et al.,1982). The components of hot mix asphalt were examined at the Texas Transportation

Institute (TTI) in 1994-1995 (Saarenketo, 1997) and the results indicated the absolute dielectric values of dry aggregates varying between 4.5 and 6.5, with higher values recorded for carbonate-rich rock types, such as limestone. These materials were found to be dielectrically frequency independent, that is, they are dispersive when absolutely dry. The tests also showed that ageing of the bitumen samples in the sun for 6 months had no appreciable effect on the dielectric values. The basic assumption was that the dielectric value of a dry asphalt core is a function of the volumetric ratios of asphalt, air and rock and their respective dielectric values.

3.3.4 Dielectric Properties of Older Pavements

Studies on old asphalt road pavements have shown that after the paving year, their dielectric values rise up one unit, but the value of the asphalt remains constant until after 5 - 10 years, when it begins to rise slowly. The rapidity of the rise depends on the traffic volume and the use of chlorides. A few years before the pavement starts to crack, water molecules start to penetrate between bitumen and aggregates, thus breaking the bonds, and this is often seen as rapidly increasing dielectric values. Dielectric values start to decrease rapidly when the pavement starts to crack. This is due to the fact that cracks increase the volumetric proportion of air voids in the pavement.

3.3.5 Dielectric Properties of Hot-Mix Asphalt

Al-Qadi (1992) studied the dielectric properties of HMA in the frequency range of 12.4 to 18.0 GHz. His experimental set-up consisted of a focused conical horn antenna and an HP 8510B network analyzer. It was found that for dry HMA specimens, the real part of the dielectric constant ranged from 3.7 to 5.2, while the imaginary part ranged from 0.05 to 0.16. For the wet HMA specimens (volumetric water content ranging from 1.2% to 8.2%), the real

part of the complex dielectric constant varied from 4.1 to 5.3, and the imaginary part varied from 0.10 to 0.30. A correlation was established between the calculated dielectric constant and the HMA moisture content. Shang et al. (1999) developed an apparatus to measure the dielectric properties of HMA over the frequency range of 0.1 MHz to 1.5 GHz. Results indicated that asphalt content and mix type did not significantly affect the measured complex dielectric constant. However, moisture content was found to be a predominant factor on the measured complex dielectric constant. It was found that the average real part of the complex dielectric constant was 6.0 ± 0.15 for the dry specimens, and 6.52 ± 0.99 for the soaked specimens over the frequency

range of 8 to 900 MHz.

Table 3.2: Dielectric values of typical road pavement materials: Saarenketo, (2006).

Material	**Dielectric Constant (ε_r)**
Air	1
Freshwater	81
Ice	4
Sand	4 - 6
Silts	16 - 30
Silty sand	7 - 10
Bedrock (granite)	5 - 7
Peat (natural)	60
Peat (under road)	40
Clay	25 - 40
Glacial till (Moraine)	8 - 18

Gravel	4 - 7
Asphalt/other bituminous pavements	4 - 6
Concrete	8 - 10
Gravel road wearing course	12 - 14
Crushed base	6 - 8
Bitumen bound base	6 - 7
Cement bound base	8 - 10
Insulation boards	2 – 2.5
Road structures in average (new/dry)	5
Road structures in average (normal)	6
Road structures in average (wet/old)	7 - 8
Gravel road structures in average	7 - 9
Frozen road structures (normal)	5
Frozen road structures (wet/old)	6

3.3.6 GPR Systems

The Ground Penetrating Radar technology (commonly called GPR) was developed from the radar (Radio Detection and Ranging) technique of using radio waves to detect the presence of objects in the atmosphere. Radar was designed shortly before World War II with the primary aim of detecting the presence of aircrafts within some ranges. This geophysical method offers a high resolution electromagnetic technique designed primarily to investigate the shallow subsurface of the earth, building materials, roads and bridges. It is a time-dependent geophysical technique developed for the past 30 years and can provide both 2-D and 3-D pseudo image of the subsurface, including the fourth dimension of color. The GPR method

can also provide accurate depth estimates for many common subsurface objects. Under favorable conditions, GPR can provide precise information concerning the nature of buried objects. It has also proven to be a tool that can be operated in boreholes to extend the range of investigations away from the boundary of the hole. The application of GPR covers wide spectrum that includes utility mapping, site investigation studies, engineering evaluation studies for construction industries, shallow geological mapping, groundwater table studies etc. A GPR system typically comprises the following;

1. GPR control unit.
2. a pulse generator which generates a single pulse at a given frequency and power.
3. an antenna which transmits the pulse into the medium to be surveyed.
4. display unit or the monitor and the connecting cables.

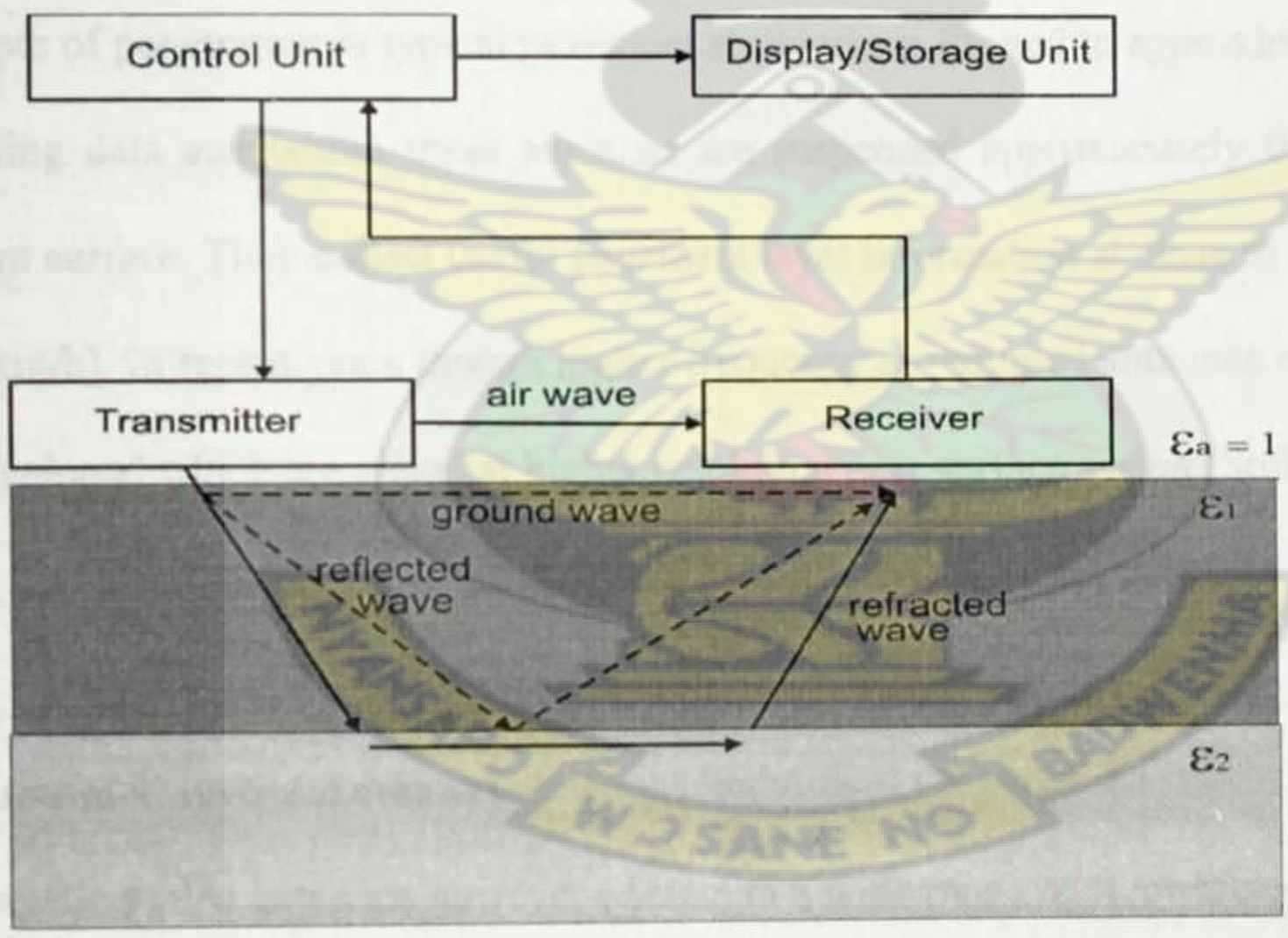

Figure 3.7: EM wave transmission and reflection in a GPR system.

Traffic infrastructure surveys with the GPR system also involve the use of a Global Positioning System (GPS) and a digital video. The GPS is meant for projecting the survey results onto a survey line whereas the video aids the GPR data interpretation as it provides a picture of the profiles or surroundings of the antenna as the data is picked. Other pavement studies have utilized infrared thermography cameras with the GPR data collection especially on bridge decks and concrete runways (Manning and Holt, 1986) Recently, infrared thermal cameras and temperature sensors have been used together with GPR in asphalt quality control (Sebesta and Scullion, 2002) and on railways (Clark et al., 2004).

3.3.7 Air-Coupled Antennas

The radar antennas in common use have two broad categories; the air-coupled horn antennae and the ground-coupled dipole antennas. The air coupled systems operate around 1 GHz, and their depth of penetration in typical pavement structures is limited to approximately 0.5 m (20 in). During data acquisition these antennas are suspended approximately 0.3 m above the pavement surface. They collect useful pavement layer information at close to highway speeds (40-60 km/h). In recent years though higher frequency air-coupled antennae of 2.5 GHz have been developed which are aimed at higher resolution near surface vision (Smith and Scullion, 1993).

3.3.8 Ground-Coupled Antennas

The ground-coupled antennas however operate in a wide range of frequencies, typically from 80 MHz to 1.5 GHz and signal propagation in traffic infrastructure surveys can be up to 20-30 m. During data acquisition these antenna maintain contact with the pavement or they are suspended just above it. The distance to the structure must be kept constant because the coupling changes as a function of distance. Normally, the lower the frequency, the larger the

antenna and the greater the depth of penetration. The clear advantage of the ground-coupled antennas is their depth of penetration and better vertical resolution. One disadvantage though is since they must remain in close proximity to the surface, survey of road pavements cannot be carried out at higher speeds possible with the air-coupled ones. Data collection speed with ground-coupled systems is usually 5- 30 km/h.

3.3.9 Antenna Arrangements in GPR Surveys

There are two antenna arrangements in GPR survey: profile-measurement (Common Offset) and wide-angle-measurement (CMP: Common Mid-Point). In the profile-measurement (figure 3.8), the separation of the transmitting antenna and receiving antenna is fixed, and both antennas are moved together. In the CMP measurement however, the separation of the transmitting antenna and the receiving antenna is changed in each data acquisition. In most GPR, the common-offset measurement is used, because of ease of use and the speed. However, the wide-angle measurement offers deeper surveys. In the profile-measurement, reflections from objects located just below the antennas are continuously measured and provides information on the lateral location of the objects and rough estimate of its depth. The wide-angle measurement determines the precise depth to the object. In this measurement, the position of the Common Midpoint (CMP) is fixed at one location, whilst the transmitting antenna and the receiving antenna are moved along opposite directions, at constant separations from the CMP. In this antenna arrangement, reflected wave from the same reflecting objects are measured many times. The reflected wave, which is located below the CMP, forms a hyperbolic curve, and from this, the depth of the object and the velocity can be simultaneously estimated. This technique is called NMO correction, which has been widely accepted in seismic signal processing (Sato, 2001).

3.3.10 Penetration Depth of GPR Antenna

The penetration depth of GPR is determined by antenna frequency and the electrical conductivity of the earthen materials being profiled (Daniels, 1996). Soils having high electrical conductivity rapidly attenuate radar energy, restrict penetration depths, and severely limit the effectiveness of GPR. The electrical conductivity of soils increases with increasing water, clay and soluble salt contents. The maximum penetration depth of GPR in the ground is commonly unknown among GPR users because the propagation of the electromagnetic signal depends on the electrical properties of the particular soil at hand. The electrical conductivity of the materials crossed by the EM waves introduces significant absorptive losses, which limits the penetration depth into earth formations and is primarily dependent on the water content and mineralization present.

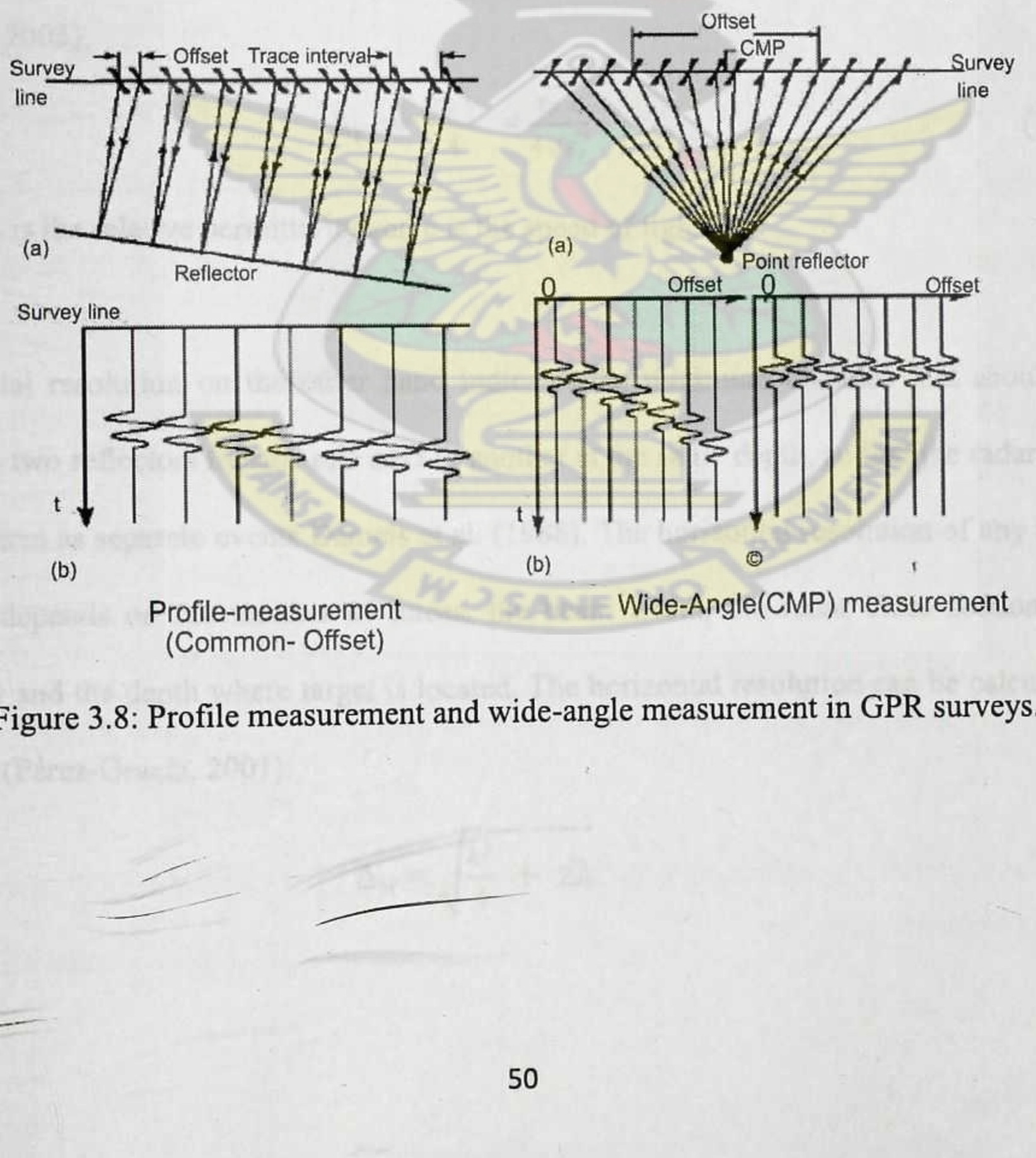

Figure 3.8: Profile measurement and wide-angle measurement in GPR surveys.

3.3.11 Resolution of GPR Antenna

In general, as the frequency of the antenna increases the resolution gets better but it diminishes the capacity of the penetration of the signal (Daniels, 2004). Resolution is an important aspect of GPR surveys and its of particular interest in civil engineering (Millard et al. (2002); Al-Qadi and Lahouar (2004); Yelf (2004)), where millimetre resolution in both, vertical and horizontal planes, is sometimes required for conducting GPR surveys. The resolution concept is essentially divided into two parts: vertical (depth) resolution (Δ_V) and horizontal (lateral) resolution (Δ_H) (Daniels, 2004). Thus the resolution can be defined as the radar capacity to discriminate individual elements in the subsurface, either in thickness or in size. Vertical resolution allows the equipment to differentiate in time two adjacent signals as different events. Expected vertical resolution can be calculated from the effective duration (τ_P) of the radar pulse and the wave propagation velocity (v) in the medium as follows (Annan, 2003);

$$\Delta_V \approx \frac{\tau_P \, v}{4} = \frac{\tau_P \, c}{4\sqrt{\varepsilon_r}} \tag{3.55}$$

where ε_r is the relative permittivity and c is the speed of light.

Horizontal resolution on the other hand indicates the minimum distance that should exist between two reflectors located one next to another at the same depth, so that the radar signals detect them as separate events Daniels et al. (1988). The horizontal resolution of any antenna mainly depends on the number of traces, the beam width, the radar cross section of the reflector and the depth where target is located. The horizontal resolution can be calculated as follows (Pérez-Gracia, 2001):

$$\Delta_H = \sqrt{\frac{\lambda^2}{4} + z\lambda} \tag{3.56}$$

where λ is the wavelength, z is the vertical distance between the antenna and reflector surface and ε_r is the relative permittivity of the medium.

3.4 Main Application Areas

GPR is an effective tool for subsurface inspection and quality control on engineering construction projects (Yelf, 2007). The numerous applications of GPR include the following:

1. Mapping pipes (including PVC pipes), cables and other buried objects.
2. Continuous inspection of layers in road pavements and airport runways. Due to the rapid data acquisition rates, it can be used at highway speeds to monitor changes in subgrade and asphalt pavement layers.
3. Mapping cavities or voids beneath road pavements, runways or behind tunnel linings.
4. To monitor the condition of railway ballast, and detect zones of clay fouling leading to track instability.
5. Detailed inspection of concrete structures, location of steel reinforcing bars and pre-and post-tensioned stressing ducts. GPR can be used in 3-D mode to map multiple layers of steel in buildings, in order to avoid damage when drilling through such structures.
6. Inspection and quality control of pre-cast concrete structures, such as bridge deck beams.
7. Detection of zones of honeycombing, voiding and chloride attack in concrete.
8. Mapping zones of deterioration and delamination on bridge decks.
9. Mapping zones of termite attack or fungal decay in trees or timber structures, such as wooden bridge beams.
10. Mapping soil, rock or fill layers in geological and geotechnical investigations, or for foundation design.

11. BH-GPR is used to detect faults and for determining the degree of fracturing of the rock mass (e.g. for investigating the structural integrity of pillars, or nuclear waste repository zones).
12. Mapping bedrock and excavation conditions along proposed cable or pipeline excavations.
13. Mapping detailed sedimentary stratigraphy, both on land and beneath rivers and lakes, particularly for pipeline crossings. (GPR will penetrate through fresh water, but is rapidly attenuated by salt water).
14. Mapping snow and ice thickness on glaciers, location of ice-core holes for climate change measurements.

3.5 Applications of the GPR in Road Pavement Surveys

Through the different phases in the lifetime of a road pavement, GPR technology can assure fundamental information with the aim of quality control or quality assurance of new pavements; as well as monitoring the structure service time; or as an inspection method to define rehabilitation strategies, forensic disputes or monitoring of structures. (Nazarian et al., 1993). The GPR in recent years has proven to be a successful and reliable tool for various road applications. These include:

- measurement of asphalt layer thickness.
- void ratio determination
- density estimation
- vertical cracks
- moisture content of base materials
- rutting
- stripping

3.5.1 Pavement Layer Thickness

Coring, Falling weight Deflectometer, and the Seismic Pavement Analyzer have until recent years been the conventional methods used to assess the conditions of asphalt road pavements, most importantly, the layer thickness. Nearly all these methods are carried out to assess the stiffness of the layered road structure. Not only are they time consuming and expensive , they only provide information at certain discrete points along the road. Therefore, the fast and continuous surveys possible with the GPR makes the asphalt layer thickness measurement the most successful application of the GPR in road related studies (ASTM, 1987). Since a pavement is made of different layers, reflections of the electromagnetic energy are expected at all interfaces. The measured time of reflection from a particular interface will allow the determination of the thickness of the layer above it. In determining the asphalt layer thickness, either air-coupled or ground coupled antennas are attached to a vehicle or dragged on the road surface (the ground-coupled antennas). The air coupled method allows for data collection at speeds up to normal highway speeds, enabling several kilometers of the road to be surveyed within a short time. The reflections from the interfaces must be strong enough to be interpreted and tracked for reasonably consistent results. Experience has shown that GPR works well on flexible pavements (asphalt) where there is a strong dielectric contrast between layers, but may be less effective on rigid pavements (concrete) where the presence of moisture in the concrete tends to attenuate the radar signal, or where the contrast between layers is minimal such as between concrete and granular base materials (Mark, 2007). Despite limitations associated with weak signals and material dielectric uncertainties, the advantages of determining thickness with GPR are considerable, since it is a nondestructive, continuous, and high-speed field test. Using GPR, layer thicknesses can be estimated in one of two ways, (1) using blind estimates and (2) using ground truth measurements. Blind estimates involve using equations 3.1 and 3.3 alone to estimate the asphalt dielectric and

thickness. Ground truth measurements involve adjusting the dielectric constant to match the predicted thickness at locations where core are taken. The thickness is determined from the dielectric constant ε and the travel time t in nanoseconds of the first peak of the electromagnetic wave.

$$h = 11.8\ t/2\ \sqrt{\varepsilon} \tag{3.57}$$

The in-situ measurement of the dielectric constant (in air-coupled antenna mode) is done from the amplitude of the reflected pulses. That is, given that the dielectric constant in air is 1, the subsurface layer dielectric constant can be calculated from;

$$\sqrt{\varepsilon} = \frac{A_m + A_0}{A_m - A_0} \tag{3.58}$$

where A_0 and A_m are respectively the reflected amplitude from the top of the surface layer and the metal plate (Loken, 2007).

3.5.2 Mapping Air Void in Asphalt Pavements

Voids in road pavement develop because of consolidation, subsidence, and erosion of the base material. Generally, voids occur beneath joints where water enters the layer and carries away the fine materials. In theory air voids and water filled voids are both detectable using GPR because the dielectric constants of both air (1.0) and water (81) are substantially different than most pavement materials (3-10). If the void is air-filled, a large negative peak will appear in the waveform, since the dielectric constant of air is much less than pavement material. Conversely, a large positive peak in the waveform will appear at the surface of a water-filled void, because the dielectric increases substantially at the interface. On the GPR record, air voids in pavement can be identified from hyperbolae with lower velocities than the average propagation velocity of the aggregate materials.

According to ASTM D 2041 or AASHTO T 209, the percent air voids in a pavement sample can be calculated using;

$$V_a = 100 \times \frac{G_{mm} - G_{mb}}{G_{mm}} \% \quad (3.59)$$

where; V_a = air voids in the compacted mixture, percent of the total volume.

G_{mm} = maximum specific gravity of paving mixture.

G_{mb} = bulk gravity of compacted mixture.

Since G_{mb} represents dry specific gravity, the calculated percent air voids is the total voids in the compacted mixture.

3.5.3 Asphalt Density Estimation

Asphalt density or equivalently, void ratio could also be estimated successfully with the GPR. The fundamental principle being that the compaction of the pavement materials would reduce the volume of air and increase the proportion of components such as bitumen or aggregate. The dielectric value of air (1.0) is less than that of bitumen (2.6) or the aggregate (6.0), thus, the compaction of the asphalt results in an increase in the value of the resultant dielectric constant of the road pavement (Saarenketo and Scullion, 1996). The asphalt road void ratio can be calculated using the following equation;

$$\emptyset = 1 - \rho_f = Ae^{B\varepsilon_a} \quad (3.60)$$

where;

$\emptyset$= void content or fractional volume of air to the total volume of the asphalt components.

ρ_f = fractional density of the asphalt.

$\rho_f = \frac{\rho_{emp}}{\rho_{max}}$, where ρ_{emp} is the emplaced asphalt density and ρ_{max} is the maximum asphalt density (at $\emptyset = 0$).

A and B are constants whose values are respectively equal to 272.93 and -1.30, determined through non-linear regression by fitting equation (3.60) to measured data in the laboratory (Loken, 2007).

3.5.4 Vertical Cracks

A number of studies have been done to determine the possibility of GPR technology in locating cracks in concrete bridge decks (Maser and Scullion (1991); Momayez et al. (2004)). Some surveys are also reported to have been carried out by Maser and Scullion et al. (1992) to locate subsurface cracks in asphalt road pavements, though most of these results have not been very encouraging, since they were done at highway speeds with only a few traces per meter. This is because such studies carried out at highway speeds offer inadequate resolution to identify vertical cracks, except where these cracks are large enough or just near the pavement surface. Nontheless, Saarenketo and Scullion (1996) were able to identify vertical cracks in an asphalt road using high frequency antenna (1.0 GHz) with a sampling density (10 - 20 scans/m). These vertical cracks appear as sharp hyperbolas on the GPR scans and are detectable at depths to 3 m.

3.5.5 Moisture Content Estimation

Moisture content, the major soil component that influences the measured base dielectric constant of water is much higher (ε_w= 81), the values for the other components of the aggregate such air is 1 whereas the dry aggregate has a value between 4 and 8 (Loken, 2007). Also, the dielectric constant of the granular base (ε_b) is assumed to be a function of the volumetric proportions of the components, thus using the complex reflective index model (Halabe et al, 1989);

$$\sqrt{\varepsilon_b} = \sum v_i \sqrt{\varepsilon_i} = n(1 - S)\sqrt{\varepsilon_w} + nS\sqrt{\varepsilon_w} + (1\text{-}n)\sqrt{\varepsilon_s} \qquad (3.61)$$

Where;

v_i= fractional volume of the i^{th} component to the total volume of the aggregate.

ε_i= dielectric constant of the i^{th} component.

n = porosity = the fractional volume of voids (air + water) to the total volume.

S = degree of saturation = fractional volume of water to the total voids.

Assuming an average specific gravity of the base solids as 2.65, equation (3.61) above can be rearranged and the moisture content (M) expressed as;

$$M = \frac{\sqrt{\varepsilon_b} - 1 - (1-n)\left(\sqrt{\varepsilon_s} - 1\right)}{\sqrt{\varepsilon_b} - 1 - (1-n)\left(\sqrt{\varepsilon_s} - 22.2\right)} \qquad (3.37)$$

where M = moisture content = the fractional weight of the water to the total weight of the aggregate.

3.5.6 Rutting Mechanism in Asphalt Road Pavements

Rutting is a longitudinal surface depression in the wheel path. In some cases, pavement uplift (shoving) may occur along the sides of the rut. Low-severity rutting may only be noticeable after a rainfall, when the wheel paths are filled with water. There are two possible mechanisms for rutting:

1. compaction of the asphalt pavement layer.
2. compaction of the base layer.

GPR can be used to identify the mechanisms of rutting, and more importantly, identify possible corrective actions. By comparing the layer thicknesses of two GPR surveys (in the wheel path and in the lane center), one can identify the layer in which the rutting (compaction) has actually occurred (Roddis et al., 1992).

3.5.7 Stripping of Asphalt Road Layers

Stripping in asphalt road pavements is a moisture-related defect in the asphalt which occurs as a result of discontinuity of the bond between the bitumen and the aggregate, thereby leaving an unstable lower-density layer within the asphalt. Stripping may not be visibly apparent since the pathway for moisture is through subsurface cracks that propagate upward

from the asphalt-base interface. This defect is the most common asphalt pavement damage inside the pavement. Stripped layers should always be detected and removed before placing a new overlay. This mechanism is accelerated by repeated wet and dry cycles, and the final result is total failure of the bond, leaving a weak unstable layer. GPR may be used to detect stripping, in a nondestructive fashion since the reflections from a lower density material will result in a large negative peak in the waveform (Saarenketo and Scullion, 1994). The link between layer density and dielectric constant can be used to detect stripping and air void ratio in the asphalt road pavement. Stripping occurs when the asphalt and aggregate bond fails, leaving a weak layer. Since stripping indicates a layer with low density, a negative reflection will be generated from the interface between the layers. Where the asphalt layer is homogeneous (no stripping), the GPR waveform will indicate reflections only at the surface and at the asphalt/base interface (Scullion and Saarenketo, 1996). Again, RMeili and Scullion (1997) used the GPR to locate stripped areas in Hot Mixed Asphalt (HMA) layers.

3.6 General Subsurface Anomalies

GPR has been used successfully to identify subsurface anomalies. These include locating buried utility objects beneath road pavements, identifying peat deposits, and locating near-surface bedrock deposits. The capabilities and limitations of the GPR for subsurface anomaly detection and location of various sizes, depths, material types and configurations was carried out by Bowders Jr. and Koerner (1982).

3.7 Benefits of Using GPR for Pavement Assessment

Accurate layer thickness estimation and distress localization are important issues for the pavement engineers. Thus for newly constructed road pavements, layer thickness measurement is essential to ensure that the constructed road layers meet the design

specifications as part of the quality control and quality assurance procedures. For old pavements, layer thickness measurement and subsurface defects mapping are important in making appropriate economical rehabilitation decisions. Some of the key advantages of the GPR method in geophysical surveys are outlined below.

- Rapid ground coverage- Antenna towed either by hand or from a vehicle, giving rise to a continuous survey within a short time frame.
- High-resolution coverage of the survey area, detecting even small objects.
- On-site interpretation possible due to instant graphic display.

3.7.1 Limitations

- Data acquisition may be slow over difficult terrain.
- Depth of penetration is limited in materials with high electrical conductivities such as clays.
- Energy may be reflected and recorded from above ground features, walls, canopies, unless antennae are well shielded.
- Artifacts in the near surface (reinforcing bars, boulders, components of made ground) may scatter the transmitted energy and complicate the received signal and/or reduce depth of penetration.
- Radar waves cannot penetrate through metal. Thus, if steel storage tanks are present on the site, GPR will not be able to see inside them, nor assess their condition. Further, objects behind steel may be obscured and thus not observable. Radar performance is driven by the characteristics of the sensor, the targets, and the competing background clutter. An object may be observable at a shallow depth, but the same object may be invisible at a greater depth.

CHAPTER 4

METHODOLOGY

4.1 Study Area Description

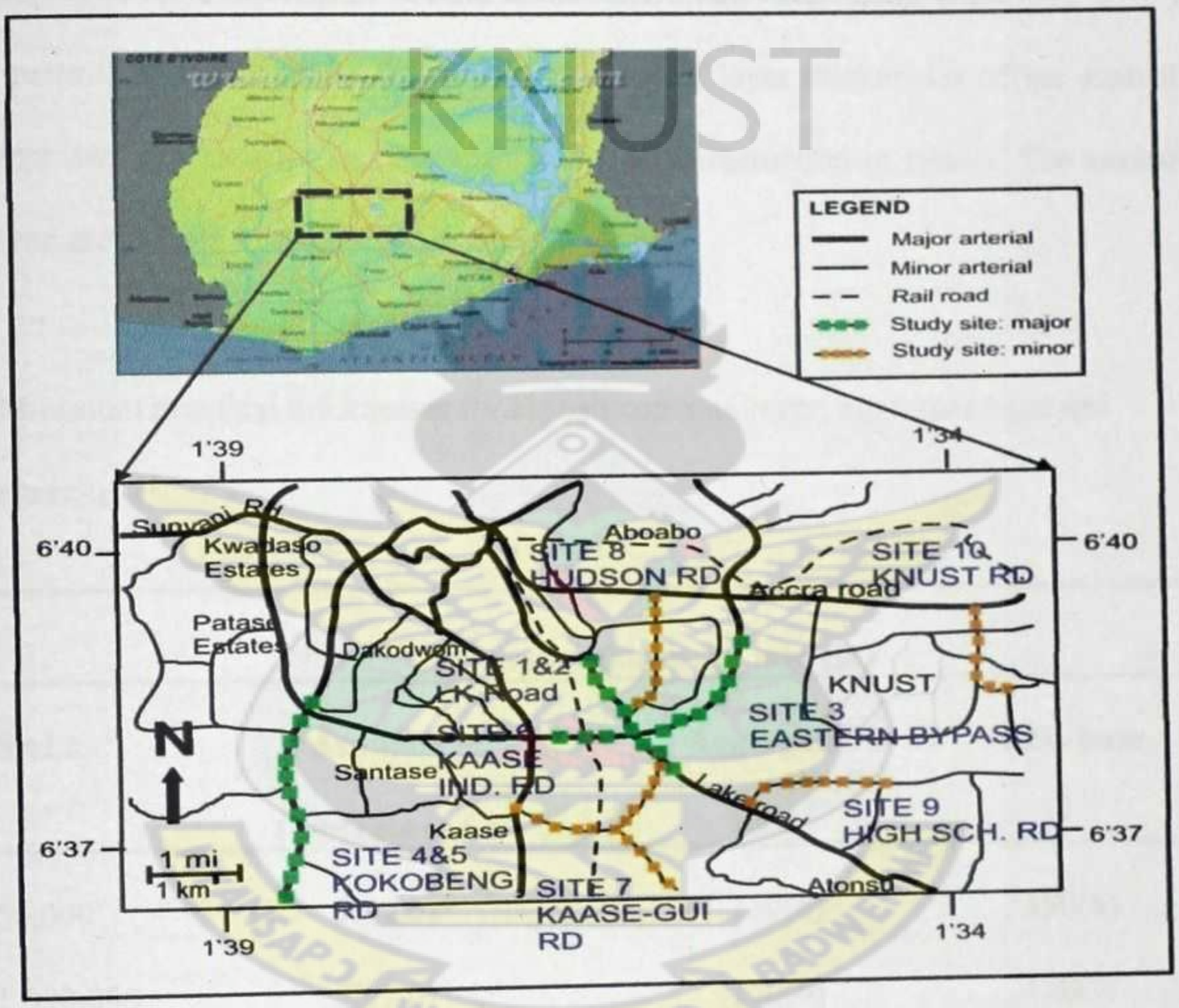

Figure 4.1: Road network of southern part of Kumasi (Modified from google earth) with the surveyed roads shown in green and orange GPS plots.

The survey was aimed at estimating the thicknesses of the wearing course (Asphalt overlay) and base layers of major and arterial roads in Kumasi and therefore, four each of them were surveyed. Thus, both new and existing roads were marked for the survey in order to fully assess the capability of the available GPR equipment for pavement thickness estimation as

well as compare the thicknesses of the older roads to the new once and ascertain their extent of deterioration relative to their ages. Majority of the surveyed road pavements are located in the southern part of Kumasi (Asokwa Sub-Metro), which can best be described as the industrial area of the city, with a number of heavy duty industries ranging from lumber companies, major construction companies and brewing companies. Thus, the roads in the area are constantly plied by heavy duty trucks, apparently causing damages to the pavements a few years after their construction. Accordingly, nearly all the road pavements of varying categories surveyed have undergone several maintenance and resurfacing treatments over a number of years. Table 4.1 shows the minimum practical layer thicknesses of the asphalt, aggregate base and sub-base for flexible road pavement construction in Ghana. The various roads surveyed are shown in table 4.2.

Table 4.1: Minimum practical thicknesses for asphalt concrete layer, aggregate base and sub-base materials.

	Minimum thickness, mm (in)		
Traffic, ESALs	**Asphalt Concrete (AC)**	**Aggregate Base**	**Sub-base**
50,001 - 150,000	50(2.0)*	150(6)	150(6)
150,000 - 1,000,000	50(2.0)*	150(6)	150(6)
1,000,000 - 2000,000	50(2.0)	200(8)	200(8)
2,000,000 - 5,000,000	76(3.0)	200(8)	200(8)
5,000,000 - 9,000,000	102(4.0)	200(8)	200(8)

* These pavement structures can use double surface treatment instead of the asphalt concrete.

** Rounded values in mm.

Source: GHA Pavement Design Manual, August 2008.

Table 4.2: Details of the various roads evaluated

Site	From	To	Total Distance Surveyed [km]	Direction
Major Arterials				
LAKE RD 1	Asafo Asokwa	Overpass	1.50	South-East
LAKE RD 2	Asokwa Overpass	Asafo	1.50	North-West
E-BYPASS	Asokwa Overpass	Anloga Jnc.	1.80	East
KOKOBENG 1	Santasi R/A	A. Kokoben	2.40	South
KOKOBENG 2	Santasi	A. Kokoben	1.60	South
Minor Arterials				
KAASE IND.	Atinga Jnc.	KBL Jnc.	1.80	East
KAASE-GUI.	Eben. Meth. Ch.	Guiness Ltd.	0.69	South-East
HUDSON	Lake Rd. Int.	Children's Park	2.00	North
HIGH SCH.	High Sch. Jnc.	Gyinyase	1.00	East
KNUST KNUST	Overpass	Coll. of Sc.	1.80	South

Most of the roads in Ghanaian urban areas involve two-layer pavements, the AC overlay (wearing course) and the base layer made of crushed rock aggregates. Some of the surveyed roads were comparatively in poor conditions (the minor arterials), some of which have been undergone several maintenance works. Road surface defects such as rutting and cracks were clearly visible on them. However, in situ information on the actual depth to the various layers

of the studied roads (cores) could not be ascertained therefore information on the actual thicknesses of the various layers (AC overlay, base and sub-base) were taken from the road contractors (in the case of the freshly built pavements), whereas that of the existing roads were obtained from the Urban Roads Department so as to assess their levels of deterioration relative to their ages.

4.2 The GPR Equipment Used

4.2.1 The Control Unit

The GPR equipment used in this research is a RAMAC system manufactured by MALA and it comprises the MALA (ProEx) Control unit, the XV Monitor powered by an external 12 V standard Li-Ion battery, and a shielded antenna unit with 800 MHz central frequency. The shielded antenna unit was mounted in a cart and pushed on the road pavement, enabling spatial triggering from the road wheel with very good resolutions and penetration depth of approximately 1.0 m. The ProEx backpack as shown in figure 4.1 is the administrator for the data collection and consists of the power supply and an analogue section that generates the crucial control signals and internal computers. It is compatible with all current MALA antennas, both shielded, unshielded, borehole, and high frequency antennas. The control unit has three parallel 32-bit processor that controls the transmitter and receiver timing, sampling and trace intervals, stores raw radar data in a temporary buffer and data transfer to a PC interface to the MALA XV Monitor. During operation, the ProEx is mounted on a backpack holder or used together with the MALA backpack.

Figure 4.2: The MALA GPR Unit used in the survey comprises; the ProEx Control Unit, XV Monitor, the 800 MHz shielded antenna and the wheel cart.

4.2.2 Operation

The moving mode employed in this research allows a radar wave to be transmitted, received and recorded each time the antenna is moved a fixed distance across the road pavement surface. The recorded signals are displayed as traces that are displayed side-by-side to form a GPR time-distance record, or GPR cross section, which shows how the reflections vary in the subsurface. If the contrasts in electrical properties (e.g. changes in permittivity) are relatively simple, then the GPR time-distance record can be viewed as a two-dimensional pseudo-image of the pavement, with the horizontal axis being the distance along the pavement surface, and the vertical axis being the two-way travel time of the radar wave. The two-way travel time on

the vertical axis can be converted to depth, if the permittivity (which can be converted to velocity) is known. The time-distance record is the simplest display of GPR data that can be interpreted in terms of subsurface features. This time-distance record of the pavement is then processed with a software for interpretation.

4.2.3 Calibration Parameters

These are the data acquisition parameters set on the GPR system for adjusting the system in order to be able to clearly map the desired target and they are set during reconnaissance surveys. For instance, for a desired penetration depth and resolution required, antennas of particular centre frequencies are selected. Other parameters include sampling time (time window), data point separation, speed etc. Therefore, in this survey, the following acquisition parameters were set for the system during data collection:

- Antenna : Shielded 800 MHz ground-coupled.
- Time window : 18.3 ns
- Collection speed : 100 m/_s
- Wheel type : Meas Wheel
- Antenna separation : 0.14 m
- Point interval : 0.023 m
- Approximate penetration depth : 1.0 m

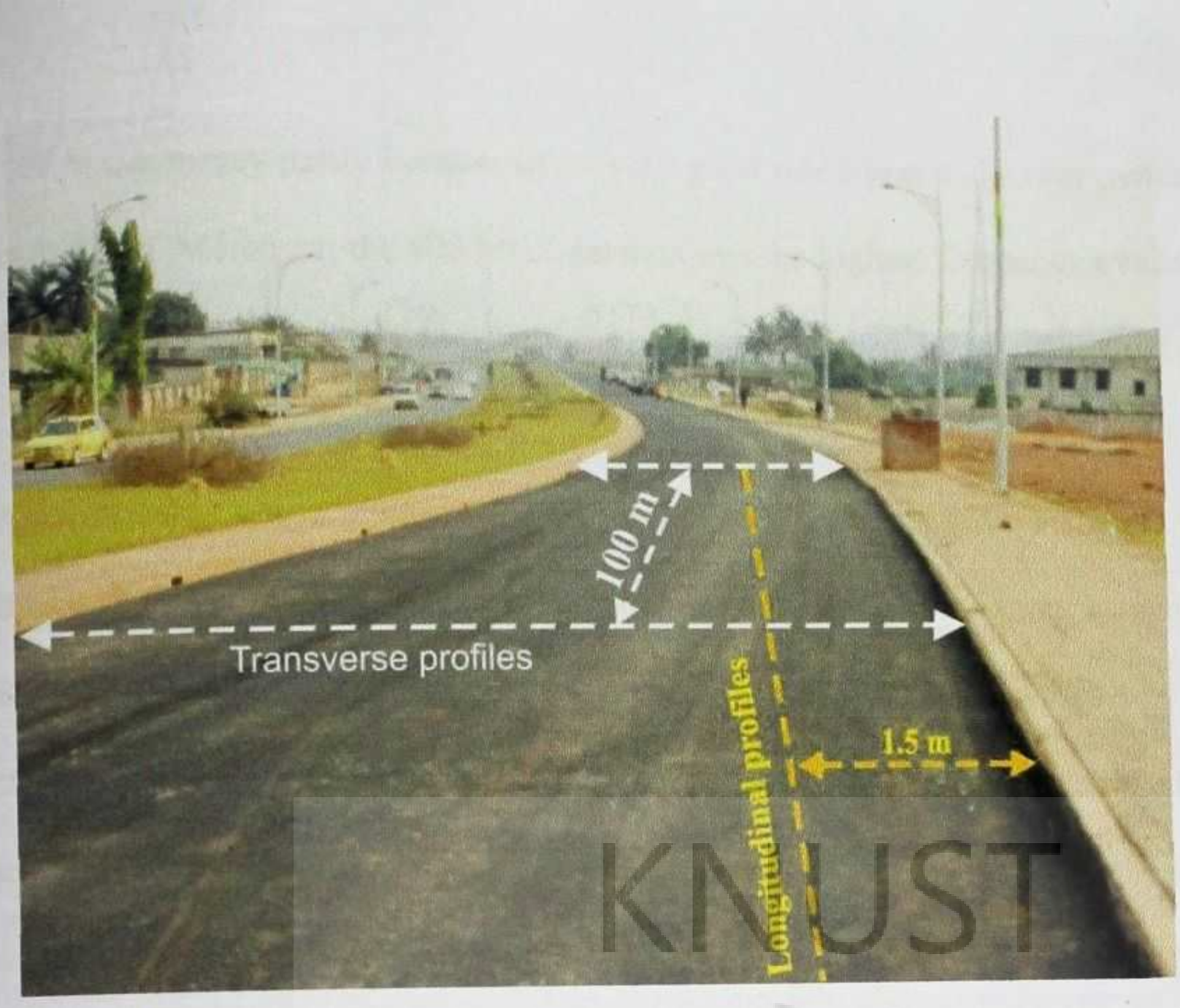

Figure 4.3: Schematic diagram illustrating the GPR profiles at the Eastern Bypass Rd.: Longitudinal profile (yellow line), Transverse profile (white line).

4.3 Field Procedure and Data Acquisition

The MALA 800 MHz shielded antenna was used with a cart (trolley) for the survey and the rate at which radar pulses were transmitted (scan rate) was set by the speed of the wheel. This is made possible by the encoder attached to one of the wheels of the cart and connected to the system pulse generator. The cart was pushed over the road pavement continuously for the entire roads surveyed. The shielded antenna consists of both transmitter and receiver antenna elements in a single housing, designed to ensure that the transmitted radar energy is only emitted from the bottom of the unit only, where it is in contact with the ground and protects the receiver element from picking external signals from the upper half space (noise). The shielded antenna construction makes the antenna suitable for urban investigations since such areas have a lot of background noise. Further, the shielded antennas offer modularity at its best and are very efficient for subsurface mapping. The 800 MHz shielded antenna was

used in the survey partly because of its very good resolution and lower penetration depth of up to 2.5 m. Moreover, the 800 MHZ antenna was the highest frequency available to offer the best resolution and the needed penetration depth of less than 1.0 m in the road pavement.

When connected to a survey wheel, different GPR systems have different maximum scan rates, and this along with the speed at which the antennae move along the ground determines the scan spacing (i.e, the number of data points picked over a given distance). The use of the pushed cart was necessary as the slow pace was meant to allow for the ample time required to acquire a detailed picture of pavement layers of interest. Calibration of the GPR equipment was done on the surveyed roads to also test the viability of the equipment for the intended study. During the on-site data collection, the GPR system parameters were set so that a scan was taken approximately every 0.023 m along each survey line and this was made possible by slowly pushing the cart. Single longitudinal survey profiles of varying lengths depending on the total length of the individual roads were taken on the roads at approximately 1.5 m from the edge of the pavement, with some transverse profiles also taken 100 m apart along the newly constructed pavements (Figure 4.3). A GPS device was also used to track the locations of the survey lines. The GPS data was picked at 100 m intervals along the roads as well as locations of prominent features along the roads that are expected to introduce anomalies on the radargrams.

4.4 Choice of Transmitting Frequency

There is an inverse relationship between frequency and penetration depth. That is, high frequency means low depth but higher resolution and vice versa. Higher frequency antennas are used for small shallow targets and low frequency antennas detect large and deeper targets. Accordingly, the following factors were considered in choosing the transmitting frequency:

- target properties (size, depth and composition of the composite road paving materials).
- the required resolution of the road pavement that can clearly display the desired features of the road.
- presence of moisture and clays in the native soil/subgrade where the roads traverse.
- topography of the site, vegetation cover and the prevailing weather conditions.
- access to the needed antenna.

4.5 Site Reconnaissance Investigation

In order to obtain as much information from GPR investigations as possible, the methodology has to be tailored to the specific site conditions and constraints. This, as with all site investigations, should start with a review of any available existing site information before beginning to plan the on-site investigation, and if necessary the investigation methodology should be revised and tailored as the on-site investigation is conducted. Planning of GPR surveys is carried out with due consideration for the expected subsurface material properties, the nature and depth of the targets and finally, the limitations of the GPR equipment available for the study. All road materials and sub-grade soils are composite materials with their dielectric properties being a combination of their individual dielectric constants of the components, volume fractions of components, their geometries, and the electrochemical interactions between them (Knoll & Knigth, 1994). These materials include: air, water, mineral aggregates, clays, colloidal particles, asphalt binders and others. All these materials combined complicates the dielectric constant of the pavement.

The most important component affecting the dielectric permittivity of soils and unbound road materials is water which, to a greater or lesser extent, also affects their mechanical properties.

However, the magnitude of these effects depends on the material properties, moisture content and even the saturation history of the layer (Saarenketo & Scullion 1994). Further, to effectively evaluate road pavements with the GPR equipment, penetration depth of less than 2 m would be needed and this informs the choice of antennae.

Reconnaissance surveys were initially carried out on selected roads with the available 800 MHz ground-coupled antenna to determine if the available GPR equipment could provide vital information about the road pavement thickness and other defects. Results from these preliminary surveys was encouraging, although the poor conditions of the aged roads studied introduced great difficulty in the interpretation of the results. The actual data acquisition was planned taking cognizance of the following; surface water conditions of the areas where the roads traverse, presence or possibility of buried utilities such as electric cables, water pipelines, wire nets in cement mortar and bracing supports, conduits, sewers pipes, nearby power transmission masts, closely spaced metal reinforcement at near-surface that may shield underlying GPR signal and generally materials containing high contents of iron ore bearing minerals such as haematite and magnetite. The exact positions of all such objects that could interfere with the GPR data and complicate interpretation of survey results were noted so that they can be marked on the radargrams. Also, potential sources of spurious reflections like above ground metal posts, vehicles, overhead cables etc were carefully noted in the course of the survey so as to distinguish them from genuine below ground reflections.

4.6 Data Collection

GPR systems are digitally controlled, and data are usually recorded digitally for post-survey processing and display. The digital control and display part of a GPR system generally consists of a micro-processor, memory, and a mass storage medium to store the field

measurement. A small micro-computer and standard operating system is often utilized to control the measurement process, store the data, and serve as a user interface. Data may be filtered in the field to remove noise, or the raw data may be recorded and the data processed for noise removal at a later time. Field filtering for noise removal may consist of electronic filtering and/or digital filtering prior to recording the data on the mass data storage medium. Field filtering should normally be minimized except in those cases where the data are to be interpreted immediately after recording. Figure 4.4 below shows data collection with the MALA GPR equipment with the 800 MHz ground-coupled shielded antenna unit placed in a cart and pushed along the pavement. As shown in the middle inset, the Rough Terrain Cart (RTC) has a pulse encoder attached to one of the wheels and calibrated to measure the profile distance.

Figure 4.4: Data collection on both new and existing road pavements in Kumasi using the MALA GPR Equipment.

4.7 Data Display and Interpretation

Data display is central to data interpretation. Thus, producing a good display is an integral part of interpretation. There are three types of displays of surface data. These are; one-dimensional trace, two dimensional cross section, a three dimensional display. The wiggle trace (or scan) is the building block of all displays. A single trace can be used to detect objects (and determine their depth) below a spot on the surface. By towing the antenna over the surface and recording traces at a fixed spacing, a record section of traces is obtained (radargrams). The horizontal axis of the record section is surface position, and the vertical axis is a two-way travel time of the electromagnetic wave. Finally, the three dimensional displays are fundamentally block views of GPR traces that are recorded at different positions on the surface. Data are usually recorded along profile lines, in the case of a continuous recording system or at discrete points on the surface in fixed-mode recording.

4.8 Assessment of Measurement Results

The quality of the data acquired on the site was assessed immediately after the field survey by examining the GPR images (radargrams) displayed on the monitor screen. In some cases, actual processing of the data was carried out at the site with the reflex software to be assured of the effectiveness of the equipment. Again, where the images displayed on the system monitor indicated doubtful features, the profiles were repeated to ensure the data was adequate to achieve the objective of the survey. Sources of stray signals were identified in the course of the study. Operation of mobile phones close to the antenna was avoided during recordings.

4.9 Data Processing Steps

GPR field data just like other geophysical data are subject to numerous processing steps with softwares to enhance data interpretation of the signal waveform by improving the signal-to-noise ratio of the radar profiles. The various processing algorithms applied to a particular data set often depend on both the objectives of the research and the quality of the filed data. Such processing steps can be basic ones or more advanced processing (muting, background removal, multiple frequency antenna mixing and polarization mixing). The important feature of advanced processing is that it focuses on making weaker signals visible, thereby enhancing specific components of the data for interpretation, or derives qualitative information such as velocity and attenuation from the data. Figure 4.5 below shows the block diagram of general data processing flow of 2D- GPR data.

The radargrams from the GPR data files were processed and analyzed using the ReflexW 4.5 software, to determine the thicknesses (depths) of the road pavement layers and identification of homogenous and anomalous lengths of pavement construction, indentify air voids in the pavements as well as general anomalies. The recorded data was subjected to filtering stages including corrections to allow for the fact that the GPR antennae are not in direct contact with the road surface, background noise removal and time to depth conversion within the pavement structure. The detailed processing steps applied to the recorded data are as follows:

1. Field Data Editing
2. 1D – Filters
    - Subtract-mean (Dewow)
    - Static correction (Time-zero)
    - Gain

- Bandpassbutterworth

3. 2D – Filters
   - Background removal
   - Running average
4. Layer Picking
5. Visual Interpretation

4.9.1 Field Data Editing

After recording the data, it was first edited as it was displayed on the GPR system monitor. Since data acquisition at the site is always susceptible to errors and omissions, data reorganization, data file merging, background information updates etc were carried out for a more objective interpretation.

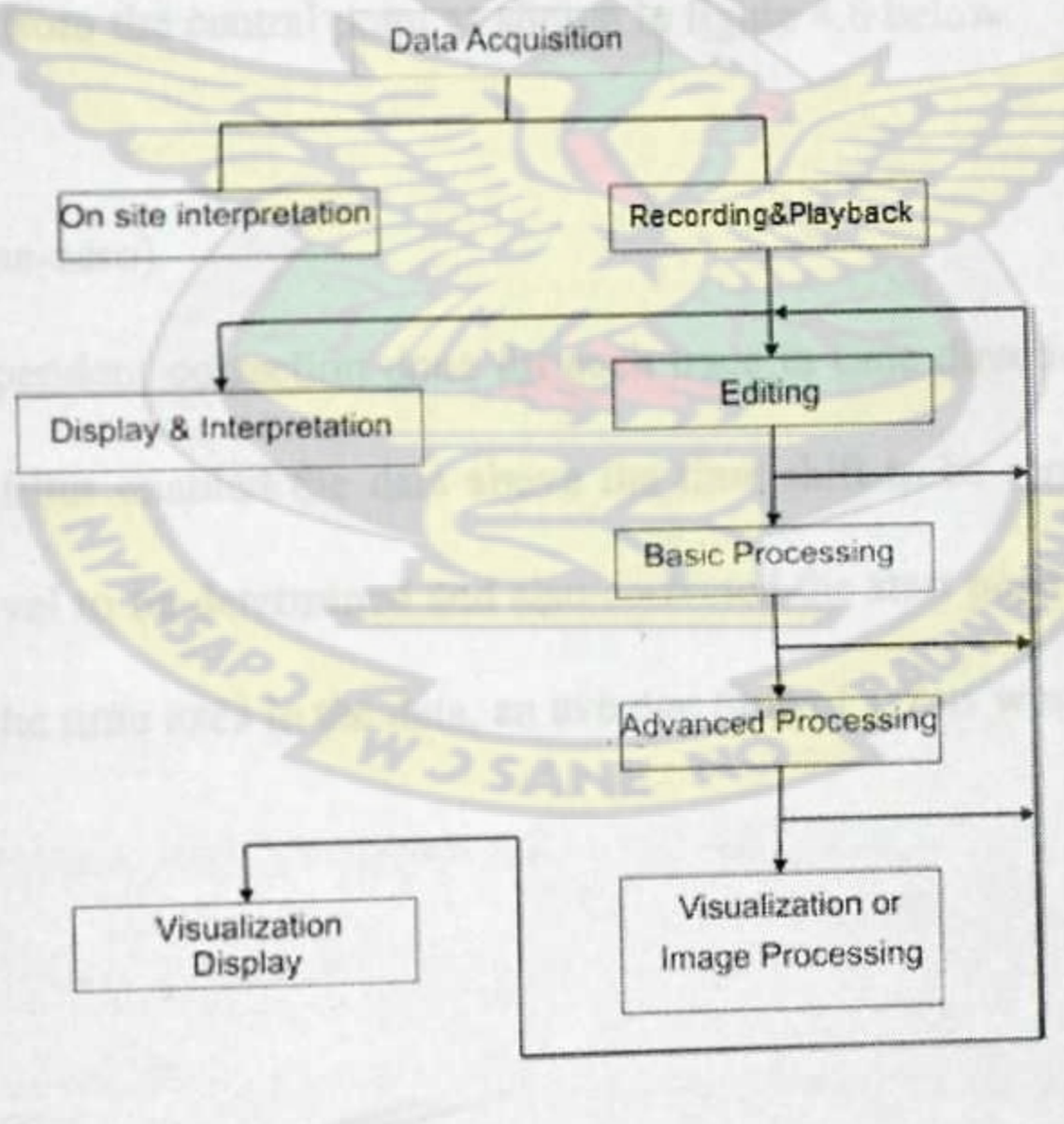

Figure 4.5: GPR Data Processing Flow.

4.9.2 Basic Processing

These are some of the fundamental manipulations applied to the data to prepare it for a more standard processing and interpretation. Because of the ultra-wide bandwidth of the impulse GPR receivers, the signals are susceptible to noise corruption. The main sources of noise that might affect GPR reflected signals when performing GPR surveys along highways are cell-phone towers, cell-phones, CB radios, and any other EM devices emitting in the GPR bandwidth (Olhoeft, 2002). The basic processing stages carried out on the data are as briefly described below:

4.9.2.1 Subtract-mean (Dewow)

This filter was used for removing very low frequency components from the data that are associated with either inductive phenomena or possible instrumentation dynamic range limitations (Gerlitz et al., 1993). Accordingly, frequency values less than 25 MHz were filtered out as unwanted low frequencies (wow). This was done by subtracting a running mean value of each from the central point as shown in figure 4.6 below.

4.9.2.2 Muting (Time-zero)

This is a time-independent correction done for each trace in time direction (figure 4.7). The application of this filter enabled the data above the time shift to be removed, allowing the significant first arrival to be determined and also corrected the start position of the time axis. In order to correct the time axes in the data, an average time of 1.7 ns was removed from each trace.

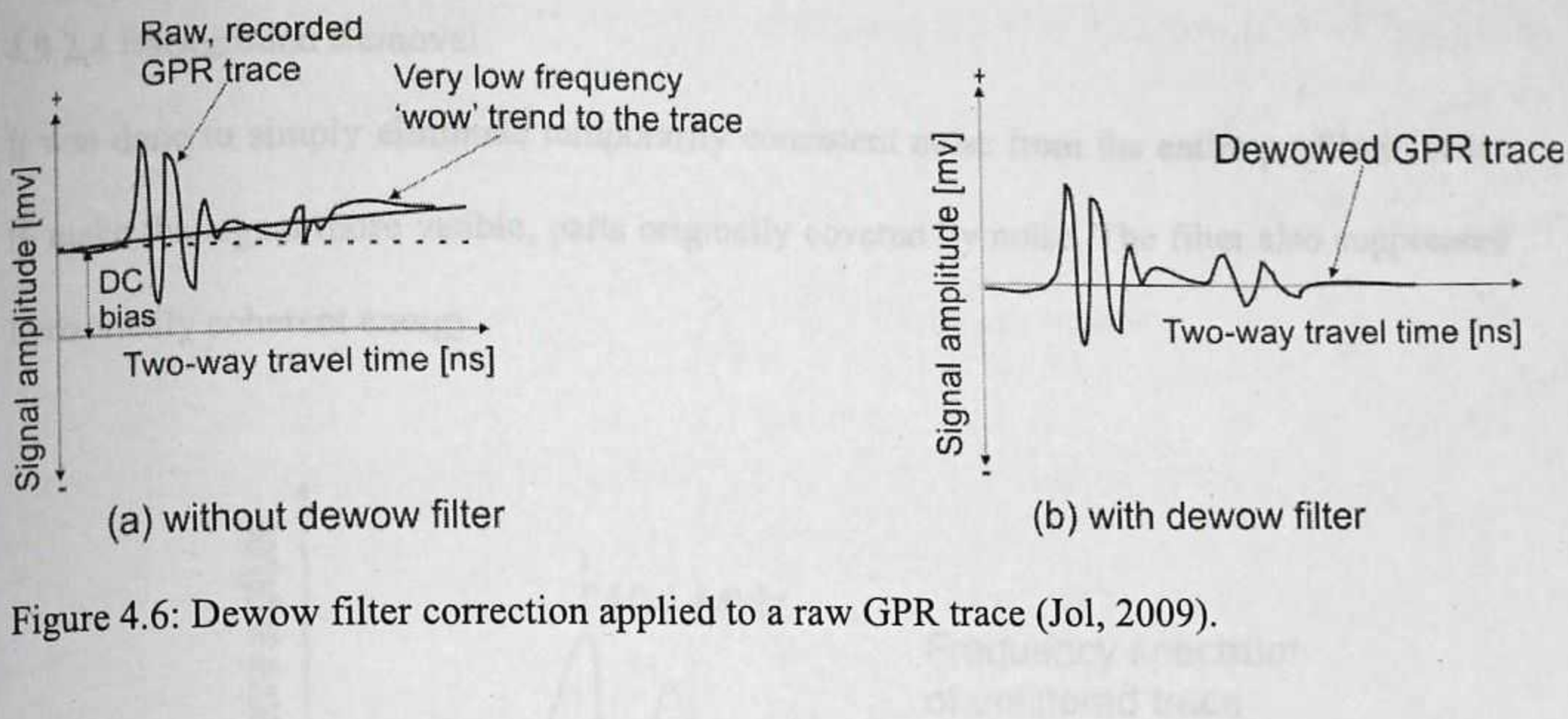

Figure 4.6: Dewow filter correction applied to a raw GPR trace (Jol, 2009).

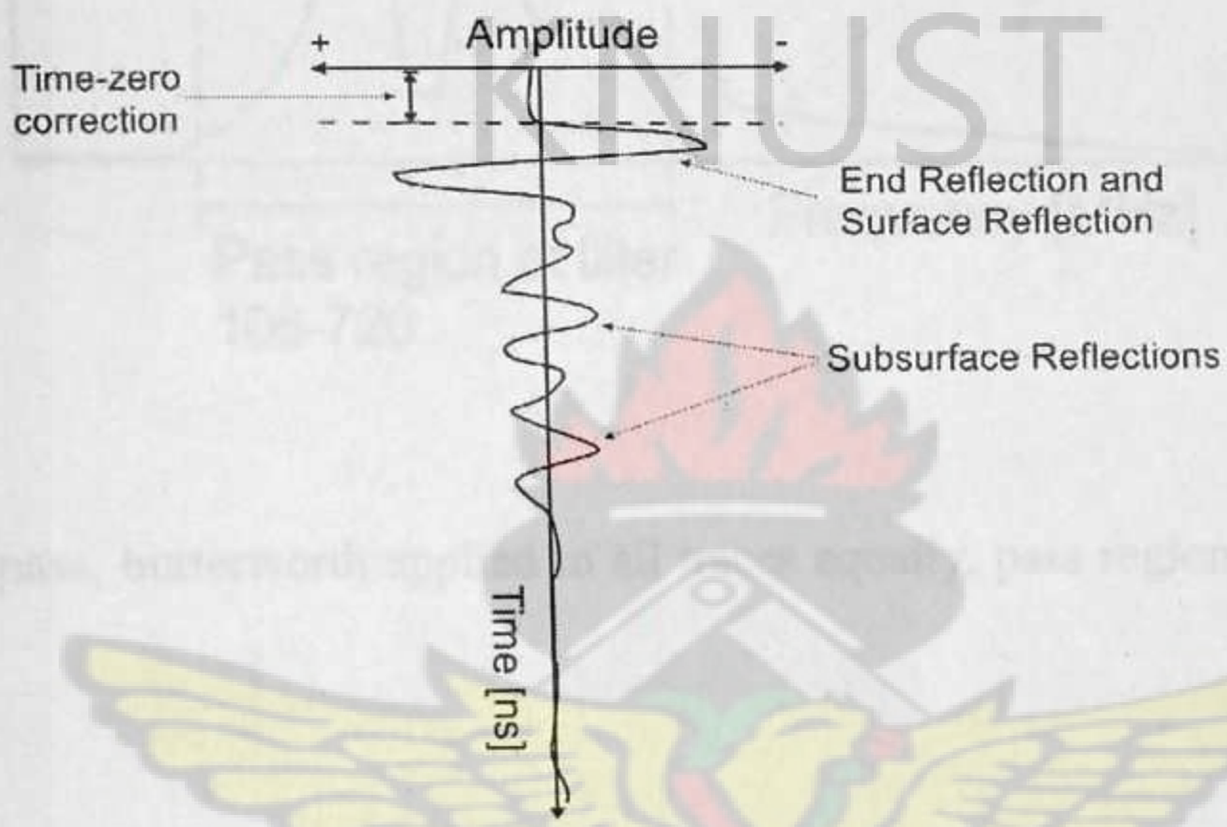

Figure 4.7: Time-zero correction applied to a raw GPR trace (Jol, 2009).

4.9.2.3 Bandpassbutterworth

This filter was applied to suppress noise with the bandpass filter when it differs from the signal in its frequency content. The filter band is specified by setting two frequency values; 25 MHz and 1200 MHz. The first point determines the lower cut off frequency , and the second, the higher cut off frequency.

4.9.2.4 Background Removal

It was done to simply eliminate temporarily consistent noise from the entire profile in order to make the signal more visible, parts originally covered by noise. The filter also suppressed horizontally coherent energy.

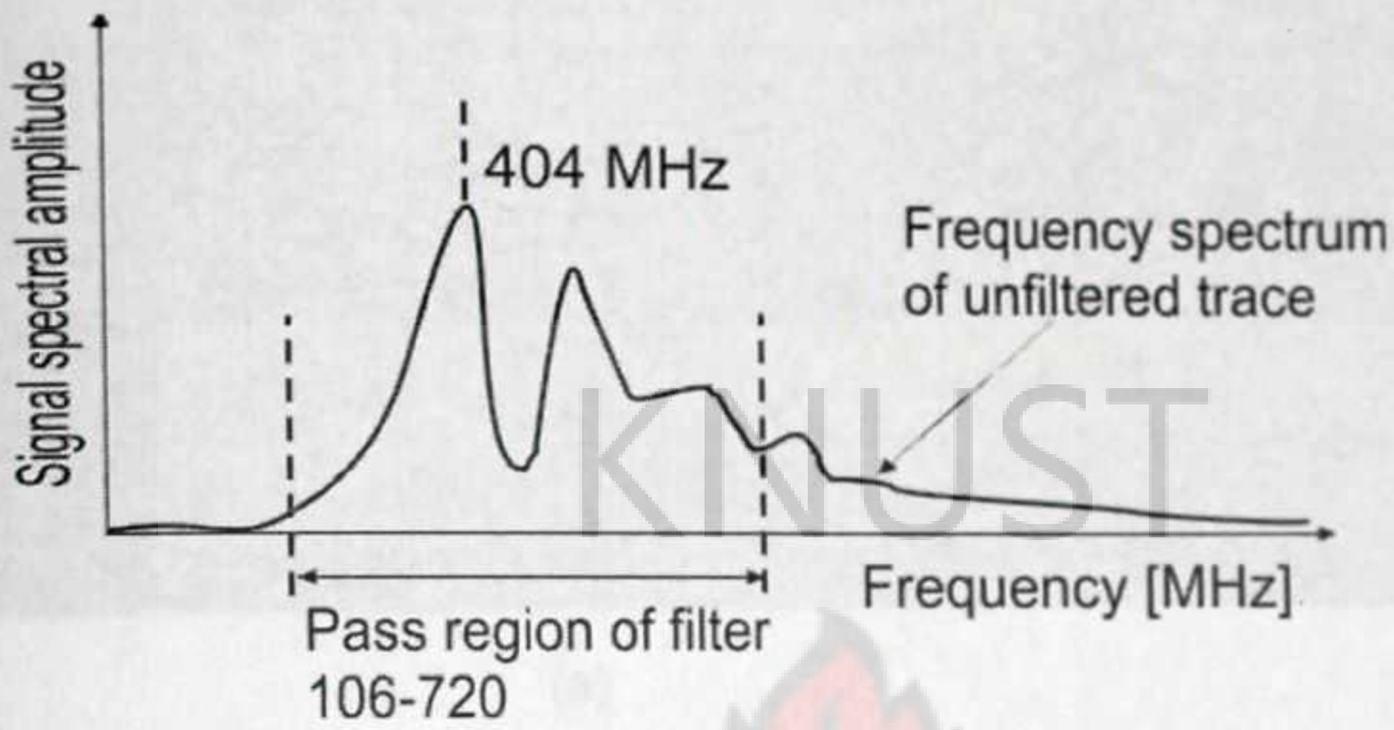

Figure 4.8: Bandpass, butterworth applied to all traces equally, pass region of 106-720 (Jol, 2009).

4.9.2.5 Gain

This filter facilitated the possibility of multiplying the data points by a given gain function. The function has options such as manual gain g(y), or g(t), energy decal or the AGC. Thus the data were multiplied by this function in order to compensate for possible damping or losses due to geometric spreading. Figure 4.9 shows the result of the application of the various filters on a GPR data. Figure 4.9 (a) is the raw data from a 1.5 km profile of LAKE ROAD 2, with indistinct features. The profile length, the travel time of the radar signals and the penetration depth are displayed in the ReflexW software window. The processed data, figure 4.9 (b), shows clear layer interface as black and white lines. That is, the quality of the data is enhanced by filtering low frequency signals (dewow), background removal, and

applying a gain function. Static correction was also done to move the start time of the traces to zero (actual surface of the pavement).

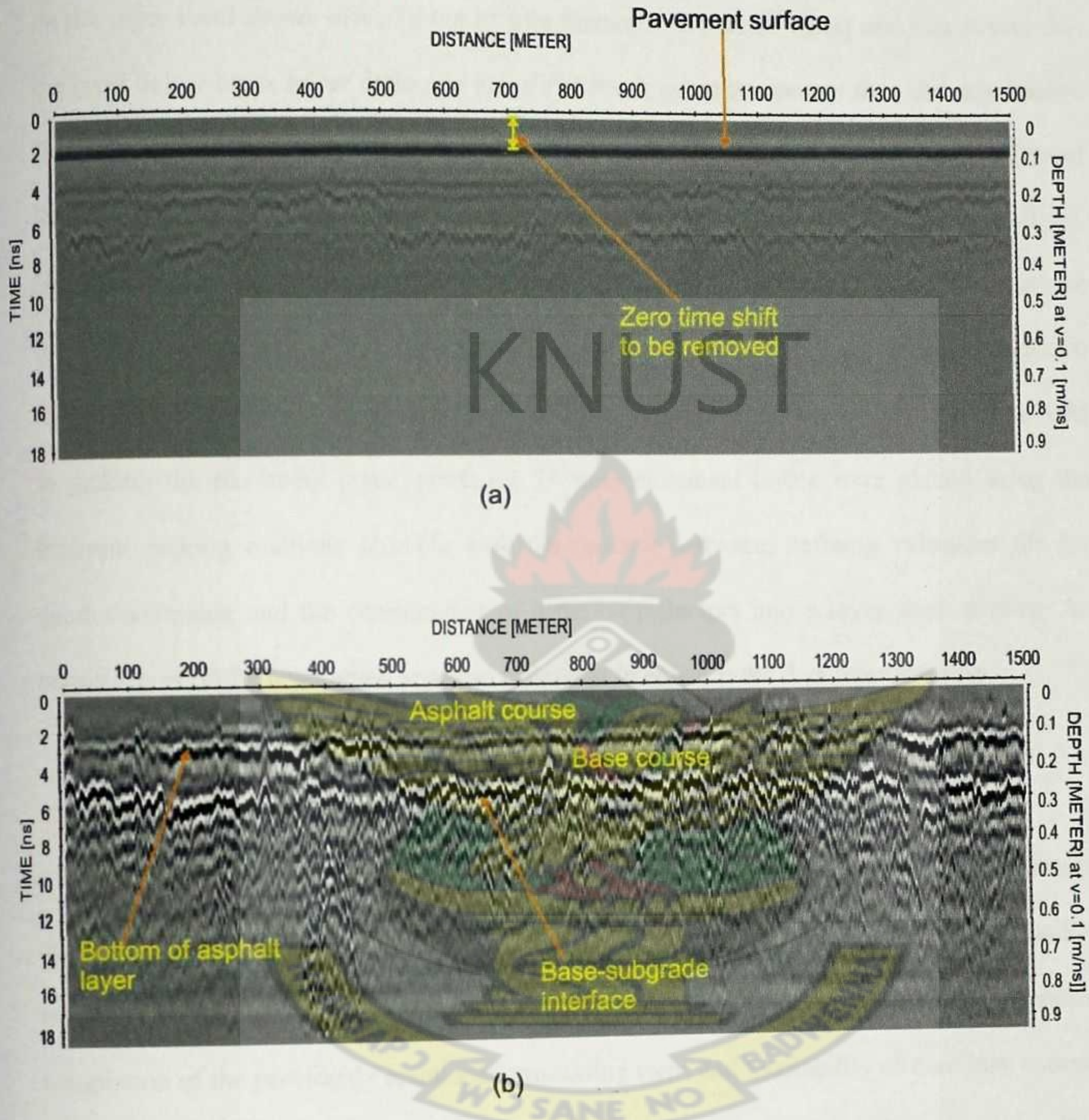

Figure 4.9: ReflexW software processing of sample data (LAKE ROAD 2) taken with the 800 MHz ground-coupled antenna.

4.10 Location of Pavement Interface

Subsurface layers appear as continuous reflectors on the radargrams which are plotted as 2-D sections using the reflexW software. The pavement bottom reflection are easily defined from the filtered data as shown in figure 4.9. Further, the polarity of the reflections provides

information on the dielectric properties (and moisture) of the road structures. Positive reflectors show white in the middle and this reveals that the dielectric value of the proceeding layer course below is higher than the dielectric value of the layers above. A negative polarity on the other hand shows black in the middle (between two white lines) and this shows that the layer below has a lower dielectric value and lower moisture content than the layer above (Saarenketo, 2006). In some of the raw data (such as the Kaase Ind. Rd. and the High School Rd.), identification of the pavement layers (Aspalt overlay and Base course) was difficult. However, upon data processing, and adjustment of the data amplitude plot-scale to enhance the contrast displayed between different reflected signal and amplitudes, it was possible to identify relatively weak interface reflectors. Figure 4.10 shows the details of the steps used in picking the pavement layer interfaces. Distinct pavement layers were picked using the different picking methods possible with the reflexw software, defining velocities for the depth conversion and the combination of different reflectors into a layer show picture. An output report of the layer show was also generated to enhance the data interpretation.

4.11 Visual Interpretation

This involves migration with various algorithms, event picking, subjective gain enhancement and amplitude analysis. This stage usually requires a good knowledge of the velocity structure in the ground or in this case the road pavement materials. All of these require completion of the previously mentioned processing steps and availability of corollary control information. For example, migration is extremely useful and reconstructs the radar image in a form which is probably a better representation of the pavement layers (Fisher et al., 1992).

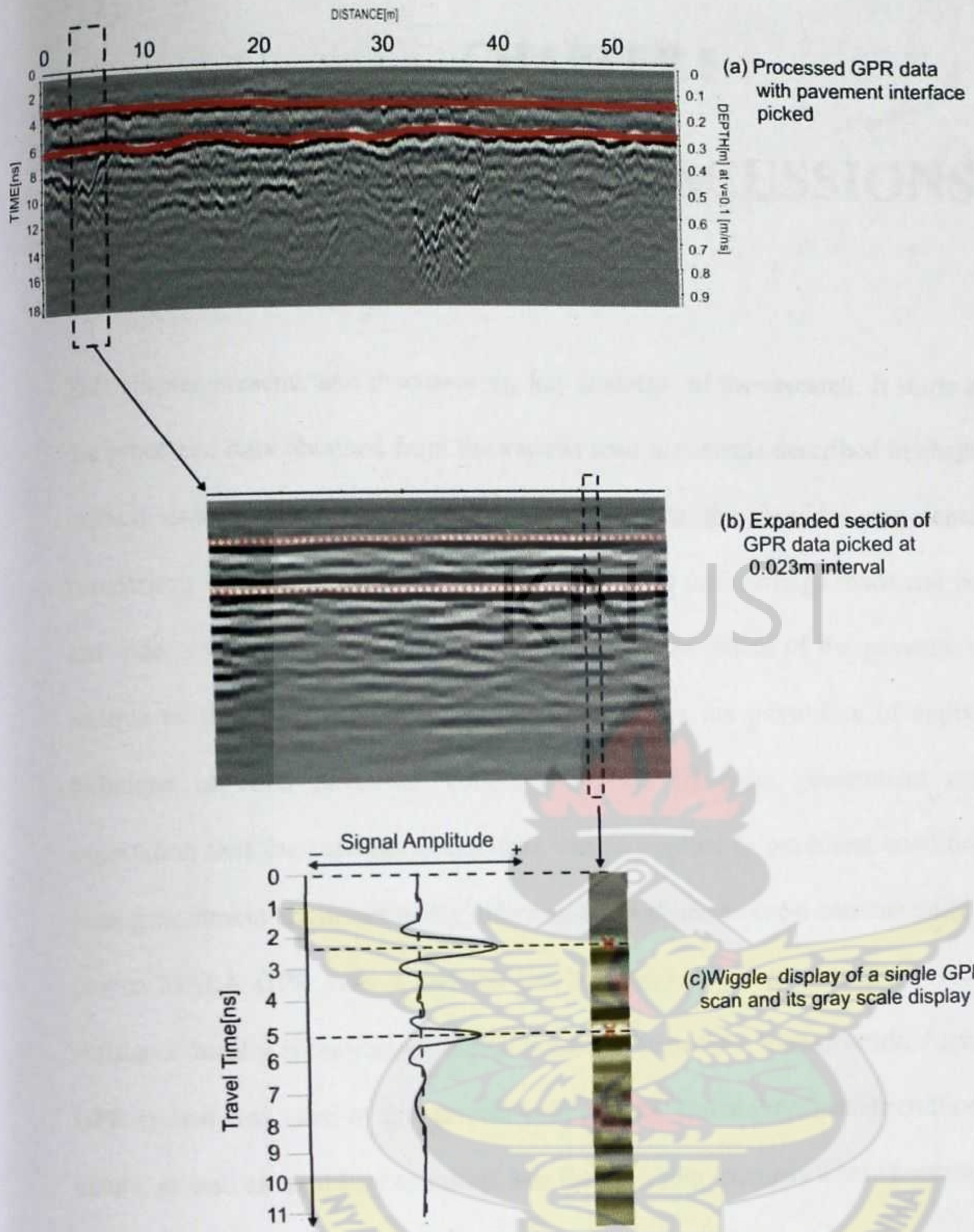

(a) Processed GPR data with pavement interface picked

(b) Expanded section of GPR data picked at 0.023m interval

(c)Wiggle display of a single GPR scan and its gray scale display

Figure 4.10: Locating pavement interface in GPR data using the ReflexW.

CHAPTER 5

RESULTS AND DISCUSSIONS

5.1 General Overview

This chapter presents and discusses the key findings of the research. It starts by presenting the processed data obtained from the various road pavements described in chapter 4, and the method used to estimate the layer thicknesses in the flexible pavements. Further, a comparison of the thicknesses of the two lanes in the dual carriage roads and between newer and older road pavements are presented to assess the extent of the pavement compression relative to their ages. Finally, the chapter discusses the possibility of applying the GPR technique in road pavement condition surveys by local government engineers. The expectation that the research undertaken can be applied in pavement condition surveys by local government engineers partly informed the decision to use a commercially available and proven MALA GPR system and the fact that these engineers can obtain readily available assistance locally if they adopt the GPR technique in their routine work. Again, the MALA GPR system was used in this project owing to its availability, user friendliness and robust nature, as well as its ability to collect data from varying antennas where necessary.

For data processing and analysis, the need for direct application of the equipment for commercial use also requires proven softwares, thus, the REFLEXW package was used. Although a number of interesting GPR road data processing softwares have been used in recent studies, the REFLEXW is an appropriate choice of GPR data processing and analysis software for this study not only because of its relative popularity, but also due to its ease of use as in data importation, filtering and interface demarcation of GPR data picked with

almost all the different commercially available GPR systems. The main findings of the GPR investigation are outlined in Appendix A, with descriptions of the various asphalt and base layers, determination of layer depths within those layers, and the identification of high variability in the thicknesses of the pavement layers along the profiles. Other notable features such as metal reinforcements in a bridge, buried utility pipes etc in some of the pavements surveyed are also presented.

5.2 Results from Major Arterial Roads

5.2.1 LKRD 1 and 2

The LKRD 1 and 2 project site is a 1.5 km dual carriage section of a major arterial road that runs south of the Asokwa sub-Metro of Kumasi and stretches from Asafo to the Asokwa overpass. It is one of the major arterial roads in the city and links the city to the Bosomtwe Lake, which is about 30 km away. According to the original construction specification, the road consists of two major structures; the asphalt wearing course which is 150 mm (6 in) thick and the base course also being 150 mm (6 in), apparently because typical urban roads undergo seasonal resurfacing with time as the road develops from a simple gravel road to its current state, obviating the need for other sub-layers as required in the case of newly constructed road pavements. The objectives of the GPR survey of the site LKRD 1 and 2 as in the other sites were precisely to estimate the asphalt and base layer thicknesses as well as detecting areas of potential stripping. Thus one longitudinal GPR profile was each run on 1.5 km sections of the south-bound (Lane 1) and the return lane (the north-bound) at approximately 1.5 m from the outer edge on the right using the 800 MHz ground-coupled shielded antenna unit pushed in a calibrated cart. After estimating the various layer thicknesses with the ReflexW software, the connectivity of the layer interface data points

were used to identify the quality of the interface. Where data on drill cores were not available, the interpretation was only based on the findings from the GPR, thus introducing some level of subjectivity in the interpretation.

Most of the results are presented in Appendix A, giving a series of dual images of different road pavement sections also with varying lengths. Figure 5.1 (a) is the processed GPR data display (radargram) depicting the asphalt course and the base course. The horizontal axis is the distance along the surveyed pavement in metres and the vertical axes represent the two-way travel times of the GPR signals in ns and their corresponding depth conversion in m. The polarity of the reflections at the various interfaces provide information on the dielectric properties (and moisture) of the road structures, resulting in easier identification of interfaces. Lighter negative peaks above and below a stronger positive peak (shown by white line between two black lines) are as a result of the wave approaching and leaving the interface. Thus, the intensity of the interface indicates the quality or clarity of the interface, that is, the more white or black the interface, the greater is the reflection amplitude and therefore the easier it is to pick the interface. Figure 5.1 (b) represents the display chart of the layers generated from the picked layers.

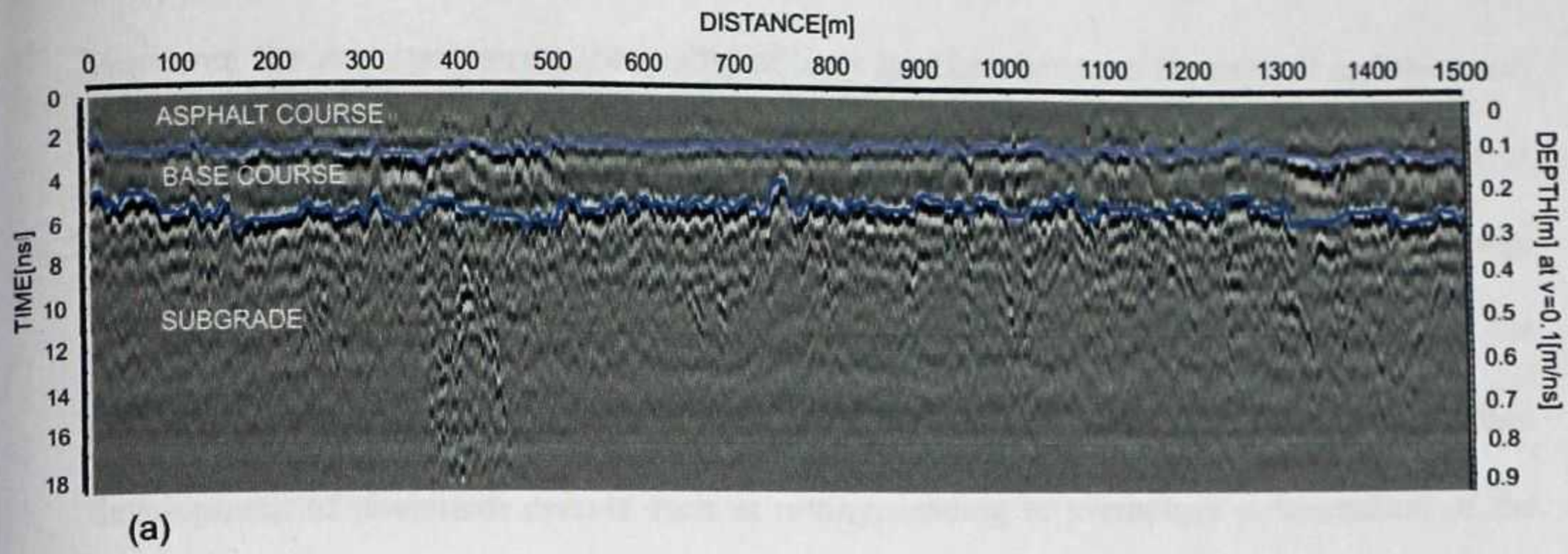

Figure 5.1: Longitudinal GPR profile of LKRD 2, taken with the 800 MHz ground-coupled antenna. Part (a) is the processed data with pavement layers picked, and (b) is a color display of the asphalt and base layers of the pavement.

The average thickness of the asphalt was estimated as 141 mm (5.5 in) with a standard deviation of 11 mm (0.43 in) representing about 8% variation. The maximum variance of the asphalt layer thickness in the LKRD Lane 1 pavement was also found as 4 mm. The base layer thickness recorded an average of 171 mm (6.7 inches), also with a standard deviation of 20 mm and maximum variance of 6 mm. Though the estimated thicknesses of the asphalt and base layers are fairly higher than the minimum Ghana Highway Authority standard range for a major arterial road (4-8 in) for the asphalt course and (6-8 in) for the base course (per the equivalent single axle loads of such a road), it can be noted that the average thicknesses measured are just about the minimum values.

Moreover, the study revealed poor quality of layer interface between the asphalt and the base. Figure 5.2 below shows a plot of the variation of the calculated thicknesses of asphalt layer from the GPR data of the south-bound lane of the Lake Road (Site LKRD 1). The high variation coefficient of the asphalt-base interface along the pavement (8 %) shows that the pavement materials are not stiff enough and this may be an indication of potential development of pavement defects such as rutting, leading to premature deterioration of the road. Further, there was a remarkable disparity between the estimated thickness variations of the dual carriage pavement of LKRD 1 and 2. That is, for the same 1.5 km GPR profile taken from each lane at the same location, the south-bound lane (Figure 5.3 (a)) registered an average asphalt layer thickness of 141 mm (5.5 in), whereas the north-bound lane (Figure 5.3 (b)) measured an average of 123 mm (4.8 in).

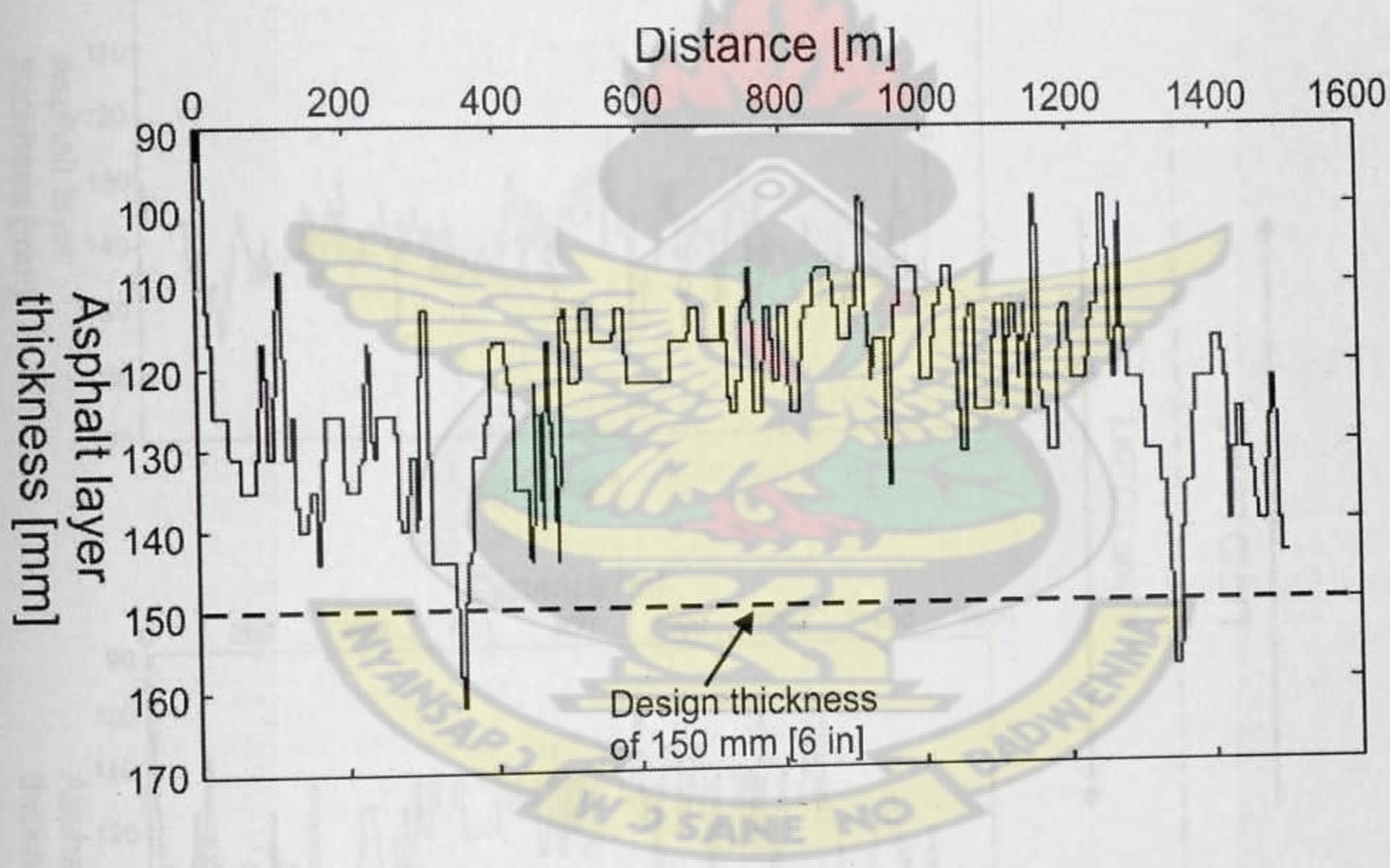

Figure 5.2: Variation of asphalt layer thickness of LKRD 2 calculated from the GPR data.

Thus, for a pavement constructed within the same time frame and apparently with the same design specifications to have an average difference in asphalt layer thickness of 18 mm (0.53 in), representing 12.5 % difference should be a matter of concern, since with all other things

being equal, the lane with the lower average asphalt thickness has the tendency to develop premature structural defects relative to the other lane. During data collection , it was noted that a number of intersections into some lumber and construction companies were located along the areas that recorded lower pavement layer thicknesses, though this may not be the only reason for the distinct disparity between the two lanes. Accordingly, quality assurance of new pavements by local government engineers should involve picking of cores at a 100 m intervals and their thicknesses measured in the laboratory to ascertain the true layer thickness variation along the road, instead of the use of only visual inspection.

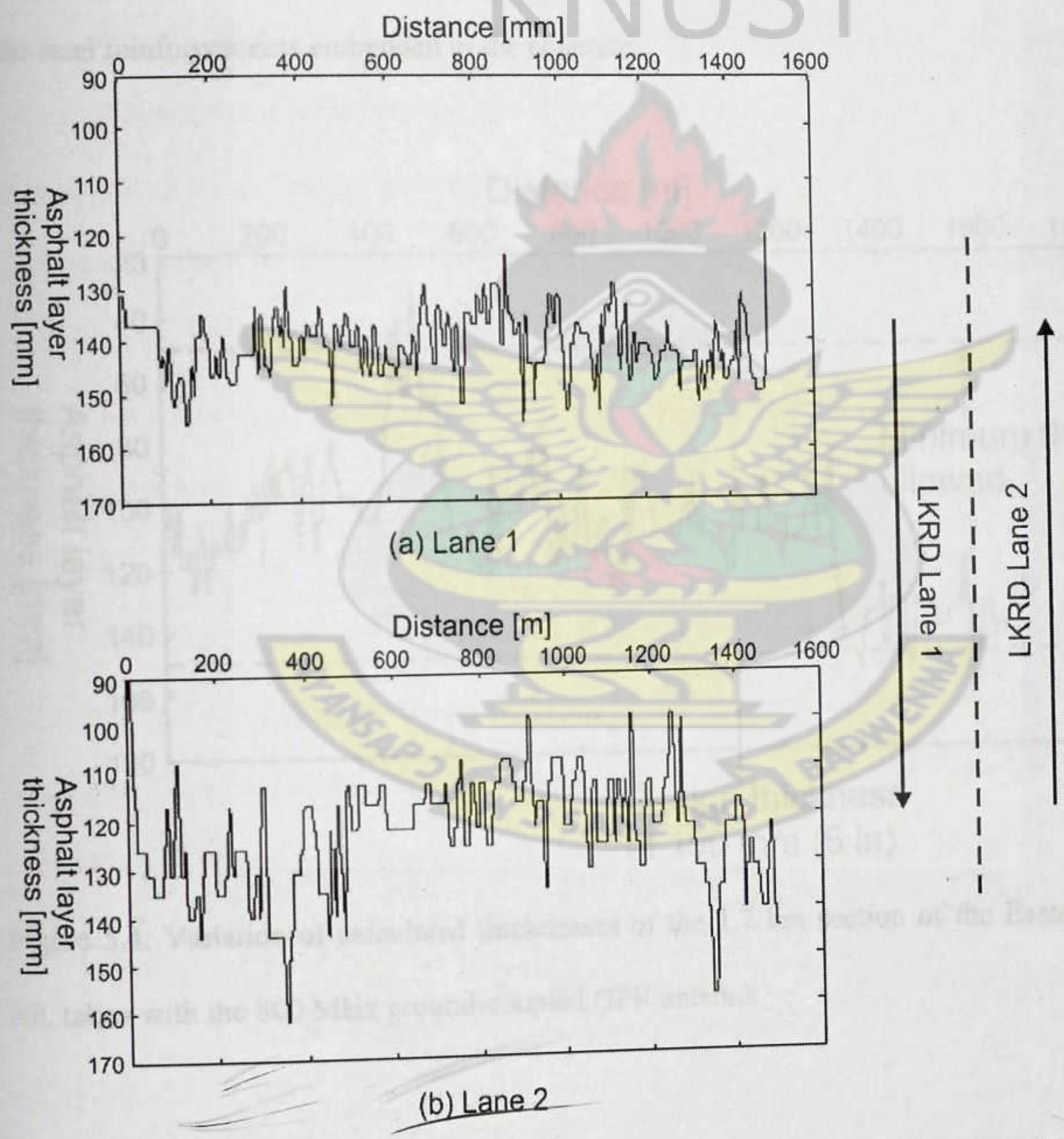

Figure 5.3: A comparison of the thickness variations of two lanes of LKRD 1 and 2.

5.3 Eastern Bypass Road.

The road at this site is a 17 km dual carriage between the Asokwa Overpass and Anloga Junction, part of which was still under construction as at the time of the survey and therefore only the fully completed 1.7 km section was evaluated to assess the pavement layer thickness and its uniformity along the traversed section. Since the project was part of the site LKRD 1 and 2, the main pavement structures included two layers; an asphalt concrete course and a base course. The road is the principal arterial road that connects the eastern part of the city to the western part. The surveyed section traverses an overpass bridge (Asokwa Overpass) which was though not fully completed at the survey time, but an effort was made to examine the steel reinforcements embedded in the concrete.

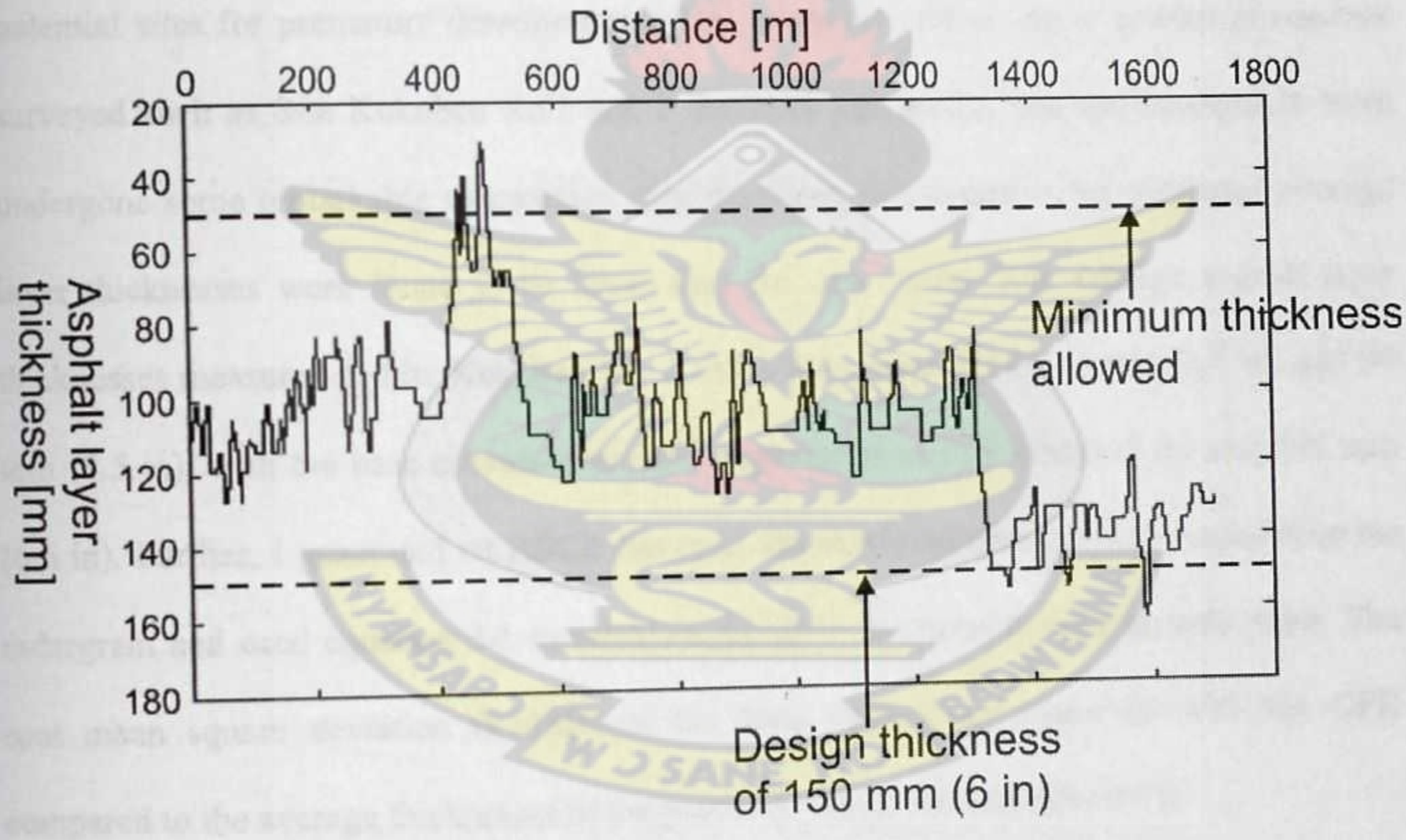

Figure 5.4: Variation of calculated thicknesses of the 1.7 km section of the Eastern Bypass Rd. taken with the 800 MHz ground-coupled GPR antenna

The variation of the calculated asphalt layer thicknesses at the Eastern Bypass Rd. is shown in figure 5.4 above. The radargram from the Eastern-Bypass road is shown in Appendix A. The estimated average thickness of the asphalt wearing course was found to be 110 mm (4.3 in), with a standard deviation of 21 mm whereas the base course recorded an average of 159 mm (6.2 in), also with a standard deviation of 21 mm. Therefore, there was some level of consistency in the average layer thicknesses of the pavements in the newly constructed roads (Sites LKRD 1 and 2, and the Eastern Bypass Rd.), though they were all found to measure quite below the 6 in. standard expected of their Equivalent Single Axle Loads (ESALs). Further, as evident from figure 5.4, a section of the Eastern Bypass road registered some asphalt layer thickness values lower than the minimum 50 mm (2 in) value allowed by the Ghana Highway Authority standard, though a very small section, such areas could be potential sites for premature deterioration of the pavement. Other major arterial pavements surveyed such as Site Kokoben Rd.1 and 2 are older pavements, and are assumed to have undergone some remarkable compaction over the years, and therefore the estimated average layer thicknesses were found to be lower than the new ones. The average asphalt layer thicknesses measured at Site Kokoben Rd. 1 and 2 were respectively 74 mm (2.9 in) and 90 mm (3.5 in), with the base courses estimated respectively as 159 mm (6.2 in) and 166 mm (6.5 in). Further, I generated an ASCII file from the measured distance-time picks from the radargram and used equation 3.1 to calculate the layer thickness at each sample point. The root mean square deviation (RMSD) of the layer thicknesses measured with the GPR compared to the average thicknesses of the pavement layers was calculated by:

$$\mathrm{RMSD} = \sqrt{\frac{1}{n}\sum_{i=0}^{n}[h_{i(s)} - h_{i(m)}]^2} \qquad (5.1)$$

where h_s is the standard thickness and h_m is the thickness measured with the GPR system. A summary of the estimated asphalt layer thicknesses of the various major arterial roads surveyed is shown in table 5.1 below:

Table 5.1: Average Asphalt Layer Thicknesses of the Major Arterial Roads

Site	Default thickness mm/[in]	Estimated thickness mm/[in]	RMSD mm/[in]
LAKE RD 1	150-200/4-8	141/5.5	11/0.4
LAKE RD 2	150-200/4-8	123/4.8	11/0.4
E-BYPASS	150-200/4-8	110/4.3	21/0.8
A. KOKOKBEN 1	150-200/4-8	74/2.8	12/0.5
A. KOKOBEN 2	150-200/4-8	90/3.5	12/0.5

Part of the pavement interface in the entire roads surveyed appeared to be in a poor condition, with areas partially deteriorated pavement material interspersed between some areas of badly compressed materials. It is worth noting here that such continuous findings about the pavement layer thickness could not have been found with other conventional methods of pavement evaluations such as coring. It is often difficult to provide a general recommendation for the number of cores required to ensure adequate information on the pavement as in the GPR method. Thus, the variability of the pavement layer thickness would determine the sampling density of the cores to be picked. For instance in the LKRD 1 pavement with high variability of layer thickness, one core per 100 m would be adequate.

5.4 Results from Minor Arterial Roads

Minor arterial roads are generally designed for traffic areas with relatively low Equivalent Single Axle Loads (ESALs) and they often link one major arterial road to another. Various GPR profiles were also taken with the 800 MHz ground-coupled antenna along five minor arterial roads, also in the Asokwa Sub-Metropolis of Kumasi with the aim of estimating their layer thicknesses as well as mapping areas of structural defects in the pavements. All of the pavements covered in this study were older ones, therefore the asphalt and base layer thicknesses were expected to be fairly below the standard values, since the pavements have undergone compaction over the years. Admittedly, locating the pavement layer interface in some of the old minor arterial pavements from the ReflexW software was indeed a challenge due to their level of deterioration. Moreover, a few of the pavements such as the High School Rd. has undergone series of maintenance work at various sections of the part surveyed. Evidence of surface defects such as cracks and rutting were clear on some of them as well. Figures 5.5 and 5.6 below are radargrams of the Kaase Ind. Rd. and the Hudson Rd. respectively, with very disturbed layer interfaces. The GPR survey was also successful in mapping clearly areas of concrete culvert along the pavement as shown in figure 5.5. Further, sections of the pavements that have undergone maintenance work are also depicted in the GPR scan (figure 5.6). Further, The average asphalt layer thicknesses estimated from the various minor arterial pavements studied are shown in table 5.2.

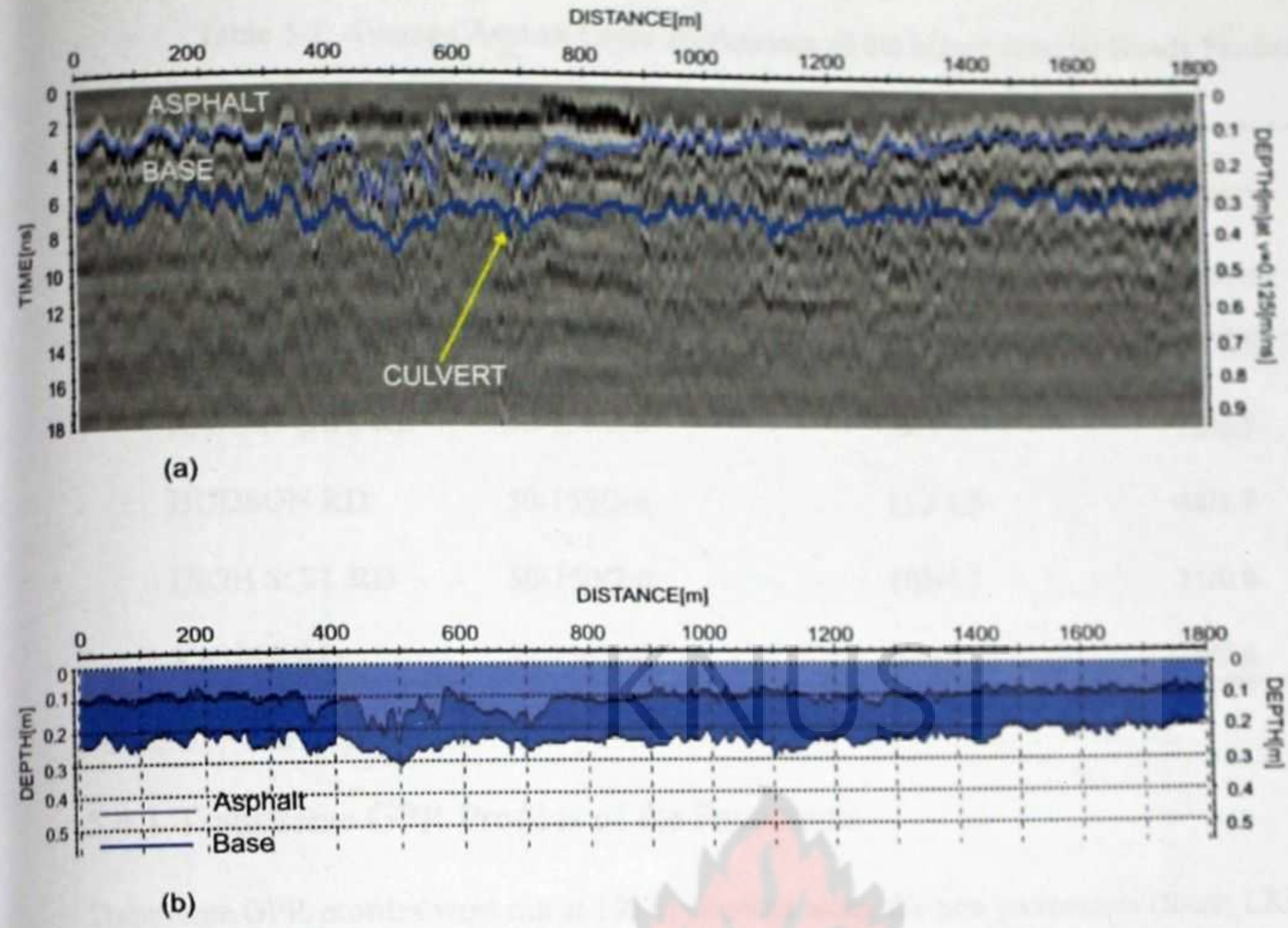

Figure 5.5: Longitudinal GPR scan of the Kaase Ind. Road.

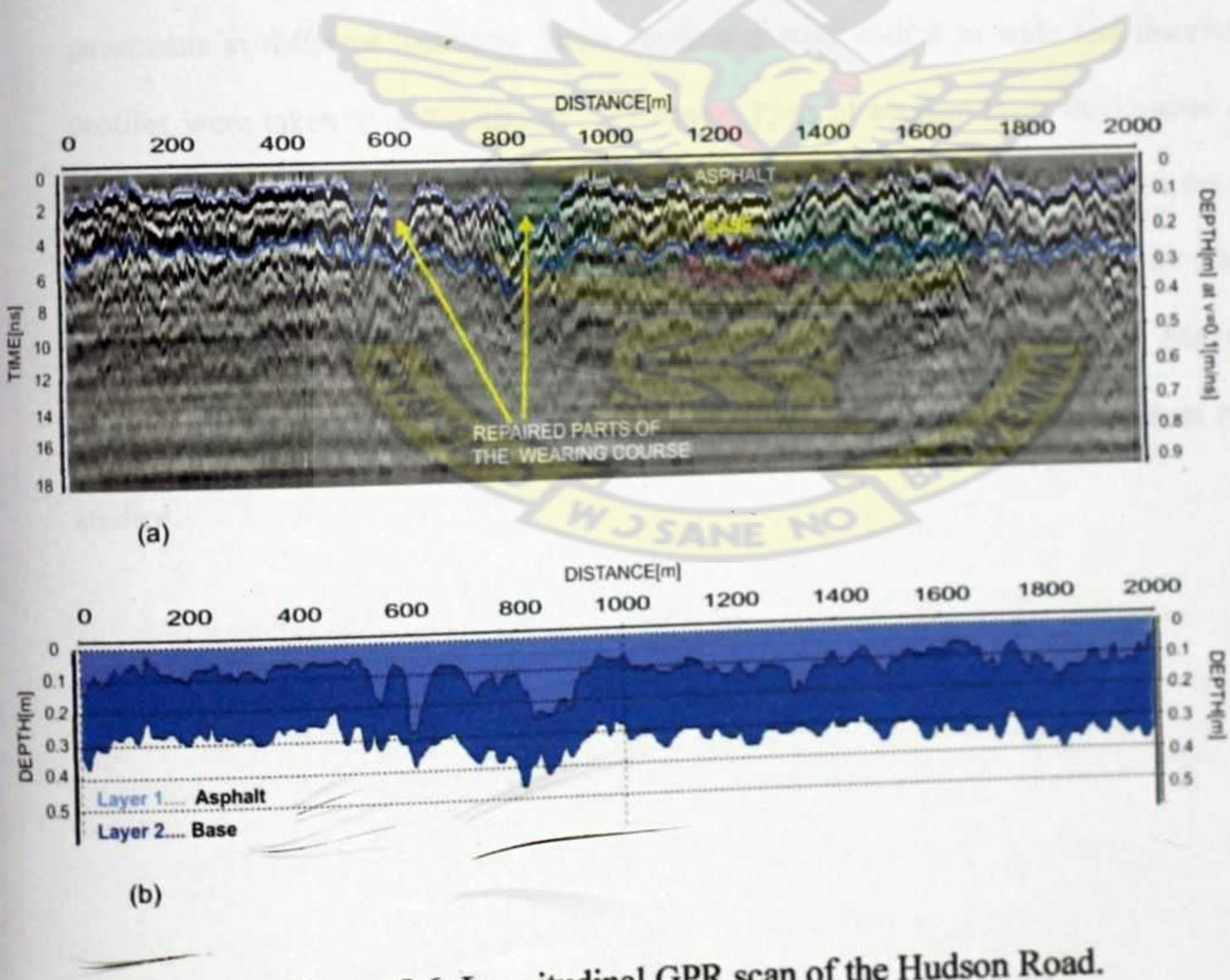

Figure 5.6: Longitudinal GPR scan of the Hudson Road.

Table 5.2: Average Asphalt Layer Thicknesses of the Minor Arterial Roads Studied.

Site	Default Thickness mm/[in]	Estimated thickness mm/[in]	RMSD mm/[in]
KAASE IND. RD	50-150/2-6	96/3.4	22/0.8
KAASE-GUI. RD	50-150/2-6	99/3.8	12/0.5
HUDSON RD	50-150/2-6	110/4.3	44/1.7
HIGH SCH. RD	50-150/2-6	103/4.1	21/0.8
KNUST RD.	50-150/2-6	80/3.1	16/0.6

5.4.1 Transverse GPR Profiles of the Pavements

Transverse GPR profiles were run at 100 m intervals along the new pavements (Sites; LKRD 1 and 2, Eastern Bypass Rd.) to assess the uniformity of the asphalt layer thickness across the pavements at different locations. These pavements were each 8 m wide and therefore the profiles were taken at a distance of 7 m across. Plots of average layer thicknesses of the transverse GPR scans are shown in Figure 5.7. Figure 5.7 (a) is the profiles from the north-bound lane of the Lake Rd. and (b) is the Eastern Bypass Rd. It was found that for the same pavement, the mean thicknesses recorded 100 m apart were not the same. Fairly high variability of the asphalt and base layer thicknesses were recorded in the various profiles studied.

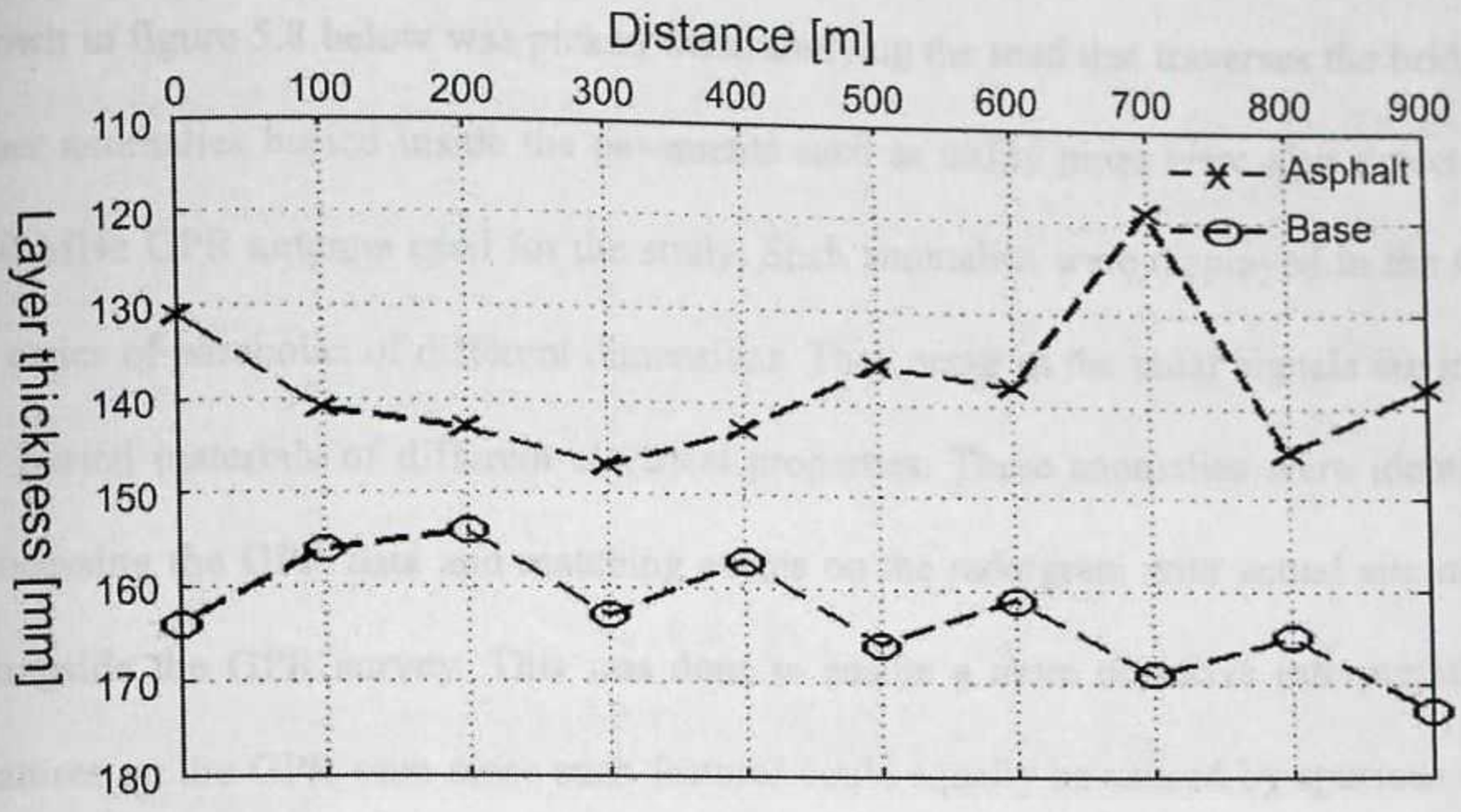

(a)

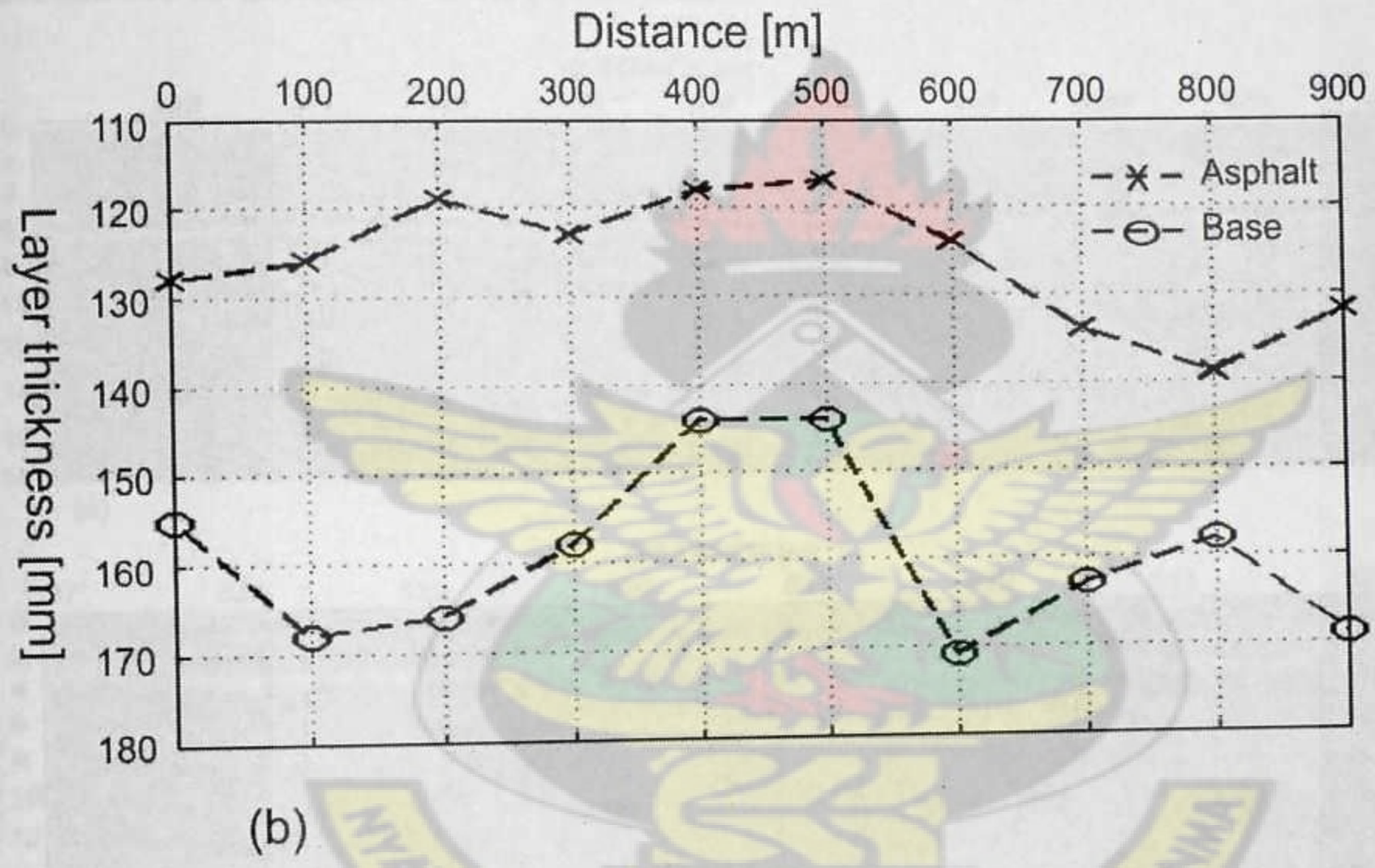

(b)

Figure 5.7: Transverse GPR scans of (a) LKRD 1 and (b) Eastern Bypass.

5.4.2 Anomaly Detection in Pavements

The 800 MHz ground-coupled shielded antenna used for this study was able to detect the metal reinforcement in the Asokwa Overpass bridge, that is, the steel inside the foundation of the bridge as well as steel mesh in the concrete bridge itself, though no special attention was given to studying the bridge. Thus the result of the GPR scan of the metal reinforcements

shown in figure 5.8 below was picked when studying the road that traverses the bridge. Some other anomalies buried inside the pavements such as utility pipes were also detected by the 800 MHz GPR antenna used for the study. Such anomalies were displayed in the GPR scan as series of parabolas of different dimensions. They occur as the radar signals are intercepted by buried materials of different electrical properties. These anomalies were identified after processing the GPR data and matching events on the radargram with actual site notes taken alongside the GPR survey. This was done to ensure a more objective interpretation of the features on the GPR scan since such features could equally be caused by spurious sources of electromagnetic energy such as telephone poles, overhead wires etc., and therefore misconstrued as anomalies in the pavements.

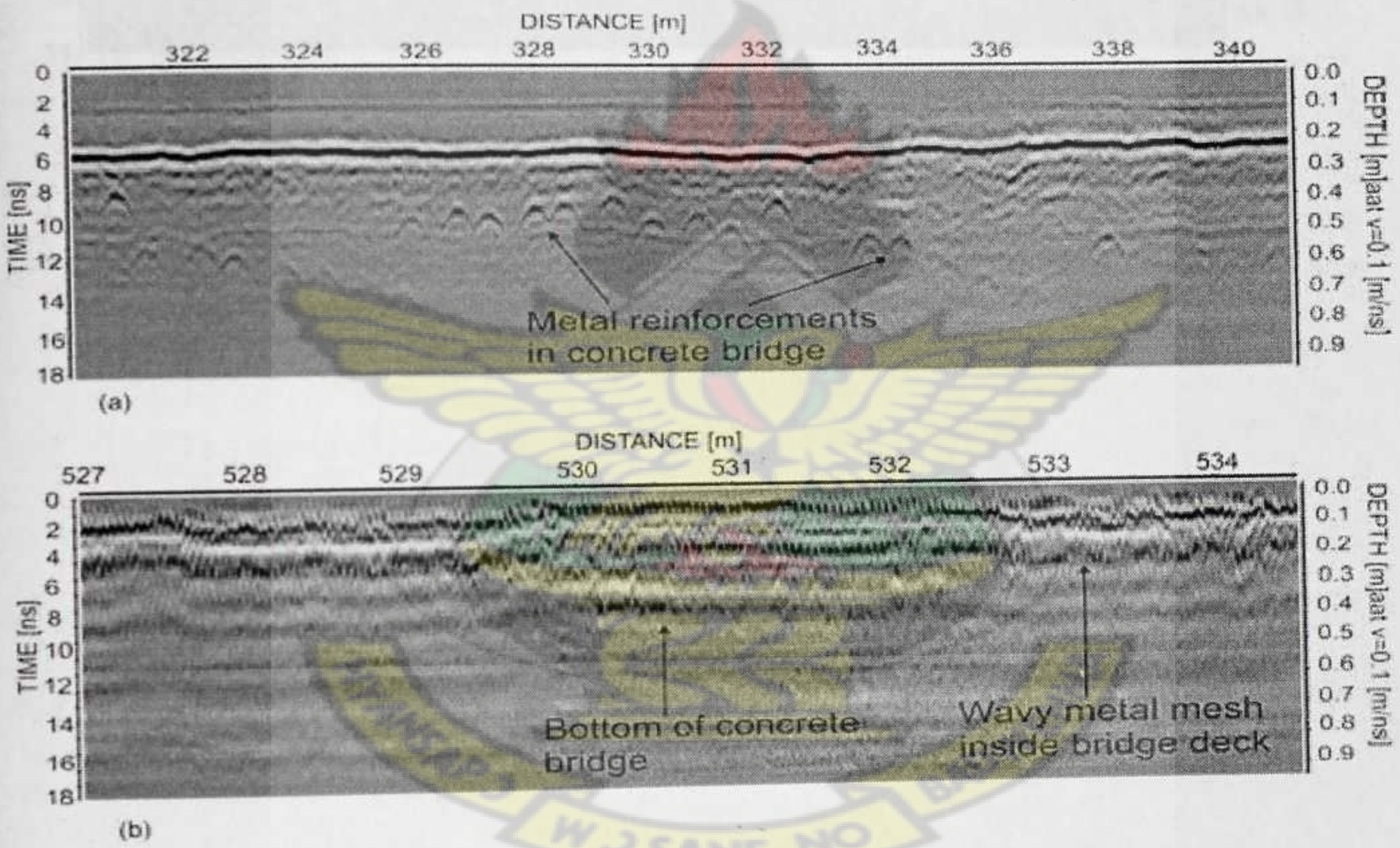

Figure 5.8: Metal reinforcements in the Asokwa Overpass Bridge, (a) is the foundation of the bridge and (b) is the actual overpass.

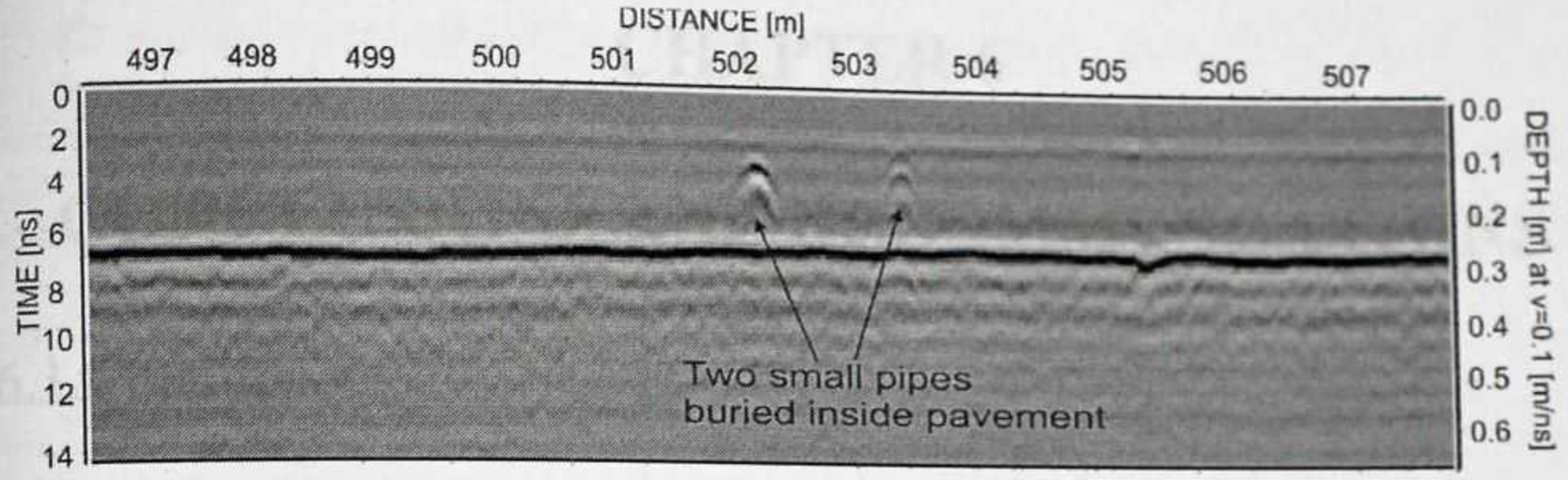

(a) Ahenema Kokobeng Rd.

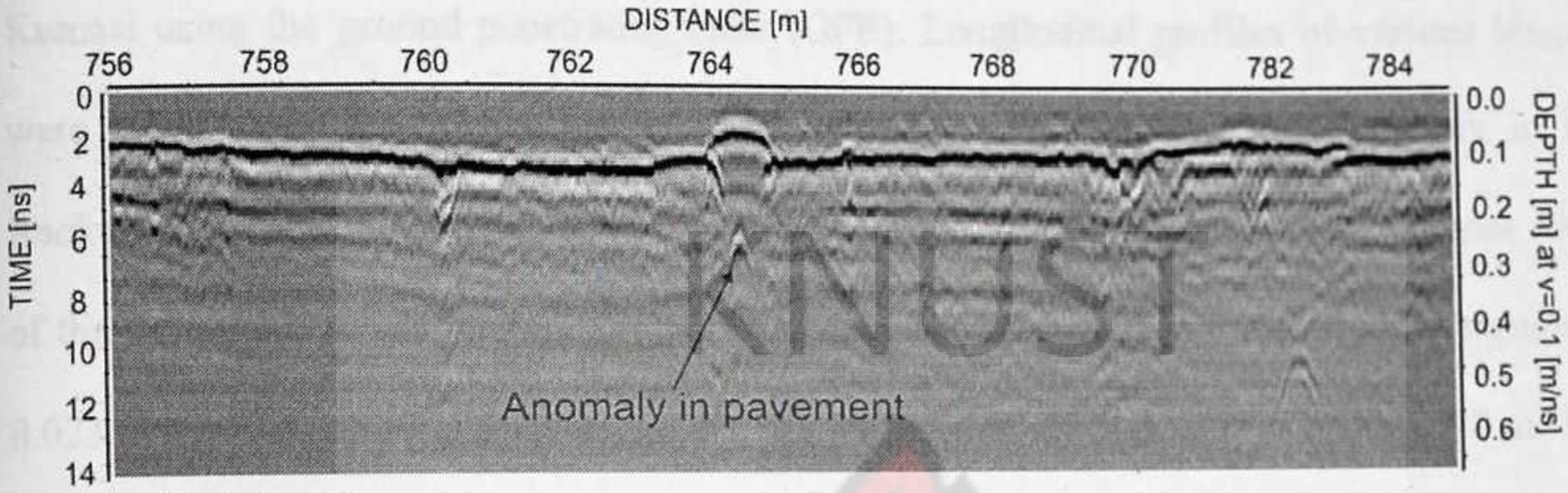

(b) Hudson Rd.

Figure 5.9: Detected anomalies in some of the pavements studied.

CHAPTER 6

CONCLUSIONS AND RECOMMENDATIONS

6.1 Conclusions

The main theme of this study has been the estimation of road pavement layer thicknesses in Kumasi using the ground penetrating radar (GPR). Longitudinal profiles of various lengths were taken along five major arterial roads and five minor arterial roads, mainly in the Asokwa Sub-Metropolis of Kumasi. Again, some transverse profiles were taken across some of the pavements to aid interpretation. The system was calibrated to transmit radar signals at 0.023 m intervals along the pavement, and at a penetration depth of approximately 1.0 m. The survey results were interpreted with due consideration for possible sources of error in the measurement and analysis since it was difficult to uniquely interpret some of the results without sample cores from the pavements. In such cases careful observation of other features at the site, including the presence of electrical junction boxes, overhead electrical cables as well as every possible sources of error were noted along the survey to help in the final interpretation. The 800 MHz ground-coupled GPR antenna used in the study was successful in clearly revealing the asphalt and base layers of the various road pavements surveyed, though GPR scans of some of the older pavements studied were poor and rendered their interpretation difficult.

The raw GPR data was processed with the Reflex software, in which the data was subjected to filtering algorithms such as background removal, subtract mean, bandpass, and gain function. The application of these filters made the identification of the pavement layer interfaces quite easy, therefore the various layer picking modes available in the Reflex software were used to mark the layer interfaces, and color shows of the layers produced.

Finally, an ASCII file of the travel times of the GPR traces, the measured thicknesses at each sample point of 0.023 m interval was generated with the software. The generated data were further plotted with MATLAB to obtain a clear display of the thickness variations in the various layers. Since no cores were taken from the pavements, the interpretation of the results was purely based on the GPR data and the notes taken from the roads as the GPR profiles were taken at the sites.

The key findings in this study are accordingly summarized as follows:

- Two main layers were identified in the pavements surveyed (asphalt wearing course and base course) and the average asphalt layer thicknesses of the newly constructed major arterial roads were found to have a range of 110 – 141 mm as against the designed layer thickness range of 102 - 200 mm, implying a RMSD of ±13.6 mm, whereas the base layers ranged between 155 - 171 mm, compared to the 150 - 200 mm designed layer thickness. This showed a RMSD of ±21 mm.
- The older major arterial roads however recorded lower average asphalt layer thickness range of 74 - 90 mm for the designed thickness of 150 - 200 mm and shows a RMSD of ±12 mm . The lower average asphalt layer thicknesses recorded in this case may be attributed to the relative consolidation of these older pavements over the years. The estimated average base course thickness range in these roads were found as 159 – 166 mm.
- The asphalt layer thicknesses of the minor arterial roads studied were found to range between 96 - 110 mm for a designed range of 102 - 150 mm, with a RMSD of ±22 mm. The average thickness range of the aggregate base layers was between 170 - 209 mm.

- Although the pavement layer interfaces were clearly identified in most cases, the interfaces in the pavements studied were generally of poor quality, and in some cases (such as the High School Rd.), layer interface identification at some areas was just impossible. High variability of the asphalt and aggregate base layer thickness was found in all the pavements investigated.
- Further, the 800 MHz ground-coupled antenna used in this study was able to detect the metal reinforcements in a concrete bridge along one of the surveyed pavements, though the bridge was not studied in detail in this survey. Other buried utilities in the pavements such as underground pipes and cables were also detected by the equipment along the pavement.
- Comparison of the measured pavement layer thicknesses with the standard design thicknesses of each of the roads (relative to their equivalent single axle loads (ESALs)) showed a RMSD of between 11 mm (0.4 in) and 21 mm (0.8 in) for asphalt layers in the major arterial roads and between 13 mm (0.5 in) and 21 mm (0.8 in) in the minor arterials. The coefficients of variation of the measured thicknesses were respectively up to 19% and 40% in the major and minor arterial roads.

It has been found through this study that the ground penetrating radar technique can be used reliably to non-destructively assess pavement systems and to estimate their layer thicknesses and distress locations. The GPR's continuous profiling capability, and ability to estimate pavement layer thickness and type without the use of cores, is a valuable precursor to ground truth, falling weight deflectometer and other road pavement evaluation methods. This capability is clearly demonstrated throughout this work.

Finally, the research results would help districts and local governments to perform continuous evaluation of the pavement conditions quickly and more accurately. In turn, this benefit will inherently increase construction efficiency and reduce the cost of pavement construction and maintenance in Ghana.

6.2 Recommendations and Outlook

The field investigations undertaken in this study provided a basis to evaluate the effectiveness of the GPR system for local traffic infrastructure condition surveys, and the lessons learnt allowed a set of main considerations to be proposed. These key recommendations are discussed below:

1. Traffic infrastructure surveys should be done with non- invasive survey methods such as the GPR for quality assurance of finished contractor jobs in Ghana.
2. Every constructed road should have load limits. Further, roads that are located in heavy duty industrial areas should have thicker layers.
3. There should be standard rules for the arbitrary cutting and refilling of roads as well as speed rumps construction.
4. For road pavement condition surveys which require shallow survey depths, higher frequency GPR antenna units should be used to effectively map all features of the pavement necessary for uniquely making conclusions about the conditions of the roads.
5. Future studies of local traffic infrastructure with the GPR system should be fully carried out with the support of the local government department and other agencies tasked with the responsibility of managing the roads, such that sample cores can be picked from the surveyed pavements and their thicknesses measured in the laboratory in order to authenticate the GPR results.

REFERENCES

1. A-CUBED (1983). General state of the art review of ground probing radar. page 89. A-CUBED, Mississauga, Ontario.
2. AASHTO (1993). Guide for Design of Pavement Structures. American Association of State Highway and Transportation Officials, Washington, D.C., USA.
3. Al-Qadi, I. (1992). The penetration of electromagnetic waves into hot-mix asphalt. Proceedings of the Nondestructive Evaluation of Civil Structures and Materials, pages
4. Al-Qadi, L. and Lahouar, S. (2004). Ground penetrating radar: State of the practice for pavement assessment. Materials Evaluation, 62(7):759–763.
5. Andreski, A. (2005). Case study of road funds in Ghana, Malawi and Tanzania. Technical report, Senior Road Executives Course.
6. Annan, A. (2003). Ground penetrating radar: Principles, procedures & applications.
7. Antunes, M. L. (1993). Pavement Bearing Capacity Evaluation Using Dynamic Non - Destructive Tests . PhD thesis, Lisbon.
8. ASTM (1987). Standard Designation: D4748-87 Standard Test Method for Determining the Thickness of Bound Pavement Layers Using Short-Pulse Radar . American Society for Testing and Materials, Philadelphia, Pennsylvania.
9. Atto-Okine, B. (1992). Investigation of post-construction failure of a lightly trafficked road in Ghana. Proceedings of the Institution of Civil Engineers, Municipal Engineer, 93(1):51–55.
10. Balanis, C. (1989). Advanced Engineering Electromagnetics. John Wiley & Sons,, New York.
11. Berg, F. (1984). Non-Destructive Measurement of Lagstykkelser in Vejbefastelser . Road Directorate, National Road Laboratory Memo, volume 157. Denmark.

12. Birchak, J., Gardner, C., Hipp, J., and Victor, J. (1974). High dielectric constant microwave probes for sensing soil moisture. Proceedings of the Institute of Electrical and Electronics Engineers , 62:93–98.

13. Bowders Jr., J. and Koerner, R. (1982). Buried container detection using ground penetrating radar. Journal of Hazardous Materials, 7:1–17.

14. Cantor, T. and Kneeter, C. (1978). Radar and acoustic emission applied to study of bridge deck, suspension cables and masonry tunnel. Transportation Research Record, (676):37–42.

15. Carlsten, P. (1988). Peat, Geotechnical Properties and Up-to-Date Methods of Design and Construction . Number 215. Varia 215. Statens geotekniska institut, Linkoping,Sweden.

16. Carter, C., Chung, T., Masliwee, T., and Manning, D. (1992). Analysis of radar reflections from asphalt covered bridge deck structures. in: J pilon (ed) ground penetrating radar. Geological Survey of Canada, (90-4):33–40.

17. Clark, M., Gordon, M., and Forde, M. (2004). Issues over high-speed non-invasive monitoring of railway track bed. NDT&E International, (37):131–139.

18. CNR (1988). Instruction to Schedule Road Maintenance. Italian regulation.

19. Daniels, D. (1996). Surface penetrating radar. page 300p. Institution of Electrical Engineers,U.K.

20. Daniels, D. (2004). Ground penetrating radar. The Institute of Electrical Engineers, London, United Kingdom.

21. Daniels, D., Gunton, D., and Scott, H. (1988). Introduction to subsurface radar. 135(4):278–320.

22. Davis, J. and Annan, A. (1989). Ground-penetrating radar for high resolution mapping of soil and rock stratigraphy. Geophysical Prospecting, 37:531–551.

23. Department of Urban Roads, 2002, Accra-Ghana

24. Fernando, E. G, Maser, K. R. and B. Dietrich, (1992) "Implementation of ground penetrating radar for network-level pavement evaluation in Florida," *GPR* '94, Proc. of the Fifth International Conference on Ground Penetrating Radar, Vol. I of 3, Kitchner, Ontario CA (June 12-16, 1994) pp. 351- 365.

25. Fisher, E., McMechan, G., Annan, A., and Cosway, S. (1992). 15. Examples of reverse- time migration of single-channel, ground-penetrating radar profiles. Geophysics, (57):577–586.

26. Franceschetti, G. (1983), Performing Electromagnetics, Basic Books, Torino, Italy

27. Gerlitz, K., Knoll, M., Cross, G., Luzitano, R., and and, R. K. (1993). Processing ground penetrating radar data to improve resolution of near-surface targets, Proceeding of the Symposium on the Application of Geophysics to Engineering and Environmental Problems . San Diego, California.

28. Graves, C. R. and Drnevich, V. P. (1991). "calculating pavement deflections with velocity transducers", transportation research record. Technical Report 1293, TRB, National Research Council, Washington, D.C.

29. Halabe, U. B, Maser, K. R., Kausel, E. A. (1989). "Condition assessment of reinforced concrete structures using electromagnetic waves, ACI Materials Journal, vol. 92, No. 5, pp 514-523.

30. Heikkilä, R., Jaakkola, M., and Saarenketo, T. (2004). Modeling Information Flows for Automated Road Rehabilitation Process. ISARC'2004, 21st International Symposium on Automation and Robotics in Construction, Jeju, Korea.

31. Herkelrath, W., Hamburg, S., and Murphy, F. (1991). Automatic, real-time monitoring of soil moisture in a remote field area with time domain reflectometry. Water Resource Research, 27:857–864.

32. Hicks, R. (1991). Moisture Damage in Asphalt Concrete. Synthesis of Highway Practice 175, Transportat Research Board, 175 edition.

33. Irwin, L. H. (2002). Backcalculation: An overview and perspective. FWD/ Backcalculation Workshop 3- 6th International Conference on the Bearing Capacity of Roads, .Railways and Airfields.

34. Johansson, H. (1987). Use of ground penetrating radar in different minicipal projects. Highway Authority, Home care and bridge construction. Department of Geotechnics, Sweden.

35. Jol, H.M. (2009). Ground Penetrating Radar : Theory and Applications. Elsevier Sciences, The Netherland. 524.

36. Knoll, M. D. & Knight, R. (1994) Relationships between dielectric and hydrogeologic properties ofsand-clay mixtures. In: 5th International Conference on Ground Penetrating Radar, Waterloo Centre for Groundwater Research, Canada. pp. 45-61.

37. Knoll, M. (1996). A petrophysical basis for ground-penetrating radar and very early time electromagnetics, electrical properties of sand-clay mixtures :unpublished Ph.D. dissertation ., University of British Columbia, 316p.

38. Kovacs, A. and Morey, R. M. (1977). Detection of Cavities Under Concrete Pavement. Technical Report CRREL 83-18, Cold Region Research and Engineering Laboratory , Hanover, New Hampshire.

39. Kwakye, E., Fouracre, P., and Brown, S. (1998). The urban transport policy reform in Ghana. Technical report, CODATU VIII Conference, Cape Town.

40. Loken, M. (2007). Use of ground penetrating radar to evaluate Minnesota roads. Technical Report MN/RC-2007-01, Minnesota Department of Transportation Office of Materials, 1400 Gervais Avenue Maplewood, MN 55109.

41. Loulizi, A. (2001). Development of Ground Penetrating Radar Signal Modeling and Implementation for Transportation Infrastructure Assessment. PhD thesis, Blacksburg, Virginia.

42. Liu, R., Li, J., Chen, X., Xing, H., Ekbote, A., and Wang, Y. (2006). Investigation of a new generation of FCC compliant NDT devices for pavement layer information collection. Technical Report 0-4820-S, Subsurface Sensing Lab., The University of Houston.

43. Manning, D. and Holt, F. B. (1983). Detecting Deterioration in Asphalt Covered Bridge Decks. Transportation Research Record, (899):10–19.

44. Manning, D. and Holt, F. B. (1986). The development of deck assessment by radar and thermography. Transportation Research Record, 083:13–20.

45. Mark, L. (2007). Use of ground penetrating radar to evaluate Minnesota roads. Technical Report MN/RC-2007-01, Minnesota Department of Transportation Office of Materials, 1400 Gervais Avenue Maplewood, MN 55109.

46. Maser, K. and Scullion, T. (1991). Automated detection of pavement layer thicknesses and subsurface moisture using ground penetrating radar. Transportation Research Board Paper.

47. Maser, K. and Scullion, T. (1992). Automated pavement subsurface profiling using radar: Case studies of four experimental field sites. Transport Research Record , (1344):148–154.

48. Ministry of Transport, 2007-2008, Accra-Ghana

49. Millard, S., Shaari, A., and Bungey, J. (2002). Resolution of gpr bowtie antennas. proceedings of 10th international conference on ground penetrating radar, gpr 2002. Pages 724–731.

50. Momayez, A., Ehsani, M., Ramezanianpour, A., and Rajaie, H. (2004). Comparison of methods for evaluating bond strength between concrete substrate and repair materials. Cement and Concrete Research.

51. More, J. and Erhard, J. (1978). Radar detection of voids under concrete highways.

52. Moreman, B. and Michel, F. (1997). Bathymetric mapping and sub-bottom profiling through lake ice with ground-penetrating radar. (18):61–73.

53. Morey, R. (1998). Ground Penetrating Radar for Evaluating Subsurface Conditions for Transportation Facilities. Synthesis of Highway Practice 255. National Academy Press., National Cooperative Highway Research Program, Transportation Research Board.

54. Nazarian, S., Makahaube, J., and Rozendal, D. (1993). Investigation of parameters affecting the interface bonding of thin concrete overlays due to vehicular vibration. Technical Report 1920-2, Center for Geotechnical and Highway Material Research, The University of Texas, El Paso.

55. Olhoeft, G. (1978). Electrical properties of permafrost. pages 127–131. Edmonton, Alberta.

56. Olhoeft, G. (2002). Applications and frustrations in using ground penetrating radar. IEEE Aerospace and Electronic Systems Magazine, 17:12–20.

57. Pérez-Gracia, V. (2001). Evaluation of GPR applications in archaeological, historical and artistic heritage. PhD thesis, Catalonia Polytechnic (UPC), Barcelona, Spain(in Spanish).

58. Petersen, J., Plancher, H., Ensley, E., Venable, R., and Migake, G. (1982). Chemistry of Asphalt- Aggregate Interaction: Relationship with Pavement Moisture-Damage Prediction Test, volume 843 of Transportation Research Record, pages 95–104. Washington.

59. Reynolds, J. (1997). An introduction to Applied and Environmental Geophysics. JohnWilley & Sons Ltd., Baffins Lane,Chichester,West Sussex Po19 1UD, England.

60. RMeili, E. and Scullion, T. (1997). Detecting stripping in asphalt concrete layers using ground penetrating radar. Transportation Research Record, (1568):165–174.

61. Roadex. Creating effective technical exchange & co-operation between road districts in the NP region. Technical report, Roadex Project(1998-2001), www.roadex.org.

62. Roberts, F., P.S.Kandahl, Brown, E., Lee, D.-A., and Kennedy, T. (1991). Hot Mix Asphalt Materials, Mixture Design and Construction. NAPA Education Foundation, Lanham, p. 490

63. Roddis, W., Maser, K., and Gisi, A. (1992). Radar pavement thickness evaluation for varying base conditions. Technical Report 1355, Transportation Research Record, National Research Council, Washington, D.C.

64. Roth, K., Schulin, R., Fluhler, H., NewAuthor4, and Attinger, W. (1990). Calibration of time domain reflectometry for water content measurement using a composite dielectric approach. Water Resource Research, 26:2267–2273.

65. Saarenketo, T. (1992). Ground Penetrating Radar Applications in Road Design and Construction in Finnish Lapland . Geological Survey of Finland, Special Paper , 15:161–167.

66. Saarenketo, T. (1997). Using ground penetrating radar and dielectric probe measurements in pavement density quality control. Transportation Research Record , pages 34–41.

67. Saarenketo, T. (2006). Electrical properties of road materials and subgrade soils and the use of ground penetrating radar in traffic infrastructure surveys. PhD thesis, Faculty of Science, Department of Geoscience, University of Oulu.

68. Saarenketo, T. and Aho, S. (2005). Monitoring and classifying spring thaw weakening on low volume roads in northern periphery. page 11.

69. Saarenketo, T. and Roimela, P. (1998). Ground penetrating radar technique in asphalt pavement density quality control. proceedings of the seventh international conference on ground penetrating radar. volume 2, pages 461–466, Lawrence Kansas.

70. Saarenketo, T. and Scullion, T. (1994). Ground penetrating radar applications on roads and highways. Technical Report 1923-2F, Texas Transportation Institute, College Station, Texas.

71. Saarenketo, T. and Scullion, T. (1996). Laboratory and GPR tests to evaluate electrical and mechanical properties of Texas and Finnish base course aggregates. Proceedings of the Sixth International Conference on Ground Penetrating Radar, pages 477–482, Sendai, Japan.

72. Saarenketo, T. and Vesa, H. (2000). The use of gpr technique in surveying gravel road wearing course. in :Eigth intl. conference on ground penetrating radar. SPIEE, 4084:182–184.

73. Sansalone, M. J. and Streett, W. B. (1997). Impact-echo nondestructive evaluation of concrete and masonry.

74. Sato, M. (2001). GPR and its application to environmaental study. Master's thesis, Center for Northeast Asian Studies(CNEAS), Tohoku University, Sendai, Japan.

75. Sayers, M.W., Gillespie, T. D., and Queiroz, C. A. (1986). The international road roughness experiment: Establishing correlation and a calibration standard for measurements. Technical Report 46, The World Bank, Washington, DC.

76. Scullion, T., Lau, C., and Chen, Y. (1992). Implementation of the Texas Ground Penetrating Radar System. Technical Report FHWA/TX-92/1233-1, Texas Department of Transportation.

77. Scullion, T. and Saarenketo, T. (1996). Laboratory and GPR tests to evaluate electrical and mechanical properties of Texas and Finnish base course aggregates. proceedings of the sixth international conference on Ground Penetrating Radar. pages 477–482, Sendai, Japan.

78. Sebesta, S. and Scullion, T. (2002). Using Infrared Imaging and Ground-Penetrating Radar to detect segregation in Hot-Mix Asphalt overlays. Technical Report 4126-1, Texas Department of Transportation, Texas A&M University, College Station, TX.

79. Sellman, P., Delancy, A., and Aroone, S. (1992). Sub-bottom surveying in lakes with ground penetrating radar. page 18. Hanover, New Hampshire.

80. Shang, J., Umana, J., Bartlett, F., and Maser, K. (1999). Measurement of complex permittivity of asphalt pavement materials. Journal of the Transportation Engineering , pages 347–356.

81. SITEB (2004). Maintenance of Roads. Emmevi Graphics, Varese, Italy.

82. Smith, S. and Scullion, T. (1993). Development of ground- penetrating radar equipment for detecting pavement condition for preventive maintenance. Technical Report SHRP-H-672, Strategic Highway Research Program, National Research Council, Washington, D.C.

83. Stuart, K. (1990). Moisture damage in asphalt mixtures. Volume 90. Federal Highway Administration.

84. Telford, W. M., Geldart, L. P., Sheriff, R. E. and Keys, D. A. (1976). Applied Geophysics. Cambridge University Press.

85. Topp, G., Davis, J., and A.P. Annan (1980). Electromagnetic determination of soil water content measurement in coaxial transmission lines. Water Resource Research, 16:574–582.

86. Ulriksen, C. (1982). Application of Impulse Radar to Civil Engineering. PhD thesis, Lund University of Technology, Department of Engineering Geology.

87. Victorine, T. T., Zhang, Z., Fowler, D.W., and Hudson,W. R. (1997). Basic concepts, currentpractices, and available resources for forensic investigation on pavements.

88. Technical Report 1731-1, Center for Transportation Research, Bureau of Engineering Research, The University of Texas at Austin.

89. Yelf, R. (2004). Where is true time zero?. proc. of tenth international conference on groundpenetrating radar. pages 279–282.

90. Yelf, R. (2007). Application of Ground Penetrating Radar to Civil and Geotechnical Engineering . Georadar Research Pty Ltd, 412 Eastbank Road, Coramba, Co_s Harbour, NSW 2450, Australia.

91. Yuejian, C., Shongtao, D., Labuz, J. F., and Pantelis, J. (2007). Implementation of ground penetrating radar. Technical Report MN/RC 2007-34, Minnesota Department of Transportation Office of Materials, 1400 Gervais Avenue Maplewood, MN 55109-2044.

Appendix A

A.1 Processed Radargrams of Pavements

A.1.1 Major Arterial Roads

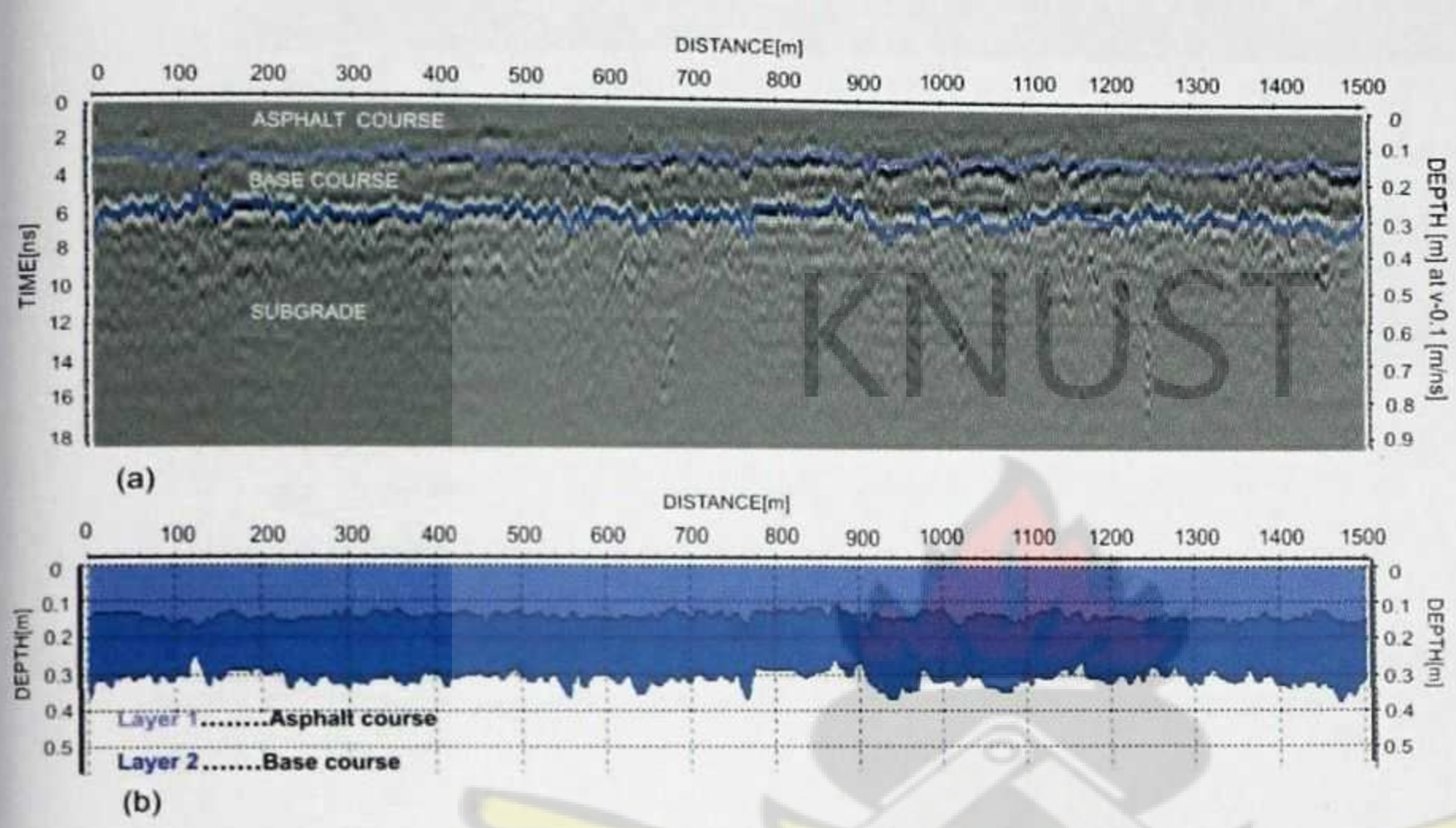

Figure A1: Radar section of the Lake Road Lane 1.

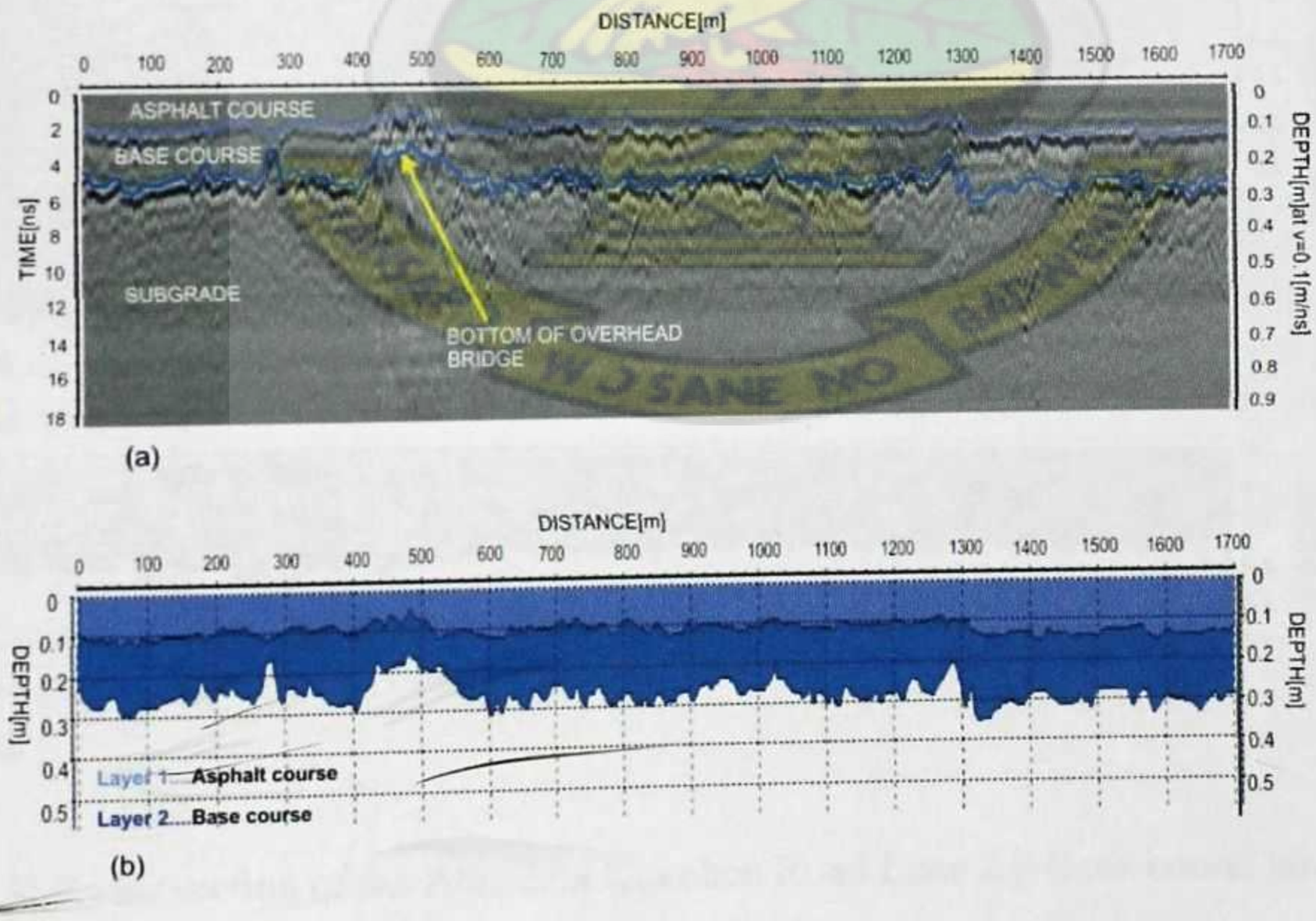

Figure A.2: Radar section of the Eastern-Bypass Road.

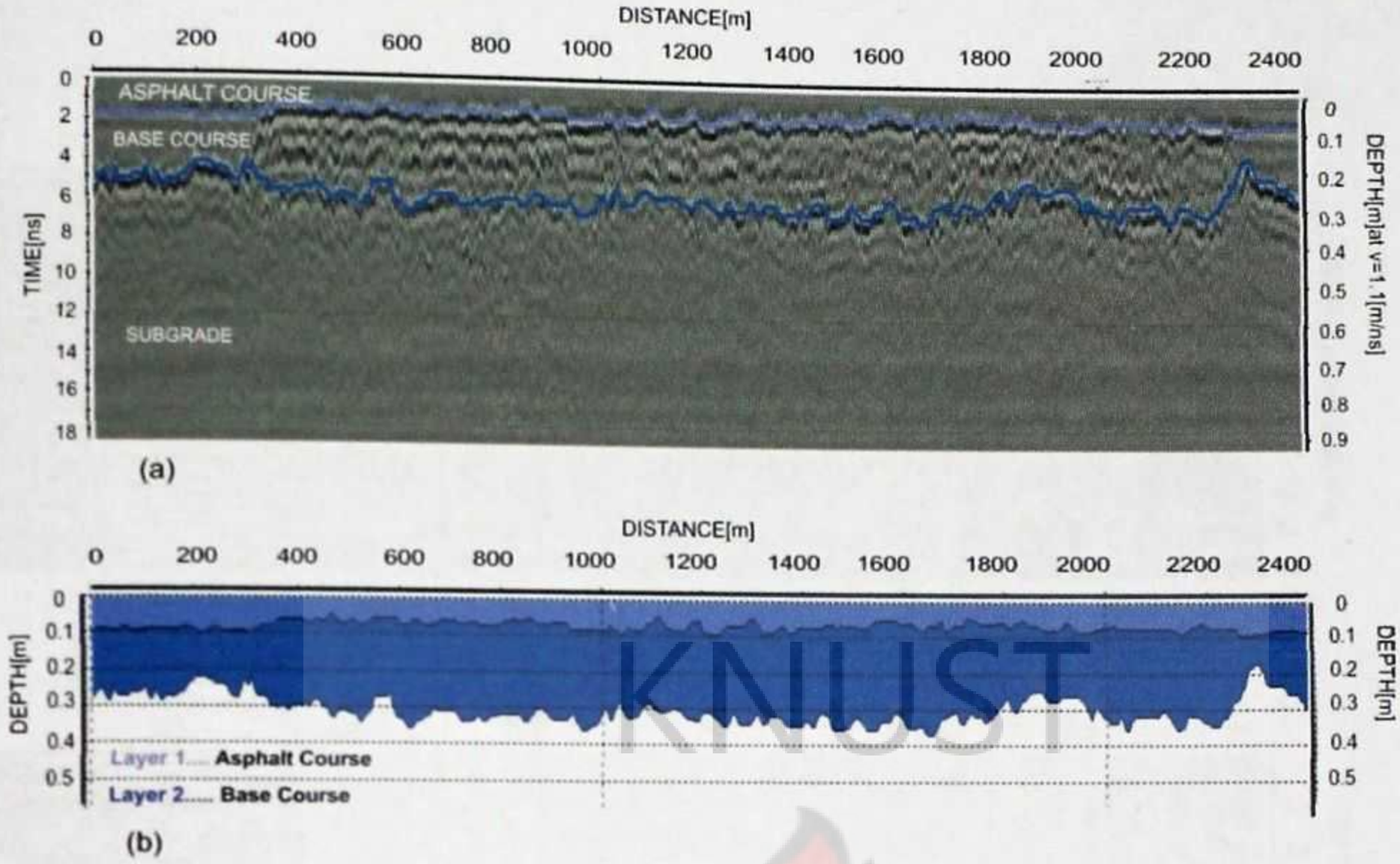

Figure A.3: Radar section of the Ahenema Kokoben Road Lane 1 (South-bound lane).

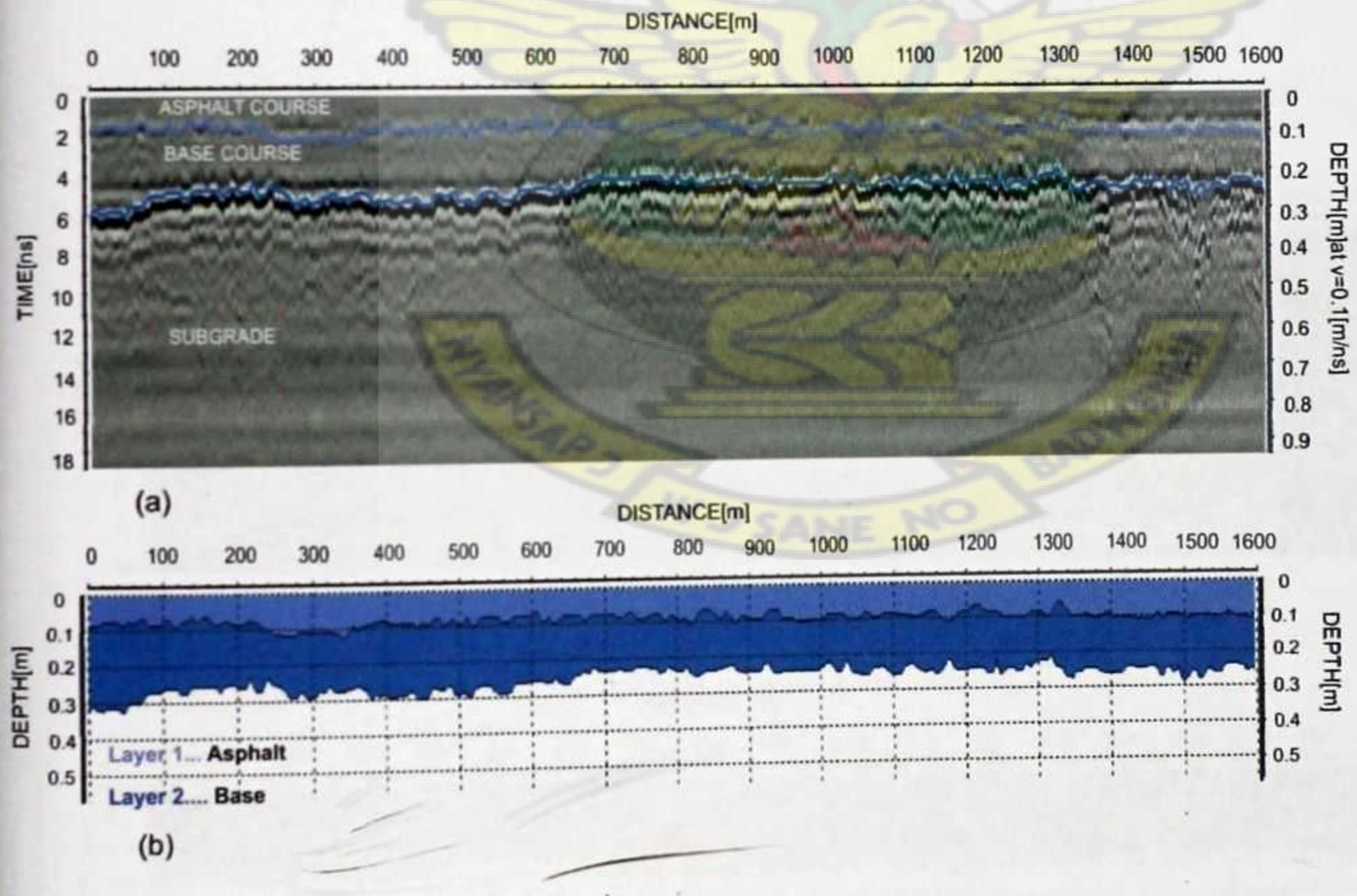

Figure A.4: Radar section of the Ahenema Kokoben Road Lane 2 (North-bound lane).

A.1.2 Minor Arterial Roads

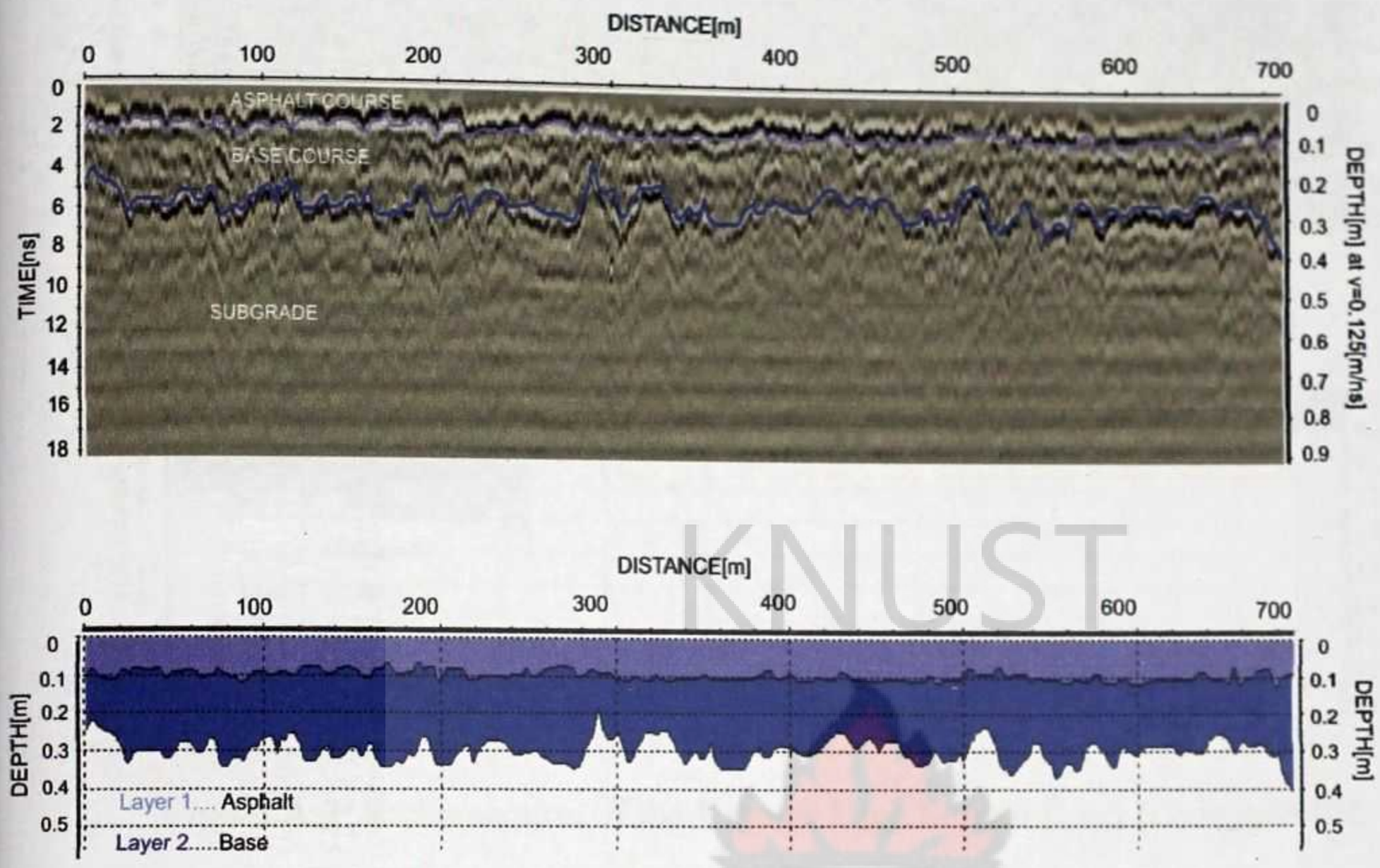

Figure A.5: Radar section of the Kaase-Guiness Ltd Road.

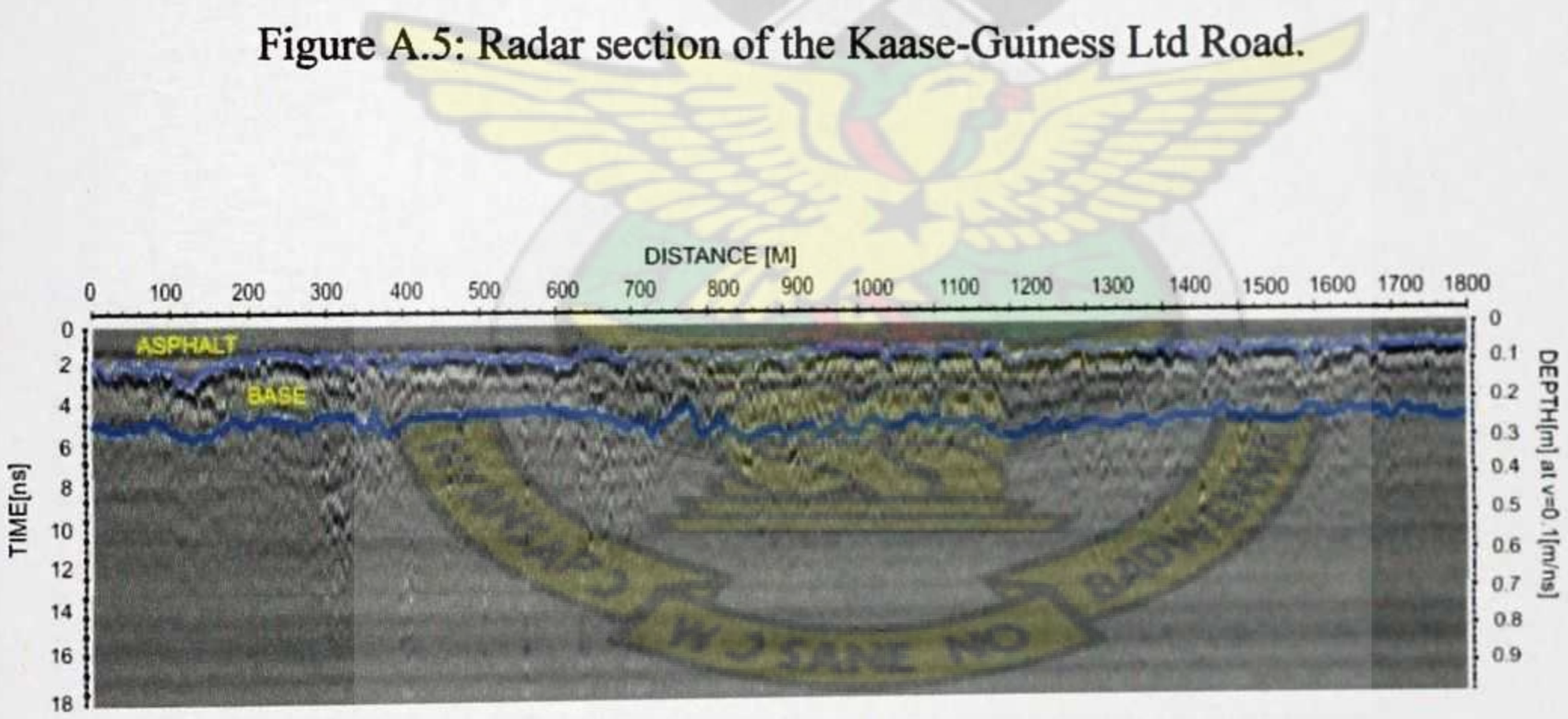

Figure A.6: Radar section of the KNUST Main Road.

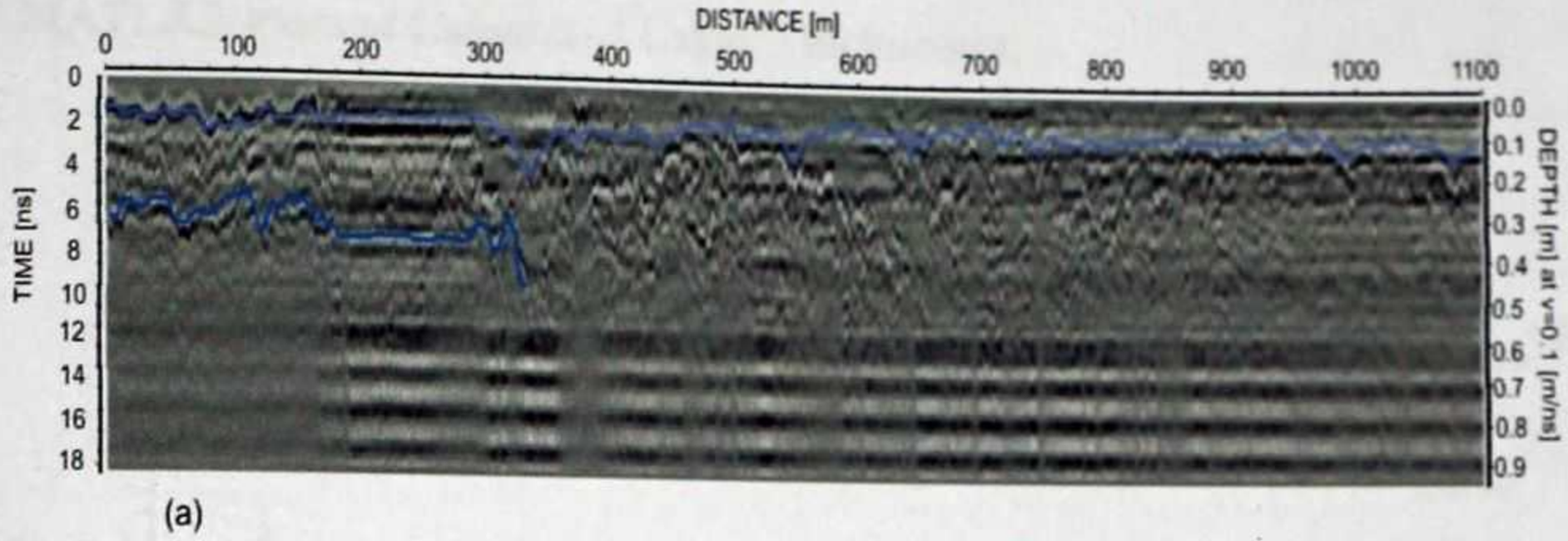

Figure A.7: Radar section of the Kumasi High School Road (Gyinyase Rd.

A.1.3 MATLAB Plots of Calculated Layer Thicknesses.

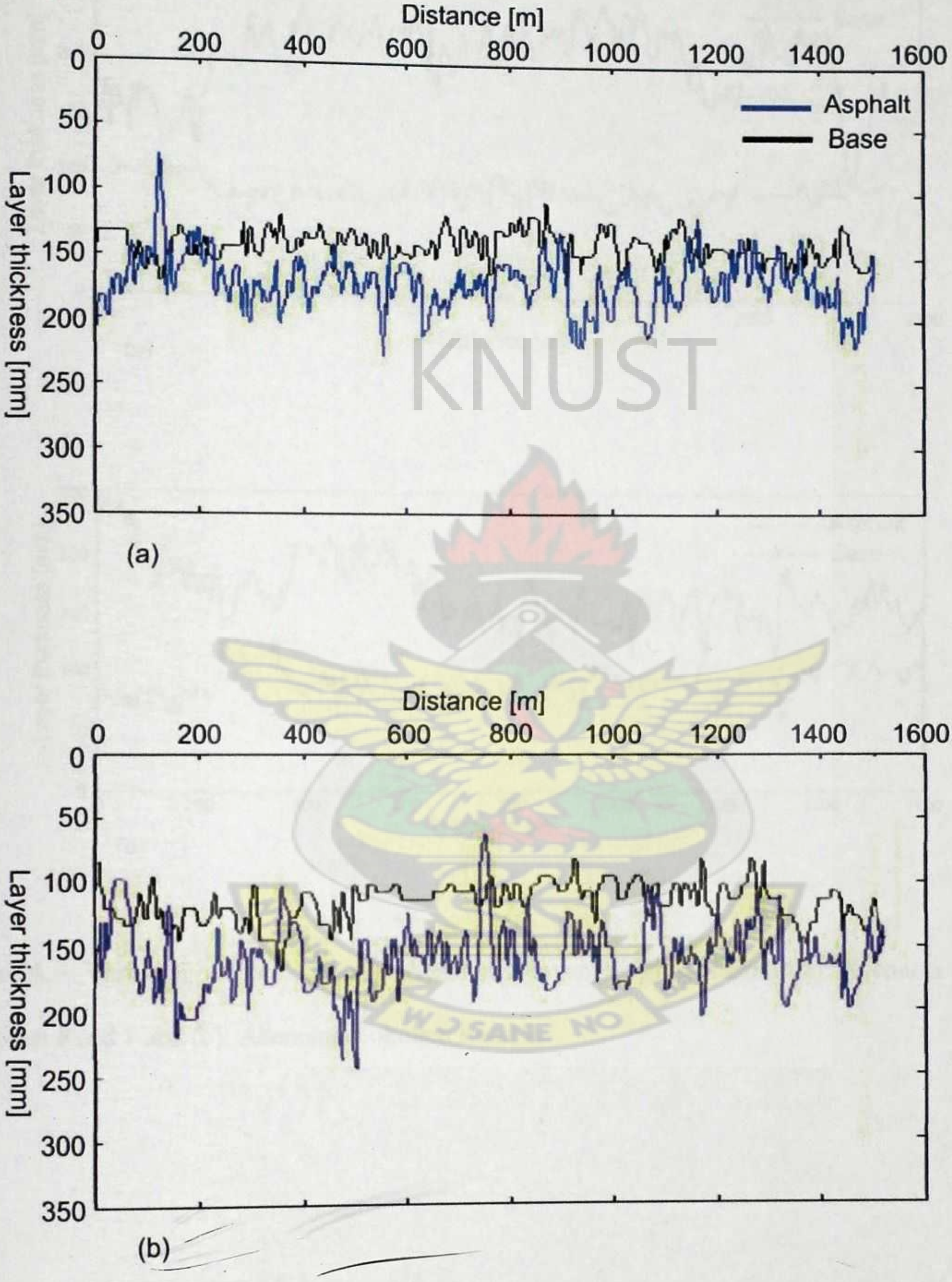

Figure A.8: Variation of calculated asphalt and base layer thicknesses along (a) Lake Road 1 and (b) Lake Road 2. The thicknesses were calculated from the GPR data.

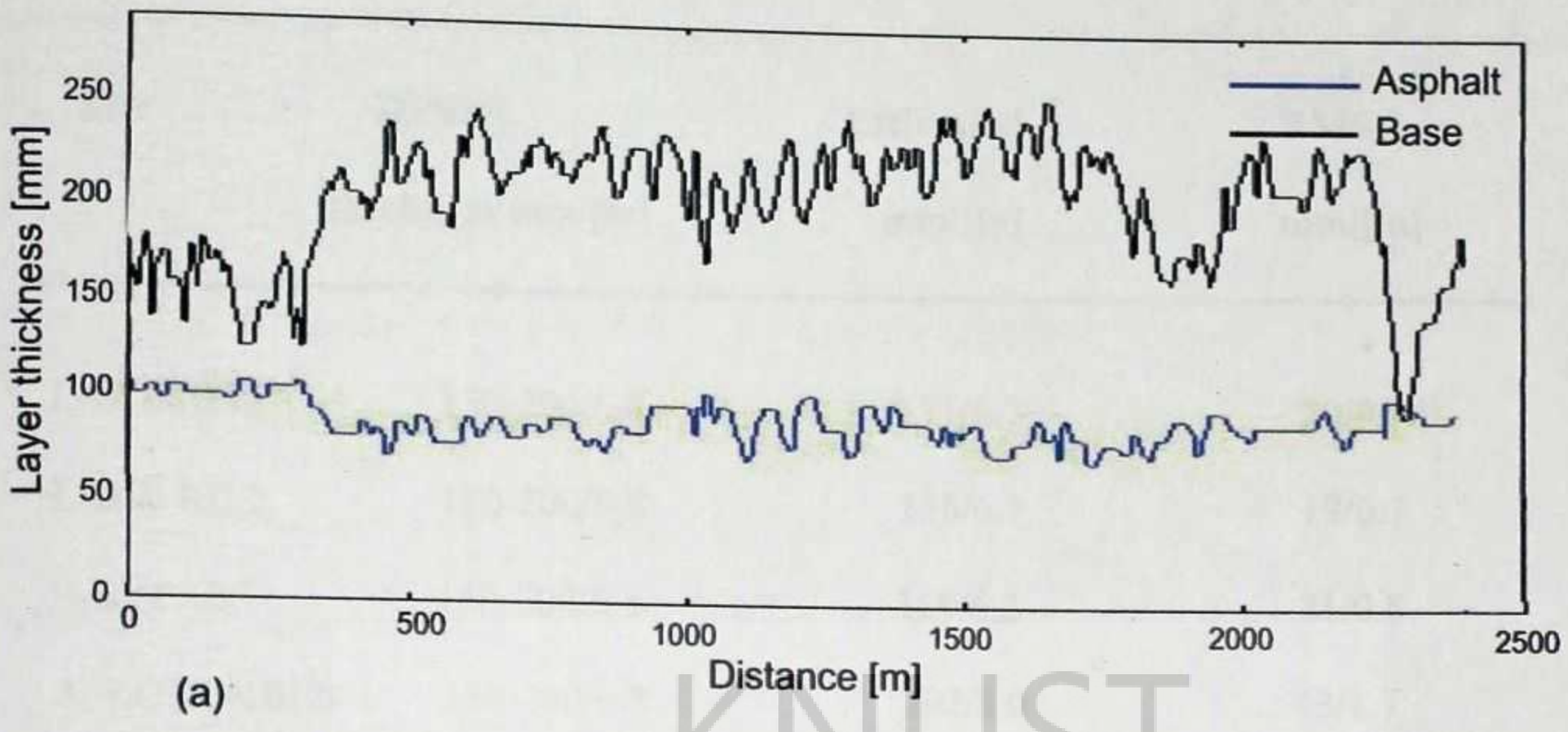

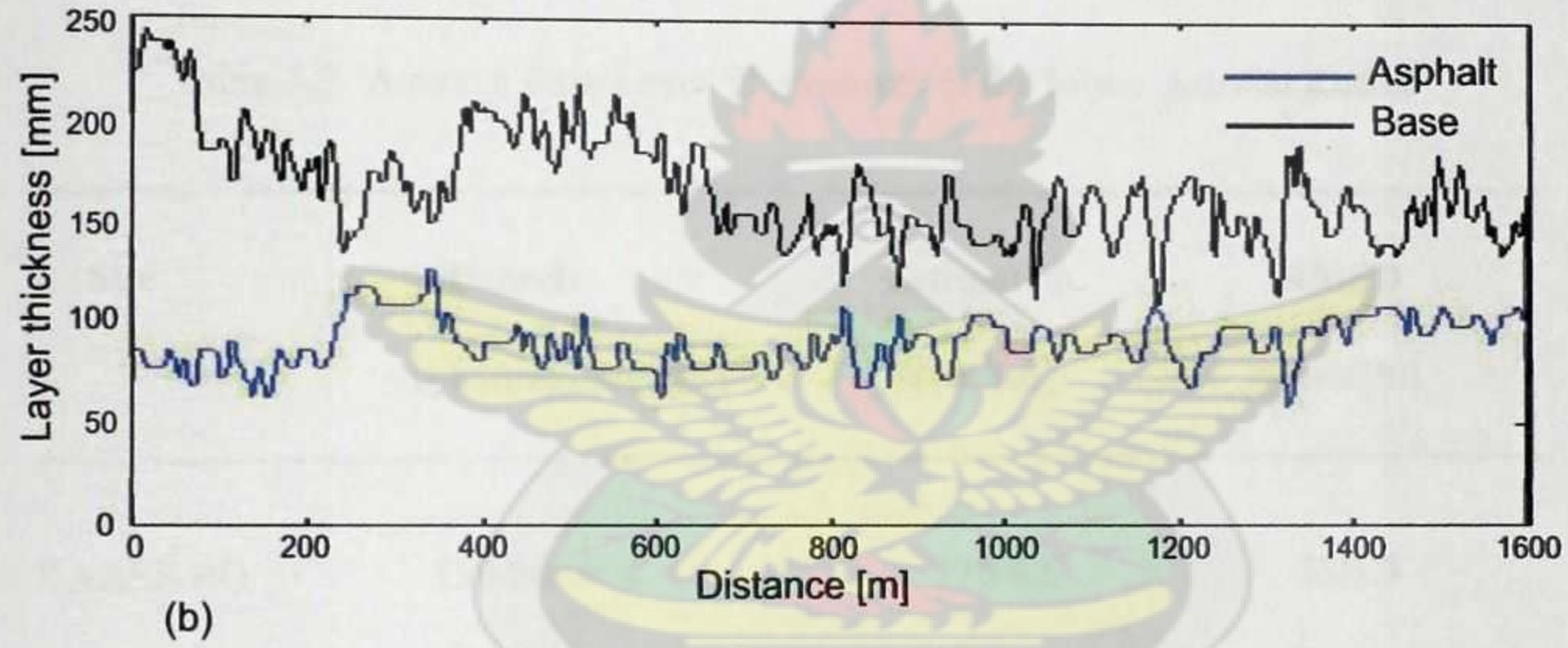

Figure A.9: Variation of calculated asphalt and base layer thicknesses along (a): Ahenema Kokoben Road 1 and (b): Ahenema Kokoben Road 2.

Table A.1: Average Base Layer Thicknesses of the Major Arterial Roads.

Site	Default thickness mm/[in]	Estimated mm/[in]	RMSD mm/[in]
LAKE RD 1	150-200/6-8	171/6.7	20/0.9
LAKE RD 2	150-200/6-8	155/6.1	19/0.7
E-BYPASS	150-200/6-8	159/6.2	21/0.8
A. KOKOKBEN 1	150-200/6-8	202/8.0	43/1.7
A. KOKOBEN 2	150-200/6-8	166/6.5	25/1.0

Table A.2: Average Base Layer Thicknesses of the Minor Arterial Roads.

Site	Default thickness mm/[in]	Estimated mm/[in]	RMSD mm/[in]
KAASE RD	150-200/6-8	170/6.6	33/1.3
KAASE-GUI. RD	150-200/6-8	187/7.3	37/1.4
HUDSON RD	150-200/6-8	209/8.0	32/1.5
HIGH SCH. RD	150-200/6-8	181/7.0	24/1.0
KNUST RD.	150-200/6-8	192/7.5	27/1.1

Appendix B

B.1 Softwares Used

- REFLEXW : for data processing.
- MATLAB: plotting pavement layer thicknesses calculated from the GPR data.
- Latex: typesetting and layout of document.
- MapInfo: Plotting GPS data and superimposing it on the site map.
- Corel Draw: Graphics.
- Microsoft Excel : data processing.